PORE-SCALE ANALYSIS OF THERMAL REMEDIATION OF NAPL-CONTAMINATED SUBSURFACE ENVIRONMENTS

A Dissertation

by

MIN AHN

Submitted to the Office of Graduate Studies of
Texas A&M University
in partial fulfillment of the requirements for the degree of

DOCTOR OF PHILOSOPHY

August 2008

Major Subject: Civil Engineering

PORE-SCALE ANALYSIS OF THERMAL REMEDIATION OF NAPL-CONTAMINATED SUBSURFACE ENVIRONMENTS

A Dissertation

by

MIN AHN

Submitted to the Office of Graduate Studies of
Texas A&M University
in partial fulfillment of the requirements for the degree of

DOCTOR OF PHILOSOPHY

Approved by:

Chair of Committee,	Yavuz Corapcioglu
Committee Members,	Hamn-Ching Chen
	Hongbin Zhan
	Eyad Masad
Head of Department,	David V. Rosowsky

August 2008

Major Subject: Civil Engineering

ABSTRACT

Pore-Scale Analysis of Thermal Remediation of NAPL-Contaminated Subsurface Environments. (August 2008)

Min Ahn, B.S., Seoul National University;

M.S., Seoul National University;

M.S., Texas A&M University

Chair of Advisory Committee: Dr. Yavuz Corapcioglu

The possible benefits of thermal remediation of NAPL-contaminated subsurface were analyzed at pore-scale. Force balance analysis was performed to provide the insight and information on the critical conditions for the blob mobilization. First, the critical blob radius for blob mobilization was calculated in terms of blob radius, temperature, and water velocity. Temperature increase enhanced the blob mobilization along with the decrease of interfacial tension. Water velocity increase also enhanced the blob mobilization. Critical water velocity provided the critical condition for the initiation of blob mobilization to distinguish singlet and doublet in blob size.

Second, the terminal (or steady state) blob velocity at the steady state blob motion was determined. Increases of temperature and water velocity raised the terminal blob velocity. When the observation of blob mobilization moved from REV scale (macro-scale) to pore-scale, terminal blob velocity showed the different phenomena according to the change of oil saturation. At macro-scale, the terminal blob velocity was smaller than

water velocity by an order or two. However, the terminal blob velocity reached to water velocity at pore-scale.

This investigation would provide the better understanding on the pore-scale analysis of residual NAPL blob mobilization by thermal remediation. Additionally, the pore-scale analysis developed in this study would be incorporated into a general conservation equation in terms of the accumulation of multiple blobs. It would derive continuum-averaged equations that accurately represent pore-level physics. In conclusion, the study on the critical conditions for the initiation of blob mobilization as a single discrete blob would have some contribution to the transport and fate of NAPL contaminant and the desired subsurface remediation.

DEDICATION

To my wife, Jeong-Soon, and my babies, Yerim and Moojin

ACKNOWLEDGEMENTS

I am deeply grateful to my advisor Dr. Yavuz Corapcioglu, who has provided the encouragement, constructive comments, and suggestions from the beginning of this research. He not only guided me in research but also enhanced my insight of what water resources engineering is and what role we play as water resources engineers. I am very honored to be his student. I am also especially grateful to my committee members: Dr. Hongbin Zhan, Dr. Hamn-Ching Chen, and Dr. Eyad Masad. I was so lucky to have an opportunity to work with them during the Ph.D. program.

I also thank my colleagues for their opinions in my research as well as their friendship: Sun Hee Yoon, Jiseok Han, and Seongha Hwang.

I would like to express my appreciation and love to my wife, Jeong-Soon, for her endless love, support, endurance, and encouragement. I can't imagine the completion of this work without her. Finally, I would like to thank my God for being always with me and bringing me strength, grace, and patience.

TABLE OF CONTENTS

CHAPTER Page

LIST OF FIGURES

FIGURE Page

FIGURE Page

LIST OF TABLES

NOMENCLATURE

A	correction factor to represent the medium-specific surface properties
d_p	soil particle diameter
F_b	buoyant force
F_d	drag force
F_p	push force
F_{st}	surface tension force
f_1	shape factor of intrinsic permeability
f_2	porosity factor of intrinsic permeability
f_R	thermal expansion coefficient of blob radius
$f_\forall$	thermal expansion coefficient of blob volume
g	gravity acceleration constant
k	intrinsic permeability
k_w (or k_o)	permeability or effective permeability of water (or NAPL) phase
k_{rw} (or k_{ro})	relative permeability of water (or NAPL) phase
M	mass
n	porosity
p_c	capillary pressure in a capillary tube
R	radius
R'	pore throat radius

S	saturation of fluid phase
T	temperature
u	velocity
$u_w^{'}$	relative velocity between water and NAPL phases
$\forall$	volume
$\forall_p$	pore volume of unit cell of porous media
$\forall_t$	unit cell volume of porous media
Bo	Bond number
Bo'	modified bond number
Ca	Capillary number
Ca_o'	modified capillary number
N_T	Trapping number
Re	Reynolds number
Δ	difference between two values of interest parameter
θ	contact angle
μ	viscosity
ρ	density
σ_{ow}	interfacial tension for NAPL-water system

Subscripts:

crit	at critical condition
o	NAPL phase

w	water phase
ref	at reference temperature (T = 20 ^{o}C)

CHAPTER I

INTRODUCTION

1.1 Problem Statement

Remediation of subsurface contamination by nonaqueous phase liquids (NAPLs) such as petroleum hydrocarbons and chlorinated solvents has been a great concern with relative issues of environmental protection and water quality monitoring (Rubin et al., 2008; Davis et al., 2002; Mercer and Cohen, 1990). NAPLs are organic chemicals which are immiscible in water. Due to their toxicity and low solubility in the water phase, a very small amount of residual NAPLs that remain as blobs, are potential long-term sources of soil and groundwater contamination.

In recent years, *in situ* thermal techniques, based on heating the subsurface, have been widely studied to remediate soil and groundwater contaminated by NAPLs as a better means of field application (O'Carroll and Sleep, 2007).

These techniques were originally developed in the petroleum industry for enhanced petroleum recovery. They were later applied to the environmental remediation industry primarily to deal with NAPL-related contamination. The various *in situ* thermal techniques include hot fluid injection (e.g. air, water, and steam), electrical heating with electrical currents or radio waves, and thermal conduction using steel wells.

This dissertation follows the style of Journal of Contaminant Hydrology.

To determinate the suitable remediation technique, the properties of contaminant and porous media both are considered (Davis, 1997; Davis, 1998). For example, steam or hot air injection is applicable for volatile or semi-volatile contaminants in the sandy or gravel aquifer. Meanwhile, hot water injection is suitable for the nonvolatile contaminants. Electrical heating is effective for most of the NAPL contaminants in the low permeability layers like the clay layer. The cost-benefit ratio and easement of operation and maintenance can also be factors for the selection of remediation technique. For a nonvolatile, viscous oil, steam and hot water injection are effective for the remediation. For this study, hot water injection is considered more appropriate, because it provides the same amount of oil recovery at a lower temperature using hot water instead of steam, saves the effort of operation and maintenance and reduces the overall cost with the same result.

According to the classification of NAPLs, highly viscous and nonvolatile oils, like crude oil, coal tar, and creosote are LNAPLs (light nonaqueous phase liquids) which are lighter than water. Viscous LNAPL in the porous media can be recovered effectively through hot water flooding. Flooding produces the several favorable effects. First, it decreases the capillary and interfacial forces between fluids and the porous media. The decrease of forces lowers the residual saturation of the NAPL phase. Second, it causes the thermal expansion of the NAPL phase. It increases the saturation of the NAPL phase and subsequently increases its mobile fraction and decreases the residual. Third, it decreases the viscosity of the NAPL phase. It also enhances its mobility.

LNAPL is generally put into the subsurface by anthropogenic episodes such as spills or wastewaters disposal from industrial activities. When LNAPL is initially released into the subsurface, it infiltrates the vadose zone in the form of continuous fluid by the force of gravity. However, when it proceeds to a certain depth, it is retained by the capillarity as a blob trapped in the pores. When a large volume spill occurs, the continuous fluid can reach the upper limit of the saturated zone and exhibit lateral movement along the water table. However, this free-phase layer is discretized to become blobs trapped in the pores around the water table from the “smearing” phenomena as the elevation of the water table fluctuates with seasonal changes (Figure 1-1).

In order to analyze the removal of NAPL blobs in the pores by hot water flooding, the critical conditions on the transport of NAPL blob through the water flow in the pores need to be observed. This observation shows the effects of blob radius, temperature and water velocity on the enhancement of blob mobilization in the pores. And, the consideration of varying relative permeabilities of fluids (oil and water) provides insights into the transport of NAPL blob in porous media at the pore-scale.

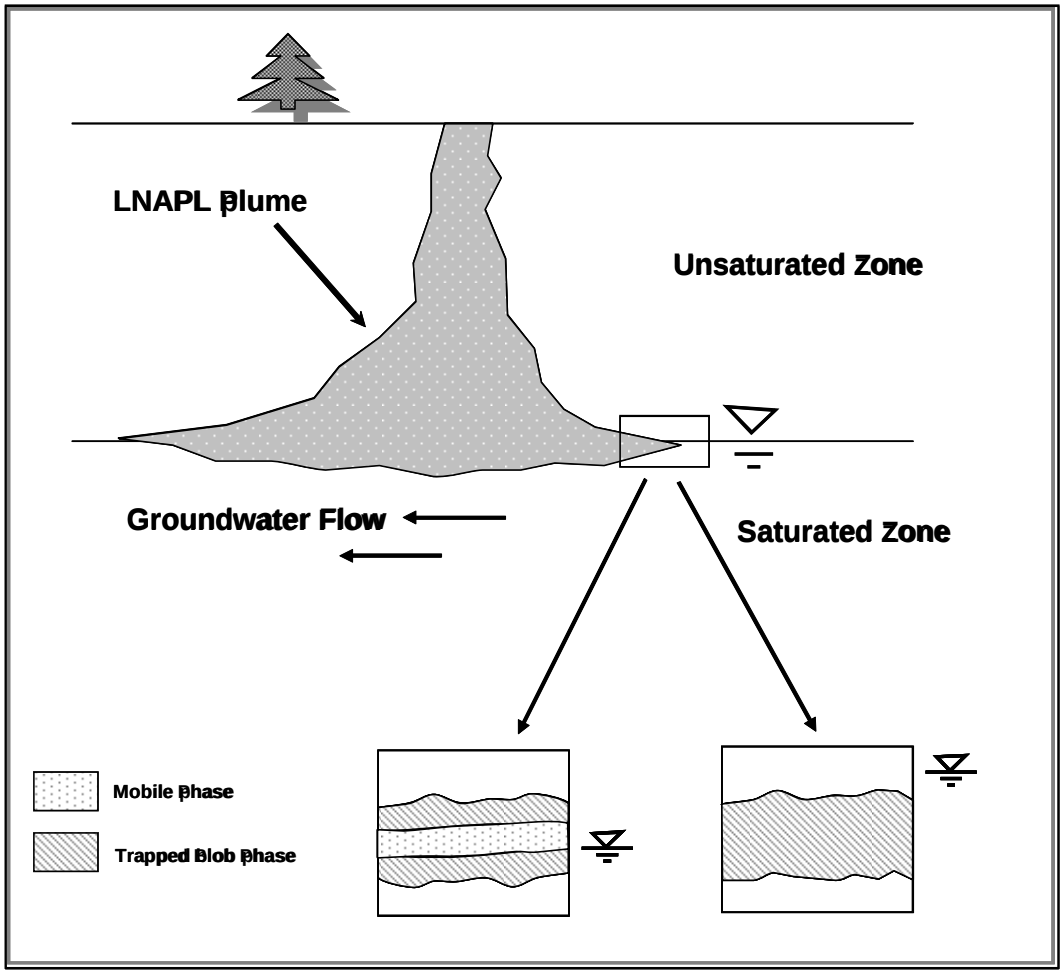

Figure 1-1 Schematic diagram of the generation of NAPL blob around the water table

1.2 Theoretical Backgrounds

1.2.1 Characteristics of NAPL Blob Trapped in the Pores

The residual NAPL phase is retained in the pores as blobs (Figure 1-2; after Han, 2007). The size of NAPL blob can be classified by the number of pore bodies observed as singlet (occupying one pore body), doublet (occupying two), or complex blobs (occupying 5 to 10 or even more). Generally, singlet-type blob represents 50~60 % of blobs, while most of the residual saturation is represented by complex blobs (Morrow et al. 1988; Wilson et al. 1990; Powers et al. 1994). The shape of the NAPL blob is classified along with its size as follows: sphere for singlet, elongate for doublet and several different forms (sphere, cylinder, and finger) for complex blobs (Powers et al. 1991; Bruell et al. 1997).

Trapped blob can be mobilized by the action of buoyant and viscous forces. Once the blob is mobilized, it may break into smaller blobs (like singlet-type blob) through snap-off and by-passing (Wilson et al. 1990). Thus, the critical condition of singlet-type NAPL blob mobilization in the pores is a crucial interest in the fate and transport of NAPL contaminant from the viewpoint of remediation.

1.2.2 Theoretical Approach on the Temperature-Dependent Blob Mobilization

The critical condition for the initiation of blob mobilization can be investigated by force balance and dimensional analyses. The mobilization of NAPL blobs in porous media is affected by the relative magnitudes of capillary forces, viscous forces, and buoyancy forces. For the relationship of these forces, dimensionless numbers such as the capillary number, *Ca*, and the bond number, *Bo*, are used.

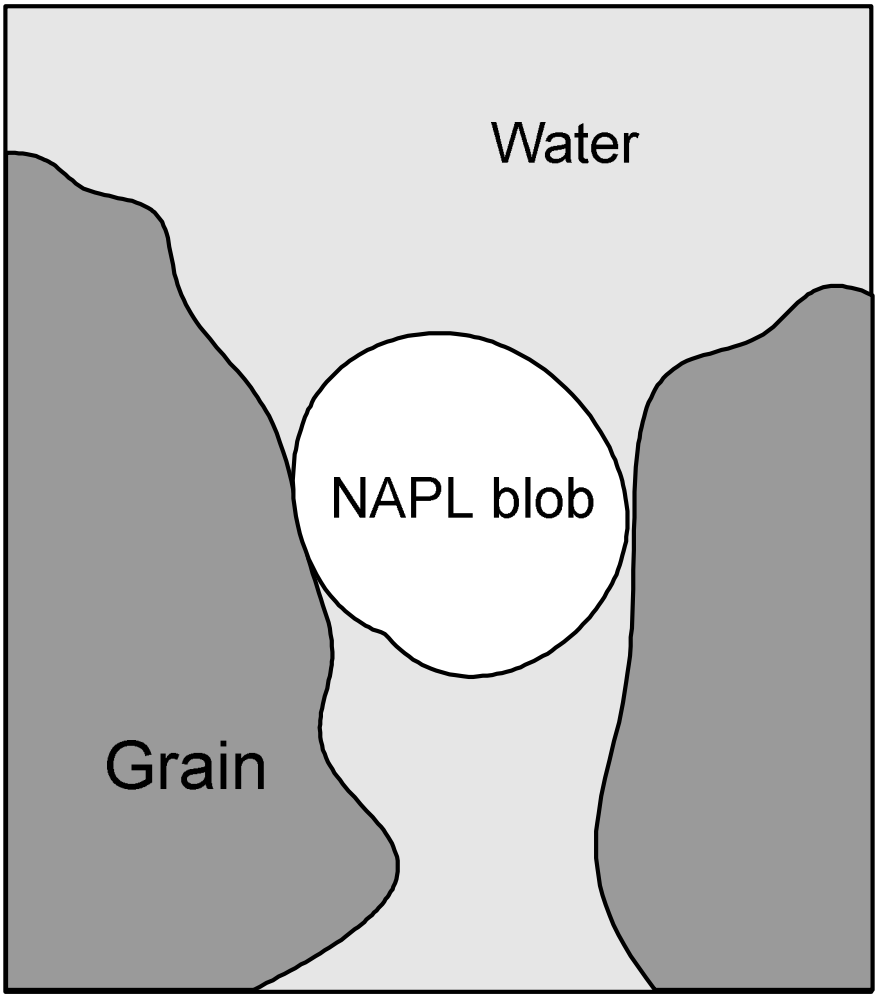

Figure 1-2 Schematic diagram of residual NAPL as a blob in water-wet porous media (after Han, 2007)

The capillary number is expressed as the ratio of viscous forces to the capillary forces, defined by $Ca = \frac{q\mu}{\sigma \cos\theta}$, where q is the Darcy velocity, μ is the viscosity of the displacing fluid, σ is the interfacial tension of the NAPL-water system, and θ is the contact angle. The bond number is expressed as the ratio of the buoyancy forces to the capillary forces, defined by $Bo = \frac{g(\rho_w - \rho_o)L^2}{\sigma \cos\theta}$, where g is the gravitational acceleration constant, ρ_w and ρ_o are wetting (water) and non-wetting (NAPL) phase densities, respectively, and L is a characteristic length.

Pennell et al. (1996) expressed the mobilization of the NAPL blob in terms of a total trapping number, N_T, defined by $N_T = |Bo \pm Ca|$. Using this number, the critical value of N_T is determined for the initiation of NAPL mobilization and for its complete displacement (Li et al., 2007; Gioia and Urciuolo, 2006; Fu and Imhoff, 2002; Anton and Hilfer, 1999).

Sleep and Ma (1997) studied the NAPL blob mobilization in terms of the capillary number over the temperature range of 20 to 90 °C. To calculate this number, they used the temperature-dependent relationships of the viscosity and the interfacial tension.

Corapcioglu et al. (2004) and Roosevelt and Corapcioglu (1998) investigated the rise velocity of air phase using the column experiment and the quantitative calculation technique. Researchers reported the calculated rise velocity of a single discrete air bubble moving upward in the water-saturated column filled with 4-mm glass beads (gravel size), not exceeding 18.5 cm/s. As a critical characteristic of the *in situ* air sparging technique, the calculation of rise velocity of a single discrete air bubble provides the insight in the upward movement of a single fluid drop in porous media.

When the fluid transport is observed in porous media, the relationship between relative permeability and saturation is another important factor. Some researchers investigated the constitutive relative permeability-saturation relationship for 2-phase flow of wetting and nonwetting fluids (Table 1-1; Dury et al., 1999). When the blob movement is observed in a REV (Representative Elementary Volume) scale, oil saturation and the corresponding relative permeability are considered as constant values. Meanwhile, at pore-scale, oil saturation and relative permeability will vary according to the change of blob size.

Table 1-1 Summary of the relative permeability-saturation relationship for 2-phase flow of wetting and nonwetting fluids (Dury et al., 1999)

Reference	Relative permeability of nonwetting phase
Corey (1954)	$k_{rn} = (1-\overline{S}_w)^2(1-\overline{S}_w^2)$ or $k_{rn} = \overline{S}_n^2\left[1-(1-\overline{S}_n)^2\right]$
Pirson (1958)	For imbibition: $k_{rn} = (1-\overline{S}_w)^2$ or $k_{rn} = \overline{S}_n^2$ For drainage: $k_{rn} = (1-\overline{S}_w)(1-\overline{S}_w^{1/4}S_w^{1/2})^{1/2}$ or $k_{rn} = \overline{S}_n\left[1-(1-\overline{S}_n)^{1/4}(1-S_n)^{1/2}\right]^{1/2}$
Wyllie (1962)	$k_{rn} = (1-\overline{S}_w)^3$ or $k_{rn} = \overline{S}_n^3$

$\overline{S}_w = \left(S_w - S_{w,r}\right)/\left(1-S_{w,r}\right)$, $\overline{S}_n = S_n / S_{n,s} = 1-\overline{S}_w$

S_w is the saturation of the wetting phase (water, subscript w) $(=\theta_w/n)$, S_o is the saturation of the nonwetting phase (NAPL, subscript o) $(=\theta_o/n)$, θ_w is the volumetric wetting-phase content $(=\forall_w/\forall_p)$, θ_o is the volumetric nonwetting-phase content $(=\forall_o/\forall_p)$, $S_{w,r}$ is the residual saturation of wetting-phase, $S_{n,s}$ is the maximum saturation of nonwetting-phase $(=1-S_{n,r})$

The theoretical work on the mobilization of a single discrete NAPL blob at pore-scale can be incorporated into a general conservation equation in terms of the accumulation of multiple blobs. The population balance model helps to derive continuum-averaged equations that accurately represent pore-level physics. So, the study on the critical conditions for the initiation of blob mobilization as a single discrete blob has some contribution to the transport and fate of NAPL contaminant and the desired subsurface remediation.

1.3 Research Objectives

The objectives of this research are to analyze the possible benefits of remediating the NAPL-contaminated subsurface using the thermal technique of hot water flooding. Specifically, this research focuses on how the temperature influences the mobilization of the immobile NAPL blob in porous media. The outline of chapters and materials presented in the dissertation is included below:

In Chapter II, the fluid properties and porous media are characterized. The temperature-dependent fluid properties include density, viscosity, and interfacial tension. Porous media is described in terms of a specific soil packing arrangement to provide information on porosity, permeability, pore volume, etc. In Chapter III, force balance analysis is executed to evaluate the critical conditions of the NAPL blob for the blob mobilization through the pores. In Chapter IV, a dimensional analysis is executed to explain critical conditions of blob mobilization through the pores. In Chapter V, the effects of water velocity is examined for the blob mobilization in porous media. To

examine the blob mobilization at pore scale, the varying relative permeability of fluid phases is applied to force balance analysis and dimensional analysis.

CHAPTER II

CHARACTERISTICS OF FLUIDS AND POROUS MEDIA

2.1 Characteristics of Fluids

This study considers water and NAPL (more specifically LNAPL) as the fluid phase. For NAPL phase, Voltesso 35 was chosen. It is viscous oil used as a transformer or electrical insulating oil. Information on the physical properties of fluid phases such as density, viscosity, and interfacial tension was gathered and used for the calculation of NAPL blob mobilization in porous media. These properties were temperature-dependent and provide data over the temperature range of 20 to 90 ^{o}C. Room temperature (20 ^{o}C) was the reference temperature.

2.1.1 Density and Temperature Dependence

NAPL density (g/cm^3) can be expressed as a function of temperature (^{o}C) (Sleep and Ma, 1997).

$$\rho_o = 0.8610 - 1.1750 \times 10^{-4} T - 2.7738 \times 10^{-6} T^2 \quad (2\text{-}1)$$

Water density (g/cm^3) is obtained as discrete data (Munson et al., 1998). Curve fitting the data gives a second-order equation similar to that of NAPL density.

$$\rho_w = 1.0020 - 1.1829 \times 10^{-4} T - 3.2280 \times 10^{-6} T^2 \quad (2\text{-}2)$$

NAPL and water densities decrease as temperature increases. The decrease of each density is about 3% over the temperature range (Figure 2-1a).

Buoyant force is directly proportional to the difference between two fluid densities ($\Delta\rho = \rho_w - \rho_o$) which decreases as temperature increases (Figure 2-1b).

2.1.2 Viscosity and Temperature Dependence

NAPL viscosity (dyne·s/cm^2) can be expressed as a function of temperature (^{o}C) (Sleep and Ma, 1997; Jayaram, 1993).

$$\ln \mu_o = -0.118 + \frac{1.890\times10^3}{273.15+T} - \frac{2.035\times10^5}{(273.15+T)^2} \tag{2-3}$$

Water viscosity (dyne·s/cm^2) is obtained as discrete data (Munson et al., 1998). Best curve fitting of these data gives the logarithmic expression.

$$\mu_w = -4.600\times10^{-3} \ln T + 2.363\times10^{-2} \tag{2-4}$$

NAPL and water viscosities decrease as temperature increases (Figure 2-2a). The decreases of NAPL and water viscosities are about 87% and 69% over the temperature range (Figure 2-2b).

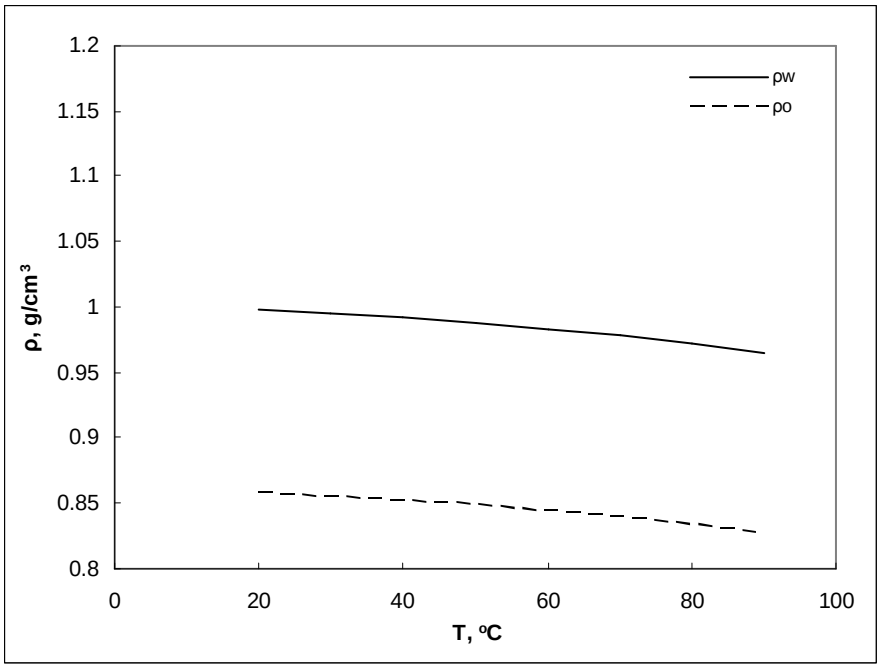

(a)

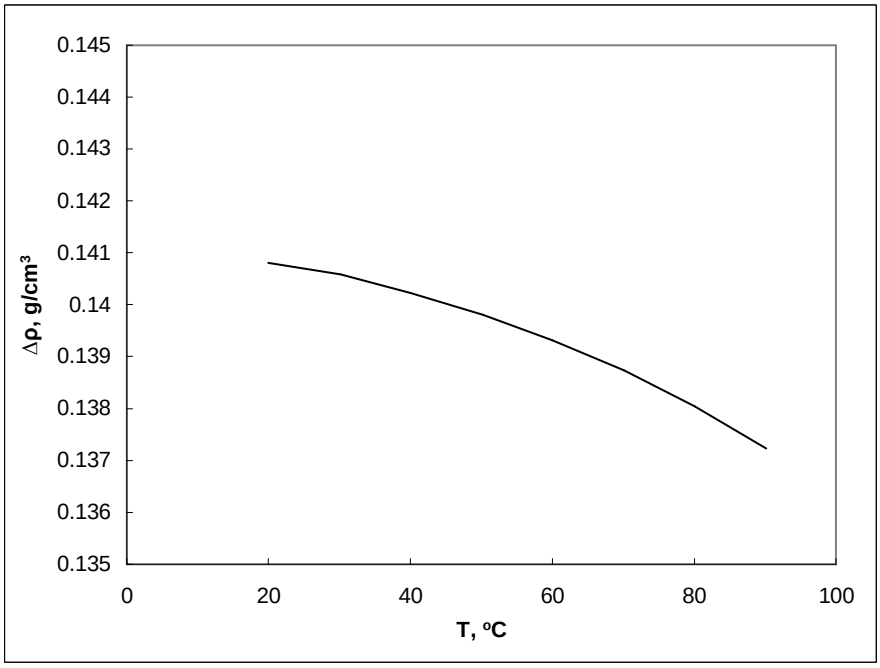

(b)

Figure 2-1 Temperature-dependent change of (a) NAPL and water densities and (b) density difference between NAPL and water densities over the temperature range of 20 to 90 ^{o}C (Sleep and Ma, 1997; Munson et al., 1998)

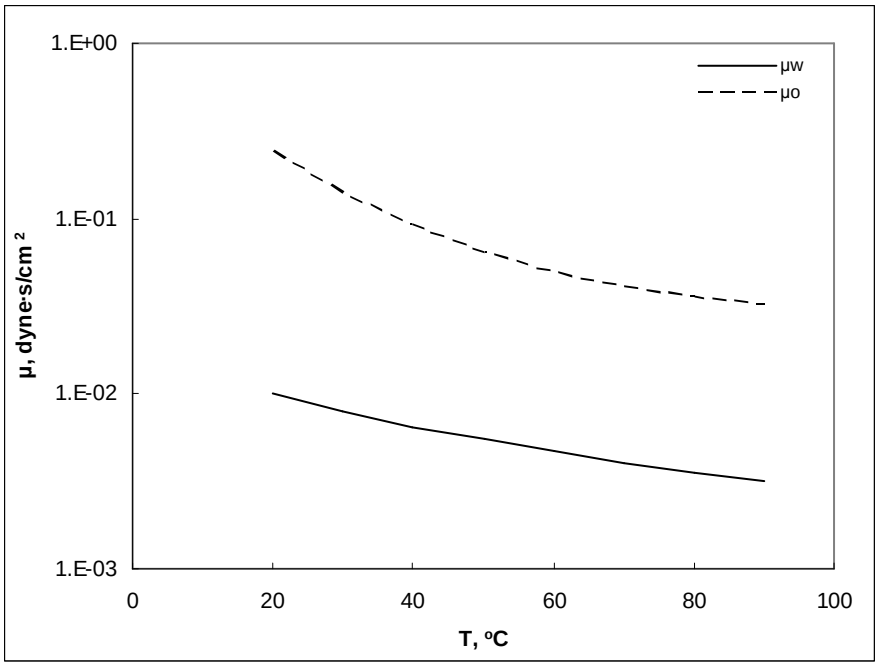

(a)

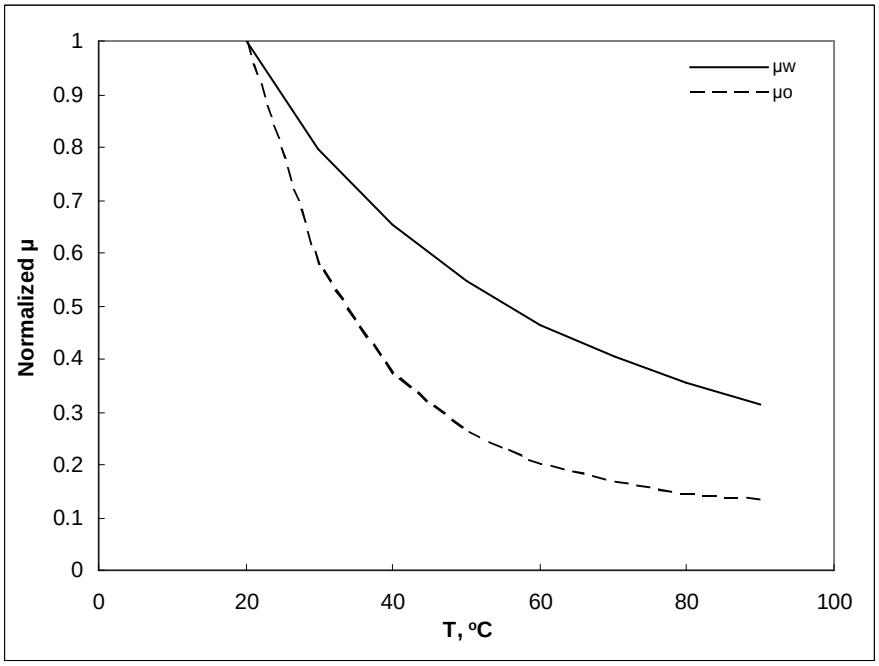

(b)

Figure 2-2 Temperature-dependent change of (a) NAPL and water viscosities and (b) ratio of viscosity at reference temperature to that at interest temperature over the temperature range of 20 to 90 ^{o}C (Sleep and Ma, 1997; Jayaram, 1993; Munson et al., 1998)

2.1.3 Interfacial Tension and Temperature Dependence

Interfacial tension (dyne/cm) for a NAPL-water system can be expressed as a function of temperature (^{o}C) (Sleep and Ma, 1997).

$$\sigma_{ow} = 47.226 - 0.244T \tag{2-5}$$

Interfacial tension decreases as temperature increases (Figure 2-3a). The decrease of interfacial tension is about 40% over the temperature range (Figure 2-3b).

2.1.4 Contact Angle and Temperature Dependence

The contact angle θ (°) shows different values depending on the kind of immiscible fluid and the corresponding type of particle material for the porous media. Keller and Chen (2003) introduced various values of contact angles for the selected NAPL phases. For the system of average hydrocarbon compounds, water and glass phases, one typical value of 34° was chosen at room temperature from their study.

Generally, the contact angle decreases as temperature increases (She and Sleep, 1998; Figure 2-4a). Thus, the decrease in contact angle gives rise to the increase in the cosine of the contact angle (Figure 2-4b). However, the changes in contact angle with temperature were small. For example, the change was –0.27°/°C for an organic-water-glass system (Poston et al., 1970).

The relationship between the capillary pressure and fluid saturation in porous media is defined by the pore size distribution and the interfacial tension between wetting and non-wetting fluids and the soil grain surface. When the porous media is simply expressed as a bundle of capillary tubes having varying diameters, the Young-Laplace equation shows the relationship (Dullien, 1979).

$$p_c = \frac{2\sigma_{ow}\cos\theta}{R} \tag{2-6}$$

where R is the radius of capillary tube. Even though increases in the cosine of the contact angle offset decreases in the interfacial angle to some degree, capillary pressures would be expected to decrease as temperature increases because the change in interfacial tension is much greater than that in the cosine of contact angle. Thus, the value in the product of interfacial tension and the cosine of the contact angle decreases as temperature increases (Figure 2-5a). The decrease of the value is about 30% over the temperature range of 20 to 90 ^{o}C (Figure 2-5b).

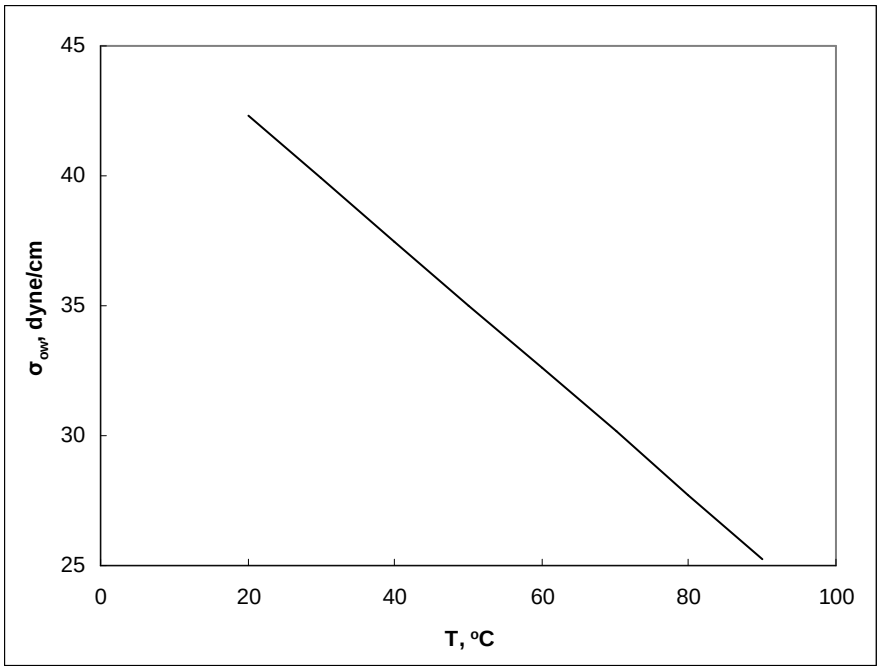

(a)

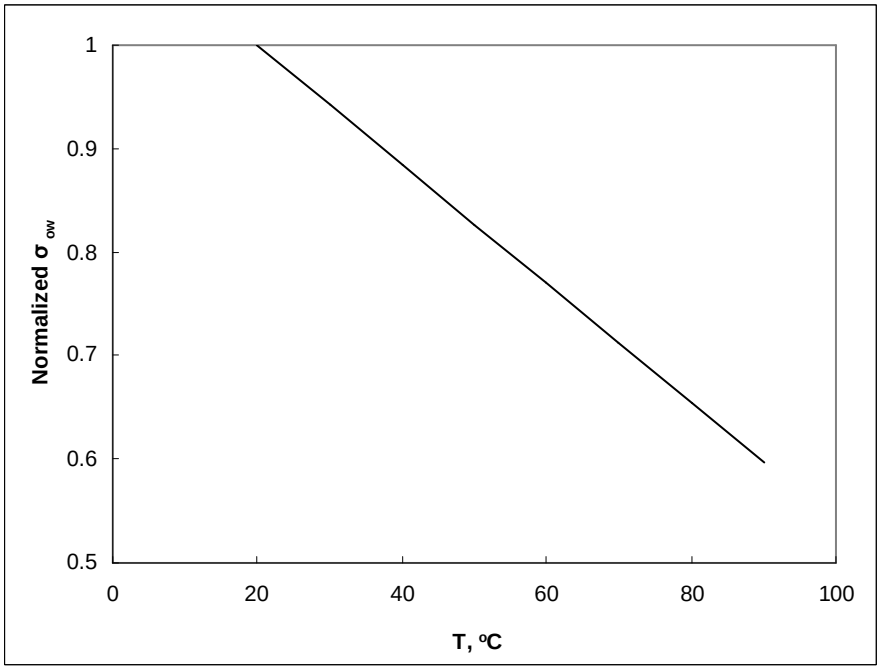

(b)

Figure 2-3 (a) Temperature-dependent change of interfacial tension for NAPL-water system and (b) ratio of interfacial tension at reference temperature over the temperature range of 20 to 90 ^{o}C (Sleep and Ma, 1997)

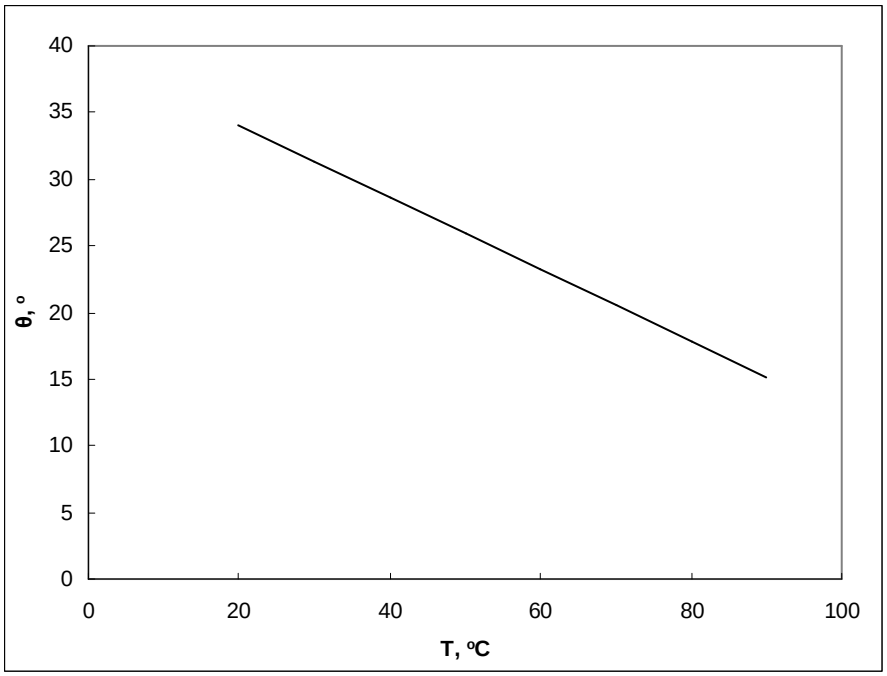

(a)

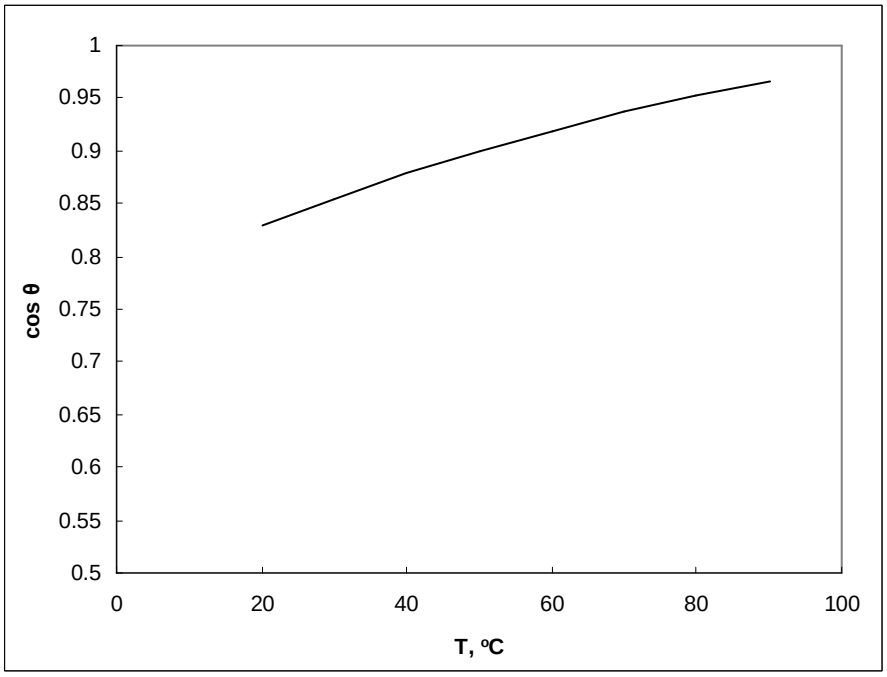

(b)

Figure 2-4 Temperature-dependent change of (a) contact angle for NAPL-water-glass system and (b) the cosine of the contact angle over the temperature range of 20 to 90 ^{o}C (Keller and Chen, 2003; Poston et al., 1970)

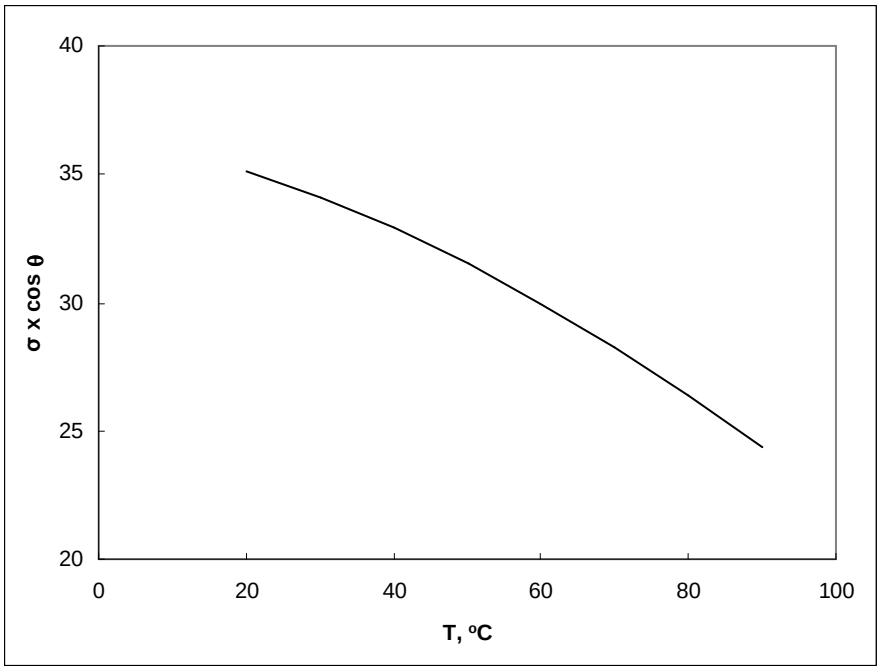

(a)

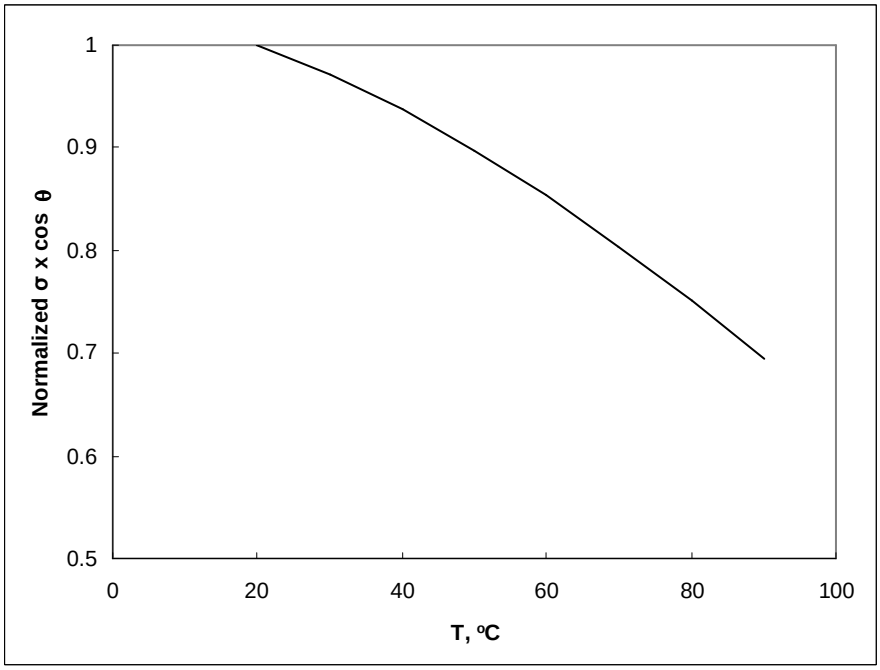

(b)

Figure 2-5 (a) Temperature-dependent change of the product of interfacial tension and the cosine of the contact angle and (b) ratio of the product of interfacial tension and the cosine of the contact angle at reference temperature to that at interest temperature over the temperature range of 20 to 90 ^{o}C

2.1.5 Temperature Dependence of Blob Radius and Volume

At reference (T_{ref}) and interest (T) temperatures, the NAPL blob density can be defined as:

$$\rho_{o,ref} = \frac{M_o}{\forall_{o,ref}}; \qquad \rho_o = \frac{M_o}{\forall_o} \tag{2-7}$$

where M_o and $\forall_o$ are mass and volume of single NAPL blob, respectively. From the ratio of two expressions, the temperature-dependent change of blob volume and radius is calculated as:

$$R_o = \left(\frac{\rho_{o,ref}}{\rho_o}\right)^{1/3} R_{o,ref}; \qquad \forall_o = \left(\frac{\rho_{o,ref}}{\rho_o}\right)\forall_{o,ref}. \tag{2-8}$$

Blob radius and volume increase from thermal expansion as temperature increases. These increases are about 1.2% and 3.6% over the temperature range of 20 to 90 ^{o}C (Figure 2-6). From Equation (2-8), the thermal expansion coefficients of the blob radius and volume are expressed as:

$$f_R = \left(\frac{\rho_{o,ref}}{\rho_o}\right)^{1/3}; \quad f_{\forall} = \frac{\rho_{o,ref}}{\rho_o} \tag{2-9}$$

where f_R and $f_{\forall}$ are the thermal expansion coefficient of blob radius and volume, respectively. These coefficients have same values as those in Figure 2-6 with respect to the temperature.

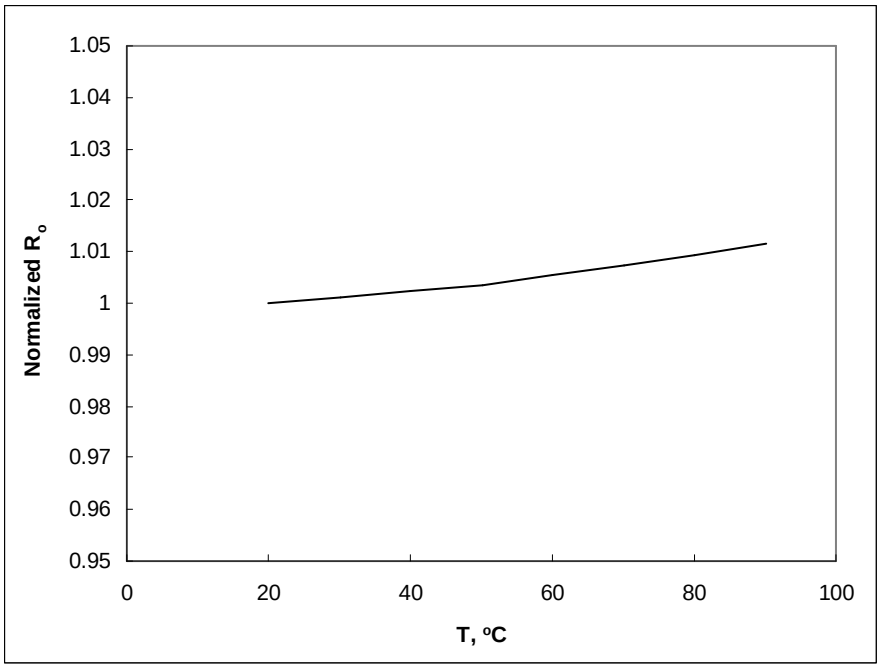

(a)

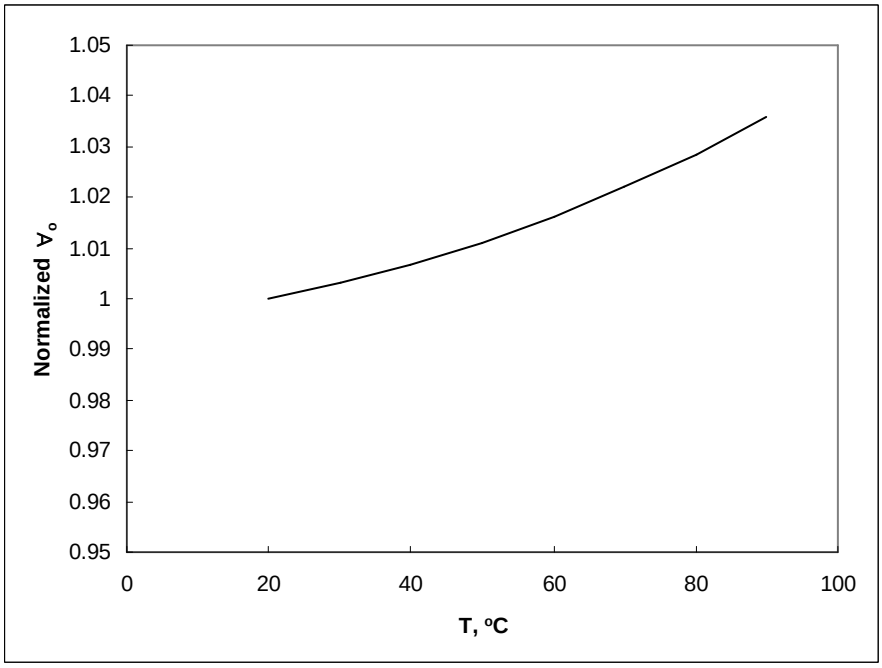

(b)

Figure 2-6 Ratio of the value at reference temperature to that at interest temperature for (a) blob radius and (b) blob volume

2.2 Characteristics of Porous Media

2.2.1 Pore Volume and Porosity

A soil packing arrangement determines the hydrologic parameters of soil system such as porosity and permeability. For example, an orthorhombic packing arrangement of soils provides the following information on the calculation of pore volume and porosity. (Table 2-1; Graton and Fraser, 1935)

Table 2-1 Calculation of unit cell, unit void volume and porosity with the orthorhombic packing arrangement at d_p = 0.4 cm (Graton and Fraser, 1935)

Unit cell volume $\forall_t$, cm^3	$6.93\left(\frac{d_p}{2}\right)^3 = 0.05544$
Unit void volume $\forall_p$, cm^3	$2.74\left(\frac{d_p}{2}\right)^3 = 0.02192$
Porosity, $n\left(=\frac{\forall_p}{\forall_t}\right)$	0.3954

If the soil particle diameter d_p is considered to be 0.4 cm, the volume of a single pore is 0.02192 cm^3. If a single blob occupies the whole space of a single pore, the maximum radius of a spherical blob is 0.174 cm.

2.2.2 Permeability

When the two-phase flow is observed in porous media, the permeability or the effective permeability of water (or NAPL) phase, k_w (or k_o) is generally expressed as:

$$k_w = kk_{rw} \text{ (or } k_o = kk_{ro}\text{)} \tag{2-10}$$

where k is the intrinsic permeability and k_{rw} (or k_{ro}) is the relative permeability of the water (or NAPL) phase. A general expression for intrinsic permeability, k would be:

$$k = f_1 f_2 d_p^2 \tag{2-11}$$

where f_1 is a shape factor, f_2 is a porosity factor, and d_p is the particle diameter (Bear, 1972). Shape factor is dimensionless and a function of particle shape, tortuosity, and other terms from the geometric form of the individual channels. The porosity factor is a function of the porosity.

Among the suggested expressions for intrinsic permeability, k, the Kozeny equation (Corey, 1994) defines it as:

$$k = \frac{d_p^2}{150} \frac{n^3}{(1-n)^2} \ . \tag{2-12}$$

When the selected orthorhombic packing arrangement of soil grains is considered, the value of intrinsic permeability, k would be calculated with values of porosity and particle diameter giving a value of 1.8039×10^{-4} cm^2.

Relative permeability k_r is a function of fluid saturation. The Wyllie equation is one of several expressions suggested for relative permeability k_r, defined as:

$$k_r = S^3 \tag{2-13}$$

where S is the saturation of fluid phase (Corey, 1994).

If the two-phase flow is considered, one fluid is in the wetting phase and the other is in the non-wetting phase. In this case, water is the wetting phase and NAPL the non-wetting phase. Thus, the relative permeability for each fluid phase can be expressed as:

$$k_{rw} = S_w^3 = (1 - S_o)^3 \tag{2-14}$$

$$k_{ro} = S_o^3 = (1 - S_w)^3 \tag{2-15}$$

where k_{rw} and S_w are relatively permeability and saturation of water phase, respectively, and k_{ro}, and S_o are relative permeability and saturation of NAPL phase, respectively. The summation of two saturations is unity ($S_w + S_o = 1$).

When the flow phenomena are observed in the macro (or REV) scale of the soil system, the value of the relative permeability is considered a constant value. However, when the flow phenomena are observed in the micro (or pore) scale of the soil system, the varying relative permeability value should be considered according to the change of saturation. For example, when the fixed oil saturation (i.e., $S_o = 0.2$) is given for the observation of parameters with the macro scale, the calculated k_{rw} and k_{ro} are 0.512 and 0.008, respectively, using Equations (2-14) and (2-15). Meanwhile, when parameters are observed with the pore scale, oil and water saturations are calculated from the NAPL blob radius first and then k_{ro} and k_{rw} are calculated from the calculated oil and water saturations (Figure 2-7).

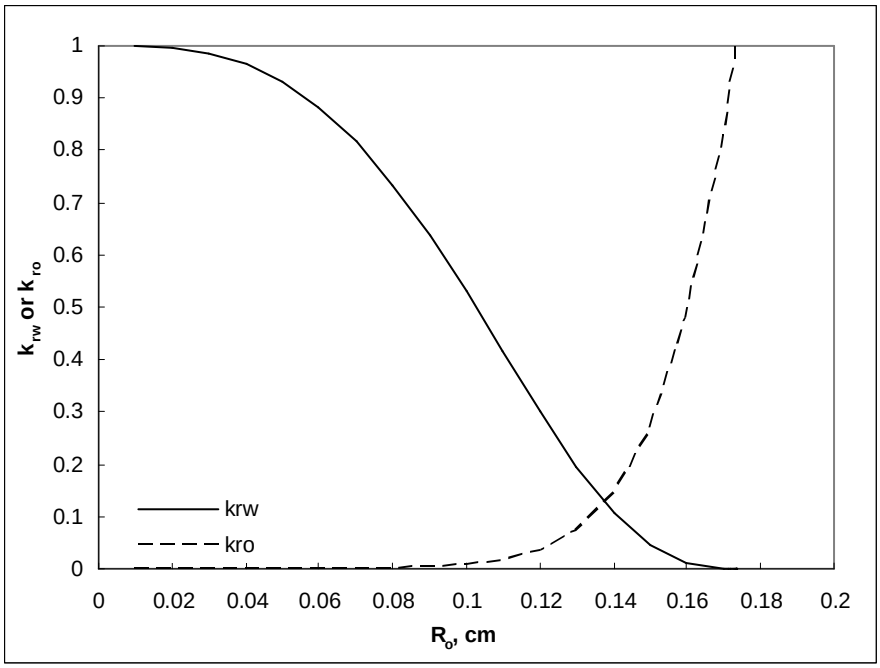

(a)

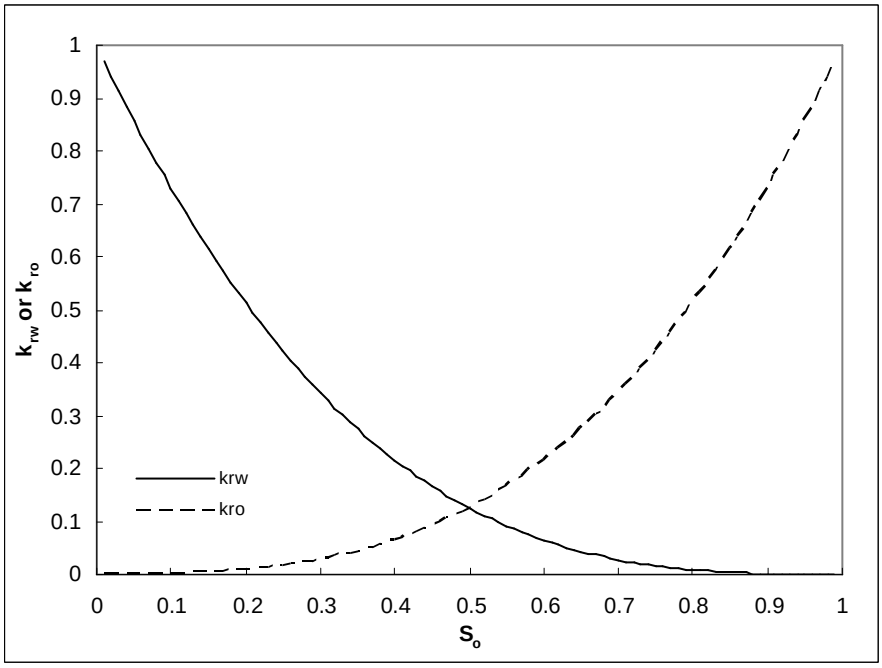

(b)

Figure 2-7 Relative permeability of NAPL and water phases as a function of (a) blob radius and (b) blob saturation

2.2.3 Limiting Pore Throat Radius

The moving blob becomes trapped in a pore when the retention (surface tension) force is equal to the driving (buoyant) force. This entrapment occurs at a certain size of pore throat radius and it is determined from the soil grain packing type (Corapcioglu et al., 2004). According to Corapcioglu et al. (2004), the limiting pore throat radius for an orthorhombic arrangement can be calculated as:

$$R' = \frac{\left(2\sqrt{3}-3\right)d_p}{6}. \tag{2-16}$$

Pore throat radius, R' is 0.0309 cm for the particle diameter d_p of 0.4 cm.

From the balance between forces mentioned above, the limiting pore throat radius can be also calculated.

$$F_{st} = F_b \tag{2-17}$$

$$2\pi R'\sigma\cos\theta = \left(\rho_w - \rho_o\right)g\frac{4}{3}\pi R_o^3 \tag{2-18}$$

$$R' = \frac{2\left(\rho_w - \rho_o\right)gR_o^3}{3\sigma\cos\theta} \tag{2-19}$$

Figure 2-8 shows the limiting pore throat radius over the temperature range at R_o = 0.25 cm. As the temperature increases, the limiting pore throat radius also increases. That is, a trapped blob in porous media at room temperature can be mobilized at some increase in temperature. It can be explained by the fact that the decrease in surface tension force in magnitude is larger than the decrease in buoyant force as the temperature increases.

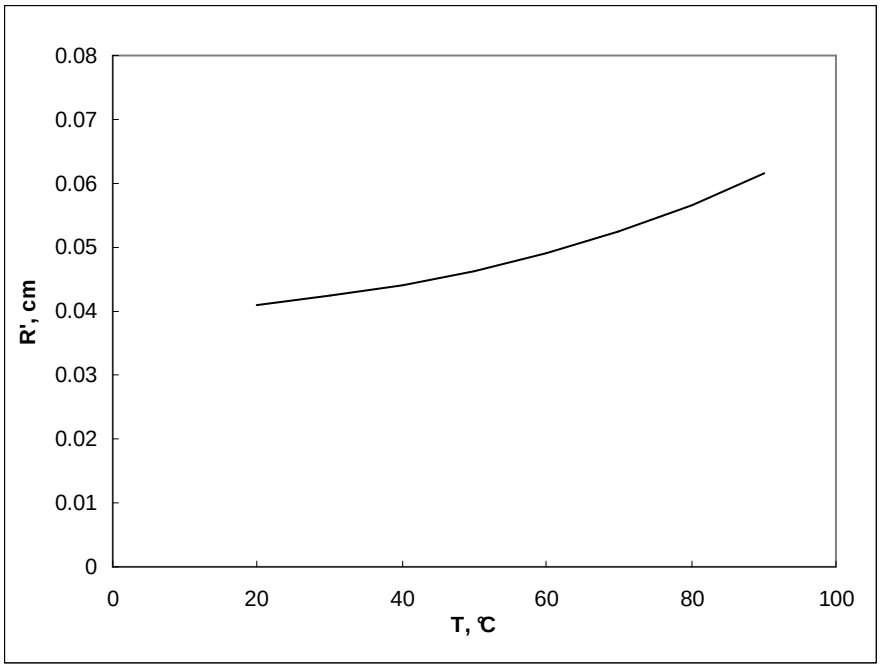

Figure 2-8 Limiting pore throat radius over the temperature range of 20 to 90 ^{o}C

CHAPTER III

FORCE BALANCE ANALYSIS ON THE MOBILIZATION OF NAPL BLOB IN POROUS MEDIA

3.1 Force Balance Approach

Force balance analysis is a critical tool to interpret the mobilization of a single, trapped NAPL blob in a single pore. This quantitative analysis provides the insight and information on the critical conditions for the blob mobilization using magnitudes of forces and ratios between forces.

The forces exerted on a trapped NAPL blob include buoyant and surface tension forces (Figure 3-1; after Han, 2007). Density difference between NAPL and water provides the positive force to help the blob move upward in water. The buoyant force, F_b is expressed as:

$$F_b = \Delta\rho g \forall_o \tag{3-1}$$

where $\Delta\rho$ is the density difference ($= \rho_w - \rho_o$), $\forall_o$ is the blob volume ($= \frac{4}{3}\pi R_o^3$), and R_o is the radius of an imaginary spherical blob having the same volume as that of a blob.

The surface tension force is the force caused by the difference between molecular attractions inside the fluid and those on the surface of the fluid. The surface tension force, F_{st} is expressed as:

$$F_{st} = 2\pi R' \sigma \cos\theta \tag{3-2}$$

where σ is the surface tension, θ is the contact angle between the NAPL blob and soil grain, and R' is the pore throat radius determined by a particular arrangement of soil grains.

If water flow exists in porous media, two additional forces are considered from "push" and drag forces. The push force is the volumetric force showing viscous effects exerted on NAPL blob while it is mobilizing through the pores (Yoon, 2007). The push force is expressed as the force the water flow pressure exerts on the NAPL blob. From the expression of Darcy's law, the push force is formulated as:

$$F_p = A \frac{\mu_w u_w}{k k_{rw}} \frac{4}{3} \pi R_o^3 \tag{3-3}$$

where u_w, k_{rw}, μ_w and A are the local velocity, relative permeability and dynamic viscosity of the water phase and the correction factor to represent the medium-specific surface properties, respectively. After the NAPL blob is mobilized, the push force F_p is expressed in the same manner, except for the term u_w (given as the relative concept).

$$F_p = A \frac{\mu_w u'_w}{k k_{rw}} \frac{4}{3} \pi R_o^3 \tag{3-4}$$

where u'_w is the local velocity relative to the moving blob velocity ($= u_w - u_o$).

The drag force resulting from the drop moving in the fluid phase can be expressed by Ergun equation (Niven, 2002) as:

$$F_d = A\left[\frac{150\mu_o u_o}{d_p^2}\frac{(1-n)^2}{n^3}+\frac{1.75\rho_o u_o^2}{d_p}\frac{(1-n)}{n^3}\right]\frac{4}{3}\pi R_o^3 = A\left(\frac{\mu_o u_o}{k_1}+\frac{\rho_o u_o^2}{k_2}\right)\frac{4}{3}\pi R_o^3 \quad (3\text{-}5)$$

The drag force consists of two terms; the viscous energy losses from the laminar flow and the kinetic energy losses from the turbulent flow. Based on the blob velocity and other terms, the blob movement reveals the laminar flow at low Reynold number having the critical number of unity. Therefore, the second term for the turbulent flow was dropped out of the equation and the first term alone was used for the drag force:

$$F_d = A\frac{\mu_o u_o}{k_o}\frac{4}{3}\pi R_o^3 = A\frac{\mu_o u_o}{kk_{ro}}\frac{4}{3}\pi R_o^3 \quad (3\text{-}6)$$

where u_o, k_{ro}, μ_o are the blob velocity, relative permeability and dynamic viscosity of NAPL phase, respectively.

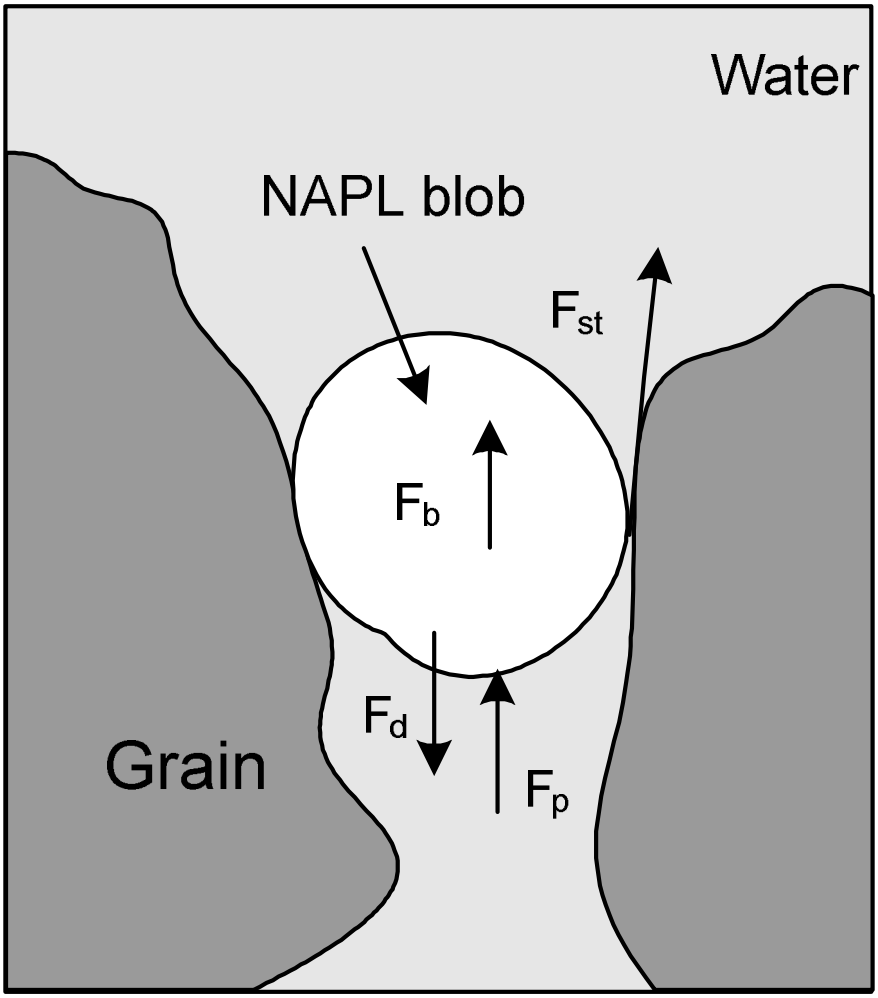

Figure 3-1 External forces acting on a NAPL blob in porous media (after Han, 2007)

3.2 Analysis on a Trapped NAPL Blob in Porous Media

For the force balance analysis, the following data and conditions are used (Table 3-1).

Table 3-1 Properties of parameters for the force balance analysis

Soil packing arrangement	Orthorhombic
Particle diameter d_p, cm	0.4
Unit void volume $\forall_p$, cm^3	0.02192
Porosity n	0.3954
Pore throat radius R', cm	0.0309
Intrinsic permeability k, cm^2	1.8039×10^{-4}
Oil saturation S_o	0.2
Oil relative permeability k_{ro}	0.008
Gravity acceleration constant g, cm/s^2	981
Correction factor A	52

3.2.1 Critical Blob Radius for the Blob Mobilization

On a single NAPL blob trapped in porous media, buoyant and surface tension forces act. The buoyant force acts as a driving force to help the blob move out of a pore and the surface tension force acts as a retention force to keep it from moving. As the blob radius increases, the buoyant force increases while the surface tension force does not. Thus, when the buoyant force overcomes the surface tension force at a certain blob radius, the blob will start to move. So, the minimum blob radius can be observed for the initiation of blob mobilization. This critical condition for the blob mobilization can be expressed as:

$$F_b \geq F_{st} \tag{3-7a}$$

$$\Delta\rho g \frac{4}{3}\pi R_o^3 \geq 2\pi R' \sigma \cos\theta \tag{3-7b}$$

$$R_{o,crit} \geq \left(\frac{3R'\sigma\cos\theta}{2\Delta\rho g} \right)^{1/3} \tag{3-7c}$$

From the above expression, the critical blob radius for the onset of blob mobilization is determined as a function of temperature. This critical blob radius, $R_{o,crit}$ decreases from 0.228 cm at T = 20 °C to 0.203 cm at T = 90 °C (Figure 3-2a). And, the blob volume also decreases from 0.04965 cm^3 to 0.03504 cm^3 along with the corresponding decrease in blob radius. With the unit pore volume from Table 3-1, the blob volume can be described as the number of unit pore volumes and this number decreased from 2.3 to 1.6 units (Figure 3-2b). In conclusion, due to the decrease of interfacial tension, the residual NAPL blob is more likely to initiate blob mobilization as the temperature increases.

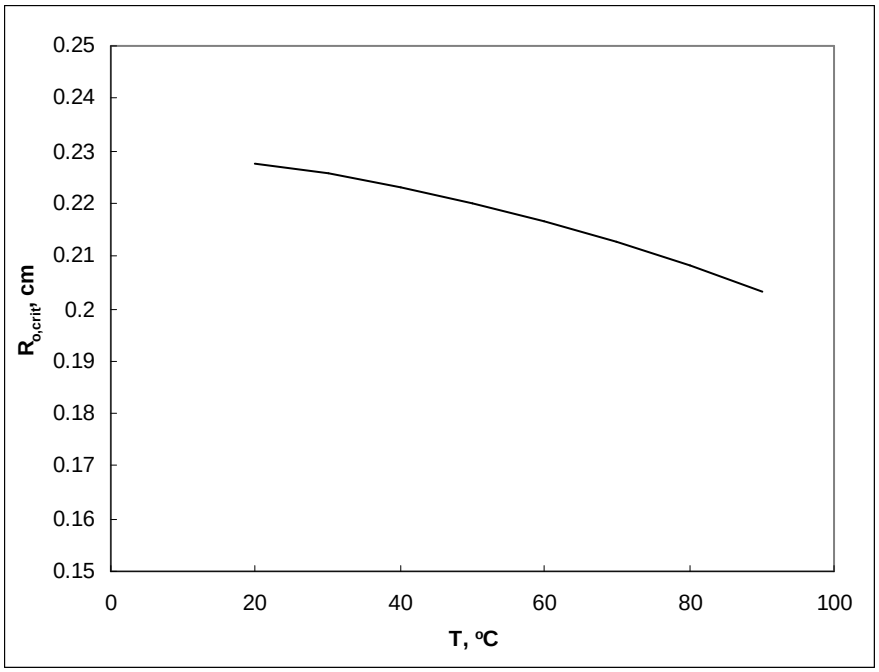

(a)

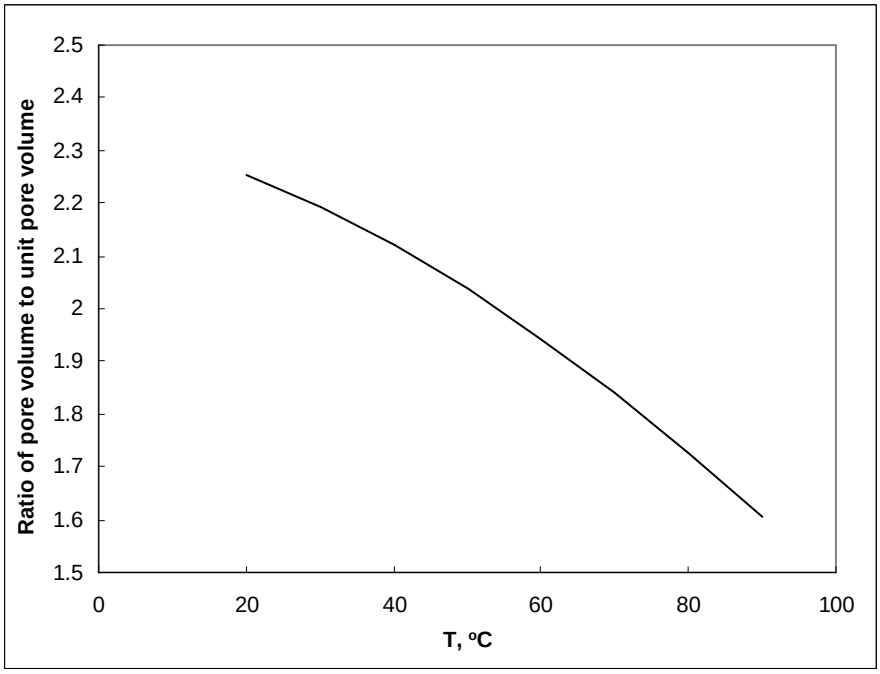

(b)

Figure 3-2 (a) Critical blob radius required for the initiation of blob mobilization over the temperature range of 20 to 90 ^{o}C and (b) the corresponding ratio of pore volume to unit pore volume

3.2.2 Magnitudes and Ratios of Forces

The buoyant force exerted on a trapped NAPL blob generally increases as the blob radius increases. The change in magnitude is directly proportional to the change in the blob volume. The surface tension force does not change with the changes in the blob radius (Figure 3-3a).

At room temperature, the buoyant force can overcome the surface tension force with blob radii greater than 0.228 cm at room temperature so to initiate the mobilization of the blob trapped in porous media. However, as the radius gets smaller, the surface tension force gets larger than the buoyant force so that the blob is trapped. From the calculation of critical blob radius for blob mobilization in Section 3.2.1, a NAPL blob as big as the one occupying more than two pores can be possibly mobilized at room temperature.

With the increasing temperature, the change in magnitude of buoyant force is insignificantly little as the change in density difference and blob volume offsets each other. The change in magnitude of buoyant force is just about 1% increase over the temperature range of 20 to 90 ^{o}C.

The surface tension force exerted on the NAPL blob generally decreases as the temperature increases. The change in magnitude of force is directly proportional to the change in the product term between interfacial tension and the cosine of the contact angle. The change in magnitude of surface tension force is about 30% decrease over the temperature range of 20 to 90 ^{o}C.

The calculation indicates that the temperature influences a trapped blob to mobilize at a lower critical blob radius, $R_{o,crit}$ of 0.203 cm at T = 90 ^{o}C (Figure 3-3b). From the calculation of critical blob radius for the blob mobilization in Section 3.2.1, a NAPL blob large enough to occupy just two pores ("doublet") can be potentially mobilized at T = 90 ^{o}C.

Since the blob is mobilized, the drag force is also exerted on the moving blob in porous media. Under the steady state of the blob motion, the surface tension force balances against the buoyant force at a smaller blob radius. However, the drag force replaces the surface tension force in the role of the retention force as the radius increases (Figure 3-4).

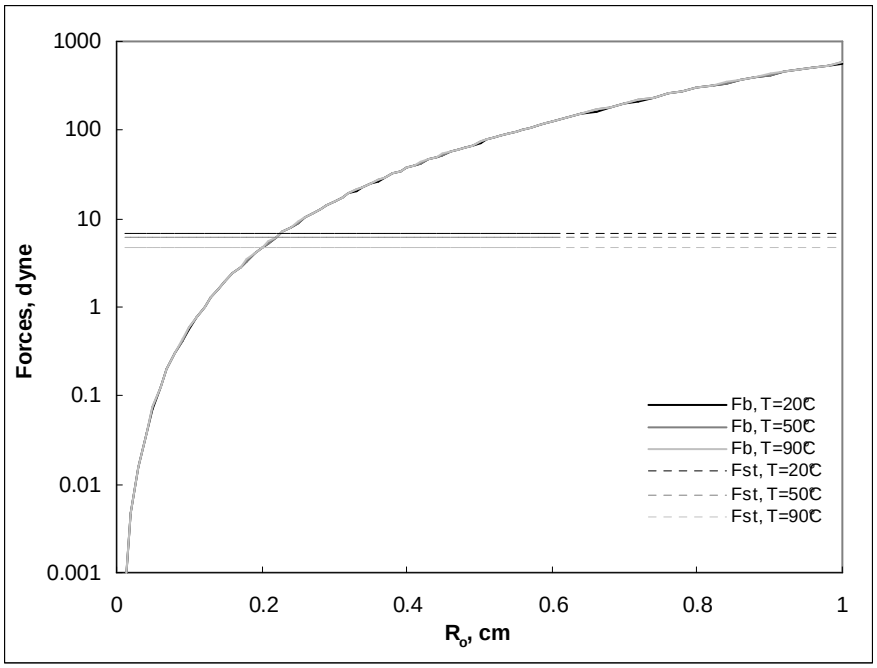

(a)

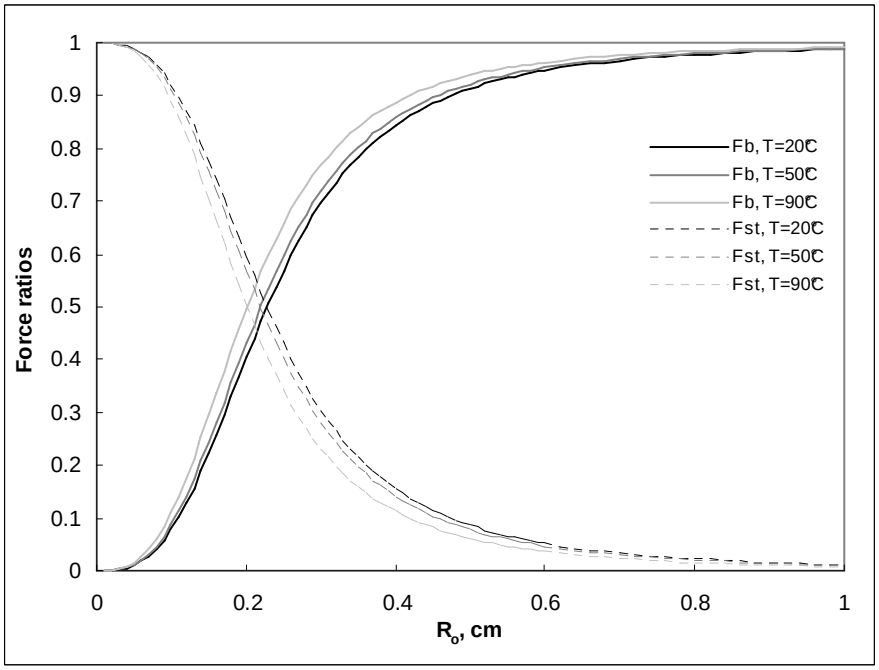

(b)

Figure 3-3 (a) Magnitudes of forces and (b) force ratios versus blob radius before the blob mobilization

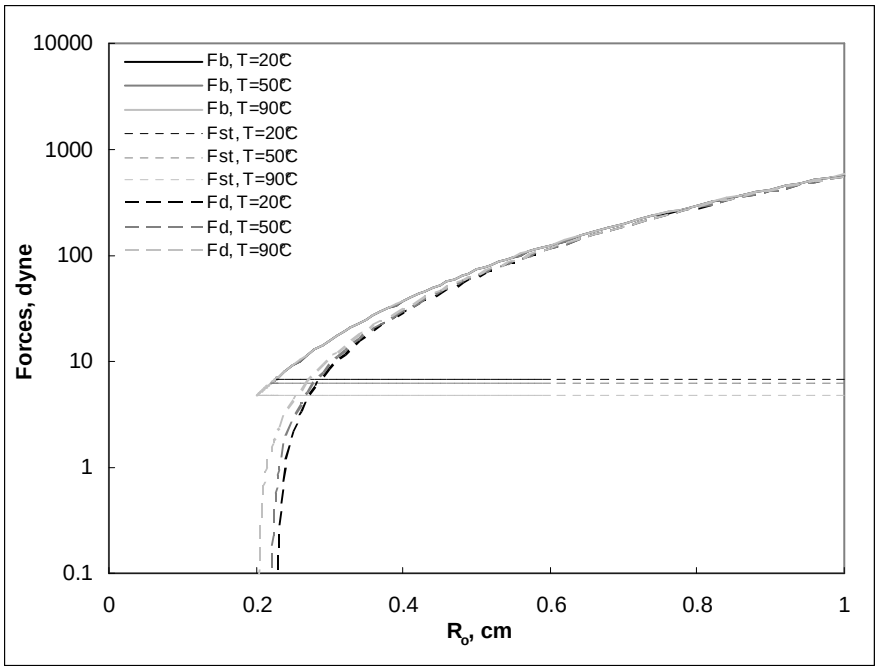

(a)

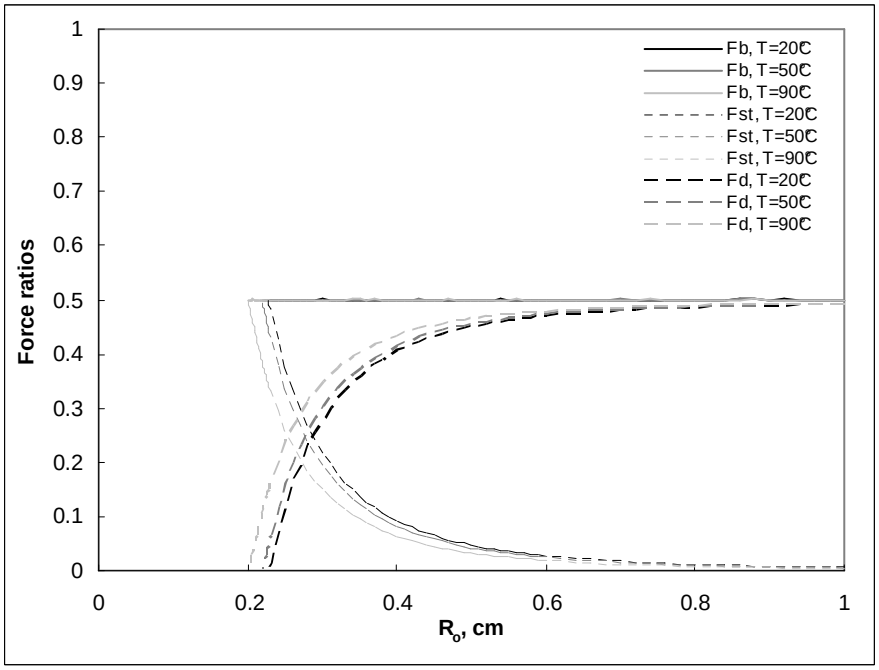

(b)

Figure 3-4 (a) Magnitudes of forces and (b) force ratios versus blob radius after the blob mobilization

3.2.3 Terminal Blob Velocity

Once the blob mobilization is initiated, the terminal (steady state) blob velocity from the steady state blob motion can be determined. This is done using the force balance equation which includes the buoyant, surface tension, and drag forces exerted on the moving blob in porous media. The blob velocity is determined from the following expressions:

$$F_b = F_{st} + F_d \tag{3-8a}$$

$$\Delta\rho g \frac{4}{3}\pi R_o^3 = 2\pi R'\sigma\cos\theta + A\frac{\mu_o u_o}{kk_{ro}}\frac{4}{3}\pi R_o^3 \tag{3-8b}$$

$$u_o = \frac{kk_{ro}}{A\mu_o}\left(\Delta\rho g - \frac{3R'\sigma\cos\theta}{2R_o^3}\right) \tag{3-8c}$$

The calculation is observed with the fixed oil saturation (S_o = 0.2) from the macro-scale (or REV scale). The calculation indicates that the terminal blob velocity is 1.55×10^{-5} cm/s at T = 20 ^{o}C (Figure 3-5). As the temperature increases, the terminal blob velocity also increases up to 1.15×10^{-4} cm/s at T = 90 ^{o}C. This blob velocity increase is due to a decrease in blob viscosity with the resultant increase in the smooth motion of blob in the pores.

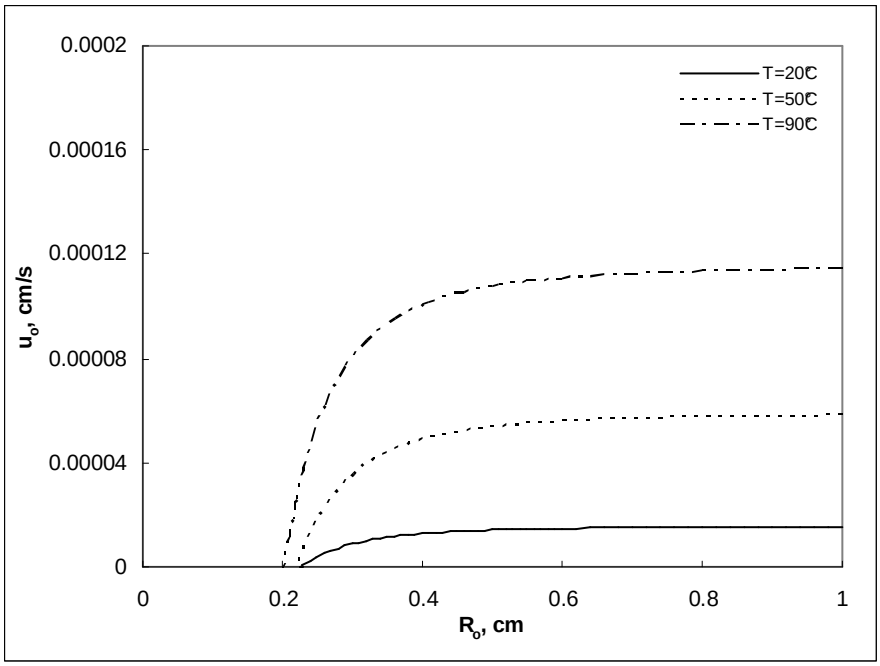

Figure 3-5 Calculated terminal (steady state) blob velocity after the blob mobilization from the force balance equation

3.3 Analysis on a Trapped NAPL Blob with Water Flow

3.3.1 Critical Blob Radius for the Blob Mobilization

When water flows in porous media, an additional force will be exerted from the water "push" on a trapped blob with the buoyant and surface tension forces. The push force acts as a driving force and supplements the magnitude of the buoyant force. Thus, when the summation of buoyant and push forces overcome the surface tension force, the blob will start to move. The condition for the blob mobilization can be expressed as

$$F_b + F_p \geq F_{st} \tag{3-9a}$$

$$\Delta\rho g \frac{4}{3}\pi R_o^3 + A\frac{\mu_w u_w}{kk_{rw}}\frac{4}{3}\pi R_o^3 \geq 2\pi R'\sigma\cos\theta \tag{3-9b}$$

$$R_{o,crit} \geq \left(\frac{3R'\sigma\cos\theta}{2\left(\Delta\rho g + A\frac{\mu_w u_w}{kk_{rw}}\right)} \right)^{1/3} \tag{3-9c}$$

From the expression, the critical blob radius for the mobilization $R_{o,crit}$ is determined as a function of temperature. With the natural velocity of water flow (u_w = 1 m/d), the critical blob radius decreases from 0.224 cm at T = 20 °C to 0.202 cm at T = 90 °C. And, the blob volume also decreases from 0.04708 cm^3 to 0.03453 cm^3 with the decrease in blob radius. Thus, the number of unit pore volumes, equivalent to the blob volume, also decreased from 2.1 to 1.6 units.

Compared to the calculations of the condition of no water flow, the radius is smaller, but the difference is insignificant (Figure 3-6). It means the existence of water flow within the range of naturally existing velocities does not significantly affect blob mobilization.

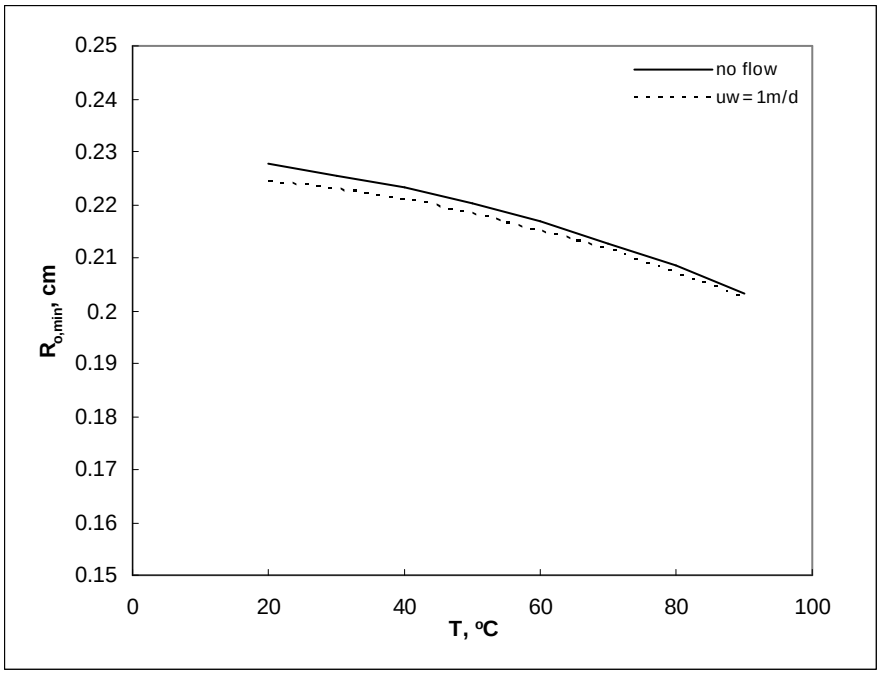

Figure 3-6 Comparison of minimum blob radius for the blob mobilization between the condition of no water flow and the condition of constant water flow as a function of temperature

3.3.2 Magnitudes and Ratios of Forces

Among the forces acting on a trapped blob, the buoyant and push forces increase as the blob radius increases, but the surface tension force does not change (Figure 3-7).

At the macro scale, the magnitude of the push force is approximately 20 times smaller than the buoyant force. Thus, the contribution of the push force to the total driving force is insignificant and has little impact on the blob mobilization when it is compared to that without the push force. The driving force from buoyant and push forces can overcome the surface tension force at a blob radius larger than 0.224 cm for the blob mobilization in a pore. That result is much similar to 0.228 cm, the critical blob radius, $R_{o,crit}$ from the condition without water flow.

For the temperature range, the ratio of the buoyant to the push force increases up to 65, which indicates that the driving force receives the most contribution from the buoyant force (Figure 3-8). Thus, temperature has little effect on the reduction of the critical blob radius, $R_{o,crit}$ to enhance the blob mobilization with 0.202 cm at T = 90 ^{o}C.

As the blob is mobilized, the drag force is also exerted on the moving blob (Figure 3-9). Under the steady state of the blob motion, the surface tension force balances against the buoyant force at the smaller blob radius. However, the drag force replaces the surface tension force in the role of the retention force as the radius increases. The ratio of the drag to the surface tension force reveals the dominance of the drag force over the surface tension force as a function of blob radius as well as temperature (Figure 3-10). The ratio change is more predominant over the radius rather than the change in ratio over the temperature.

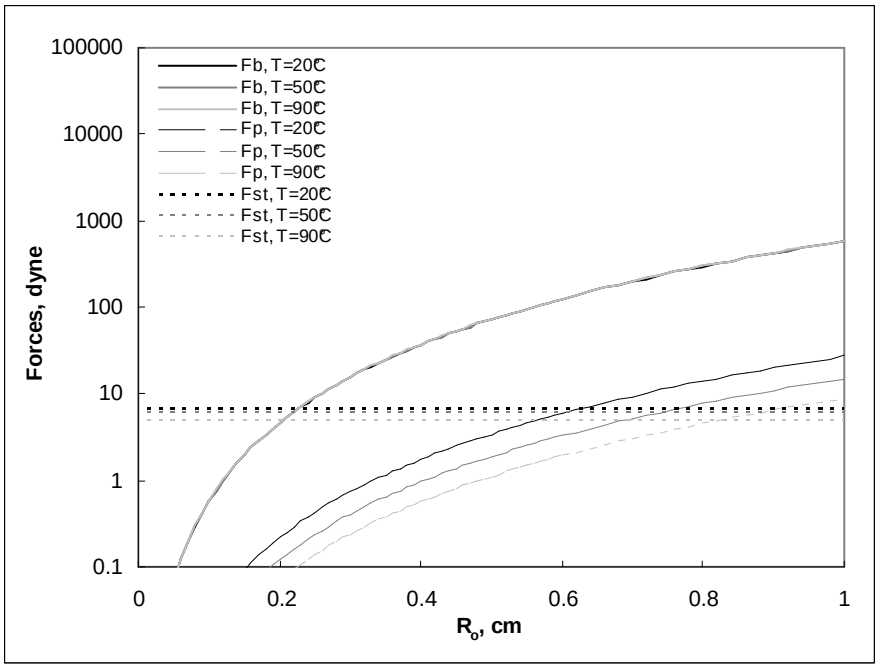

(a)

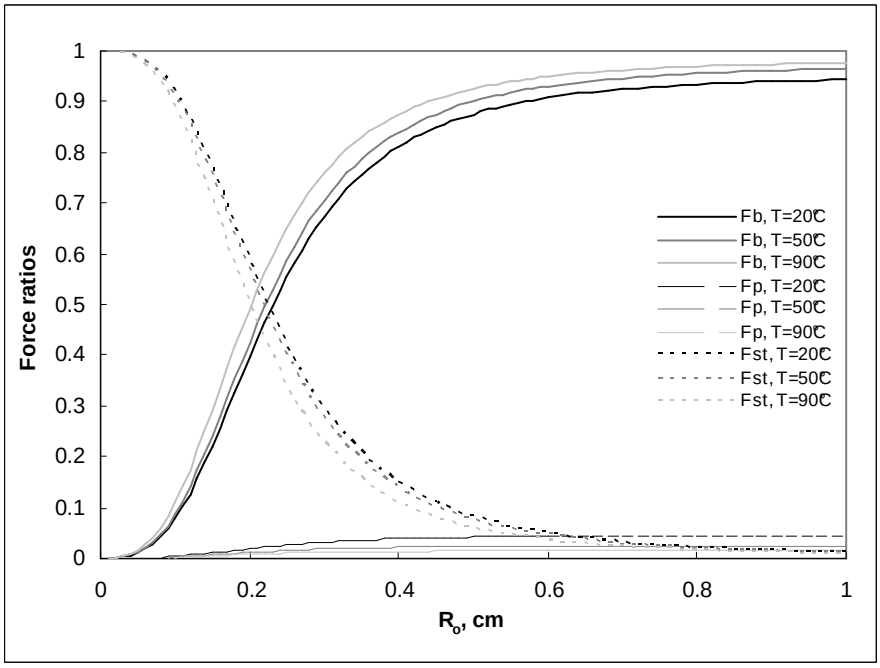

(b)

Figure 3-7 (a) Magnitudes of buoyant, push and surface tension forces and (b) force ratios between forces as a function of blob radius

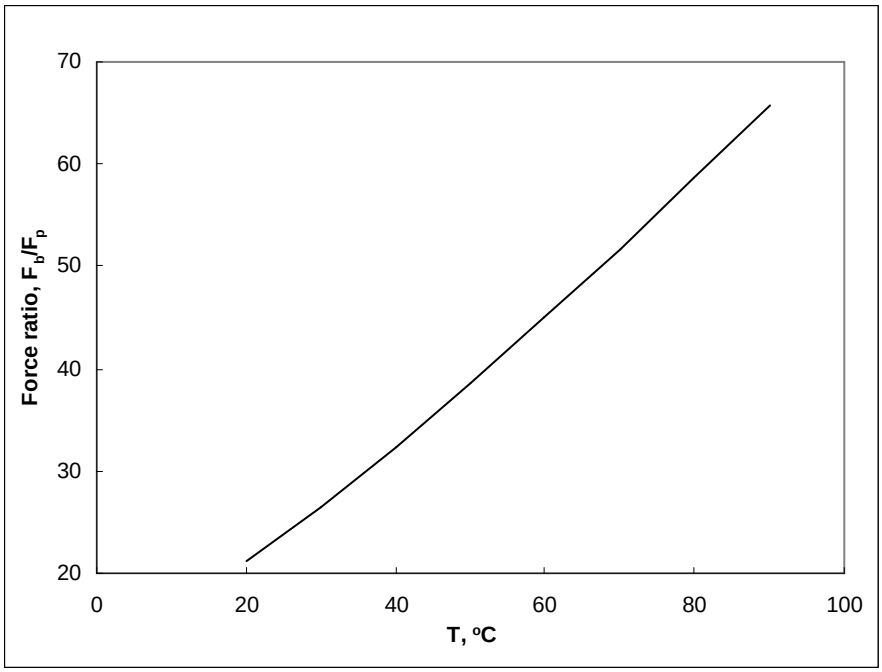

Figure 3-8 Force ratio of buoyant force to push force as a function of temperature

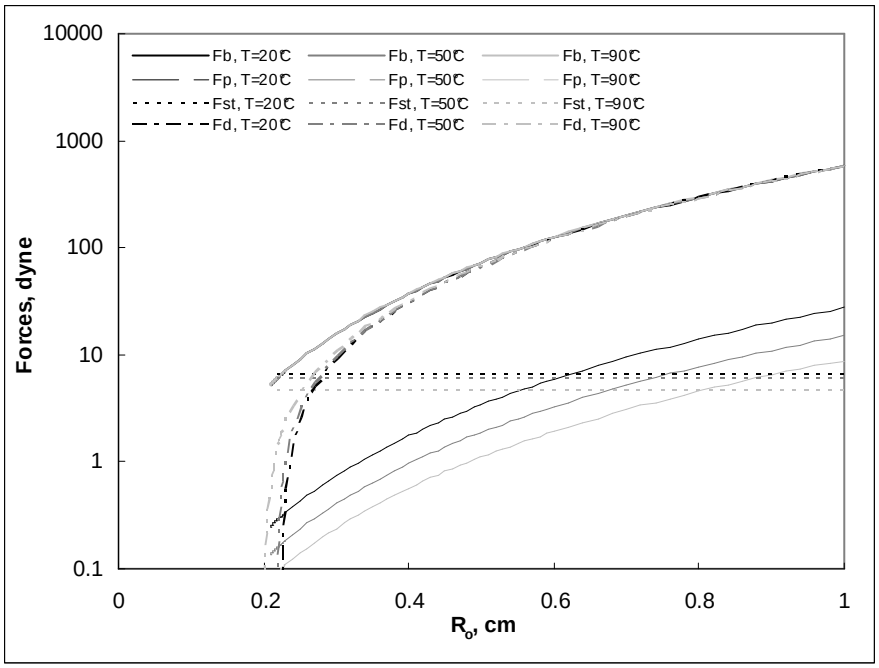

(a)

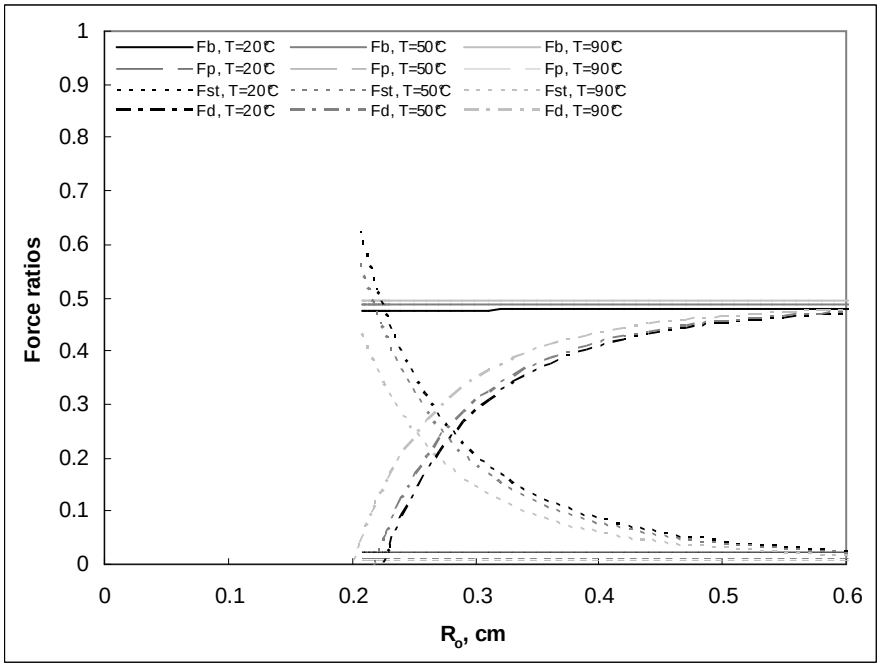

(b)

Figure 3-9 (a) Force magnitudes and (b) force ratios versus blob radius after the blob mobilization

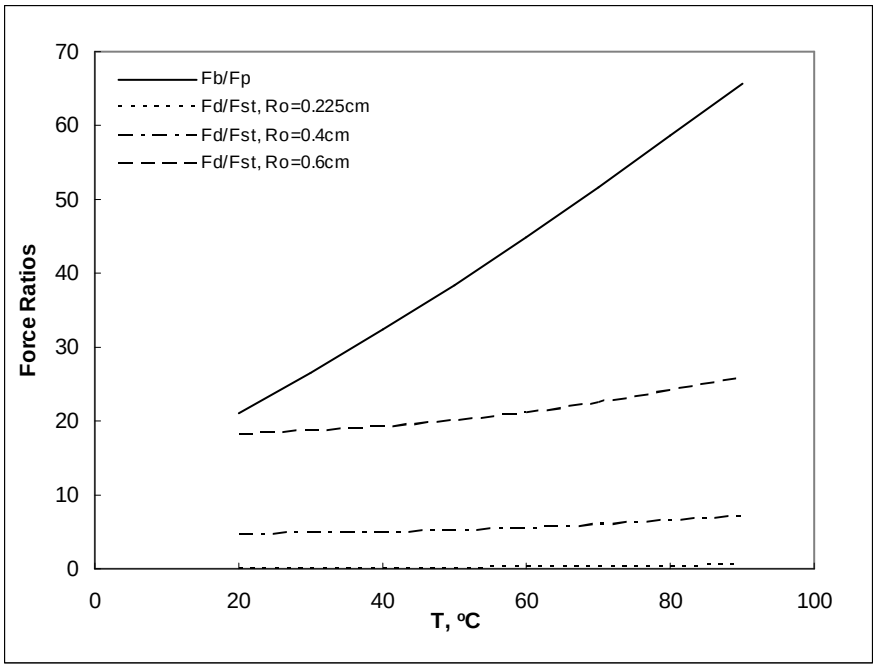

(a)

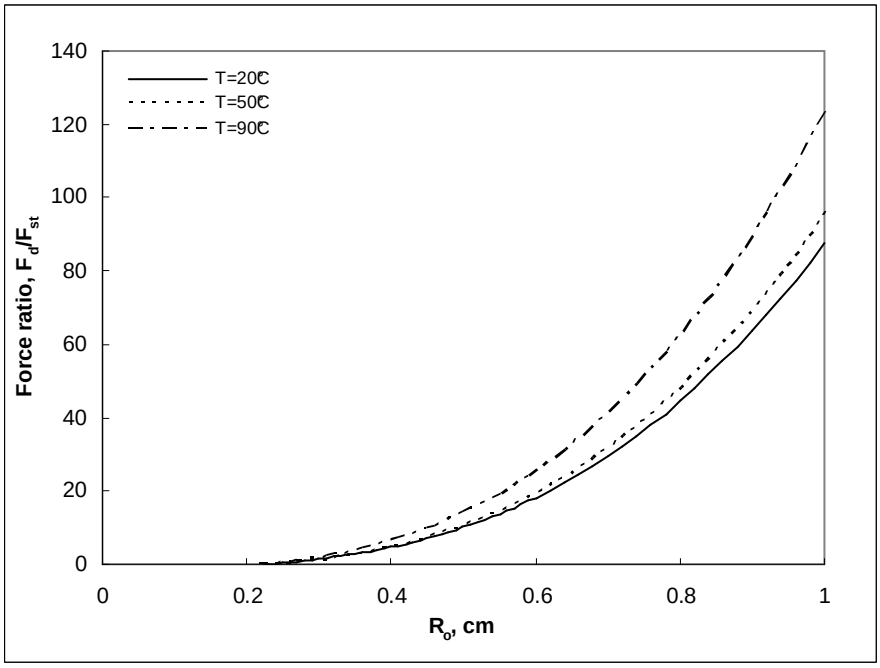

(b)

Figure 3-10 Force ratios as a function of (a) temperature and (b) blob radius

3.3.3 Terminal Blob Velocity

Once blob mobilization is initiated, the blob velocity can be determined from the force balance expression including the buoyant, push, surface tension, and drag forces exerted on the moving blob in the pore. The blob velocity is determined from the following expression:

$$F_b + F_p = F_{st} + F_d \tag{3-10a}$$

$$\Delta\rho g \frac{4}{3}\pi R_o^3 + A\frac{\mu_w u_w'}{kk_{rw}}\frac{4}{3}\pi R_o^3 = 2\pi R'\sigma\cos\theta + A\frac{\mu_o u_o}{kk_{ro}}\frac{4}{3}\pi R_o^3 \tag{3-10b}$$

$$\Delta\rho g \frac{4}{3}\pi R_o^3 + A\frac{\mu_w (u_w - u_o)}{kk_{rw}}\frac{4}{3}\pi R_o^3 = 2\pi R'\sigma\cos\theta + A\frac{\mu_o u_o}{kk_{ro}}\frac{4}{3}\pi R_o^3 \tag{3-10c}$$

$$u_o = \frac{kk_{ro}}{A\mu_o\left(1+\frac{k_{ro}}{k_{rw}}\frac{\mu_w}{\mu_o}\right)}\left(\Delta\rho g + \frac{A\mu_w u_w}{kk_{rw}} - \frac{3R'\sigma\cos\theta}{2R_o^3}\right) \tag{3-10d}$$

where u_w' is the water velocity relative to that of the NAPL blob. At the macro scale with S_o = 0.2, the calculation indicates that the terminal blob velocity is 1.62 × 10^{-5} cm/s at T = 20 ^oC. The terminal blob velocity was smaller than the water velocity by two orders of magnitude (Figure 3-11). Without the push force, the blob velocity is 1.55 × 10^{-5} cm/s at T = 20 ^oC and it can be compared to the above value with the push force. It indicates that the push force increases the blob terminal velocity insignificantly. As the temperature increases, the terminal velocity also increases to 1.16 × 10^{-4} cm/s at T = 90 ^oC, compared to 1.15 × 10^{-4} cm/s without the push force.

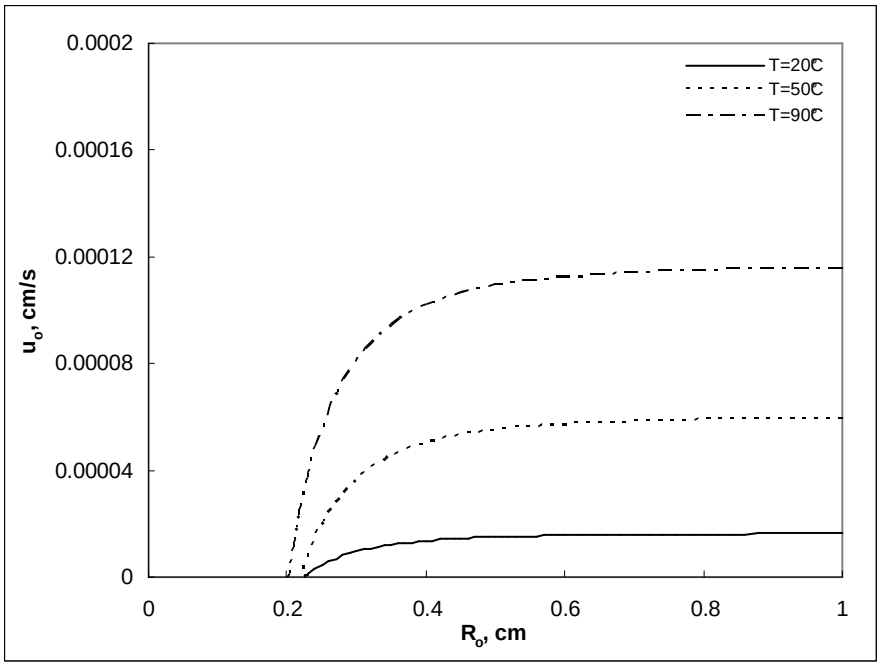

Figure 3-11 Calculated terminal (steady state) blob velocity with water flow after the blob mobilization from the force balance equation

CHAPTER IV

DIMENSIONAL ANALYSIS ON THE MOBILIZATION OF NAPL BLOB IN POROUS MEDIA

4.1 Dimensionless Numbers

A dimensional analysis using dimensionless numbers is used to delineate the NAPL blob mobilization in porous media, based on an evaluation of the effects of the forces exerted on a blob. The dimensional analysis provides a better understanding of the critical condition of the displacement of NAPL blob in porous media.

In general, the mobilization of NAPL blob in porous media is explained by the combined effects of bond number (Bo) and capillary number (Ca).

$$Bo = \frac{(\rho_w - \rho_o) g k k_{rw}}{\sigma \cos\theta} \tag{4-1}$$

$$Ca = \frac{\mu_w u_w}{\sigma \cos\theta} \tag{4-2}$$

Bond number, Bo , represents the ratio of buoyant to surface tension forces, and capillary number, Ca , represents the ratio of drag to surface tension forces. Pennell et al. (1996) introduced another dimensionless number, Trapping number (N_T) from the combination of bond number and capillary number, based on the vertical movement of NAPL blob.

$$N_T = |Bo \pm Ca| \tag{4-3}$$

For LNAPL, blob and water flow in the same direction to combine two numbers with the positive sign. Meanwhile, the negative sign applies to the movement of a DNAPL blob.

Along with the Trapping number, the initiation of blob mobilization requires the critical value of $2 \times 10^{-5} \sim 5 \times 10^{-5}$. From the force balance analysis, the equivalent terms for the bond and capillary numbers are defined, and the critical values for the initiation of blob mobilization are investigated.

4.2 Analysis on a Trapped NAPL Blob in Porous Media

For the dimensional analysis of NAPL blob movement in pores filled with stagnant water considers three forces: buoyant, surface tension, and drag forces.

$$\sum F = F_b - F_{st} - F_d = \Delta\rho g \frac{4}{3}\pi R_o^3 - 2\pi R'\sigma\cos\theta - A\frac{\mu_o u_o}{kk_{ro}}\frac{4}{3}\pi R_o^3 = 0 \tag{4-4}$$

Modified forms of existing dimensionless numbers are introduced by dividing buoyant and drag forces by surface tension force.

$$Bo' = \frac{\Delta\rho g \frac{4}{3}\pi R_o^3}{2\pi R'\sigma\cos\theta} = \frac{2\Delta\rho g R_o^3}{3R'\sigma\cos\theta} = \frac{2R_o^3}{3R'kk_{rw}} Bo = C_{Bo} Bo \tag{4-5}$$

$$Ca_o' = \frac{A\frac{\mu_o u_o}{kk_{ro}}\frac{4}{3}\pi R_o^3}{2\pi R'\sigma\cos\theta} = \frac{2AR_o^3}{3R'kk_{ro}} Ca_o = C_{Ca,o} Ca_o \tag{4-6}$$

where $Bo = \frac{(\rho_w - \rho_o)gkk_{rw}}{\sigma\cos\theta}$, $Ca_o = \frac{\mu_o u_o}{\sigma\cos\theta}$, $C_{Bo} = \frac{2R_o^3}{3R'kk_{rw}}$ and $C_{Ca,o} = \frac{2AR_o^3}{3R'kk_{ro}}$.

Bo' is the modified dimensionless number corresponding to bond number (Bo) and Ca_o' is the modified dimensionless number corresponding to capillary number for oil phase (Ca_o).

4.2.1 Effects of Blob Radius

Existing and modified dimensionless numbers are calculated with respect to the blob radius (Figure 4-1). The existing dimensionless numbers Bo and Ca_o, which have constant values for varying blob radius, do not provide representation of the role played by driving and retention forces after blob mobilization (Figure 4-1a). Meanwhile, the modified dimensionless numbers Bo' and Ca_o' do provide some useful information of the blob mobilization (Figure 4-1b).

Bo' and Ca_o' are expressed as a function of blob radius, unlike the bond and capillary numbers. Thus, as the blob radius increases, Bo' and Ca_o' increase, too. The increase of Bo' is proportional to the cube of the blob radius, corresponding to the blob volume, and the increase of Ca_o' is proportional to the product of the cube of blob radius and blob velocity. This can be understood by the definition of forces. Buoyant and drag forces include the term of blob volume to represent the increase in magnitude of forces as the blob radius increases.

In the meanwhile, surface tension force does not change with the varying blob radius. Therefore, Bo' and Ca_o' increases are due to buoyant and drag forces, respectively.

The modified dimensionless numbers show that Bo' is around unity and is greater than Ca_o' for a small blob radius such as R_o = 0.25 cm right after the initiation of blob mobilization, indicating the buoyant and surface tension forces control blob mobilization. And as the blob radius increases, the ratio of buoyant to surface tension forces increases rapidly, explaining the rapid increase in blob velocity. However, as the blob radius increases much more, the drag force increases rapidly and its contribution to the retention force overcomes that of surface tension force to the retention force and finally becomes solely significant. At R_o = 1 cm, Bo' and Ca_o' have values of 85 and 84, respectively, indicating the buoyant and drag forces control the blob mobilization. Due to the effects of drag force, the blob velocity approaches steady state.

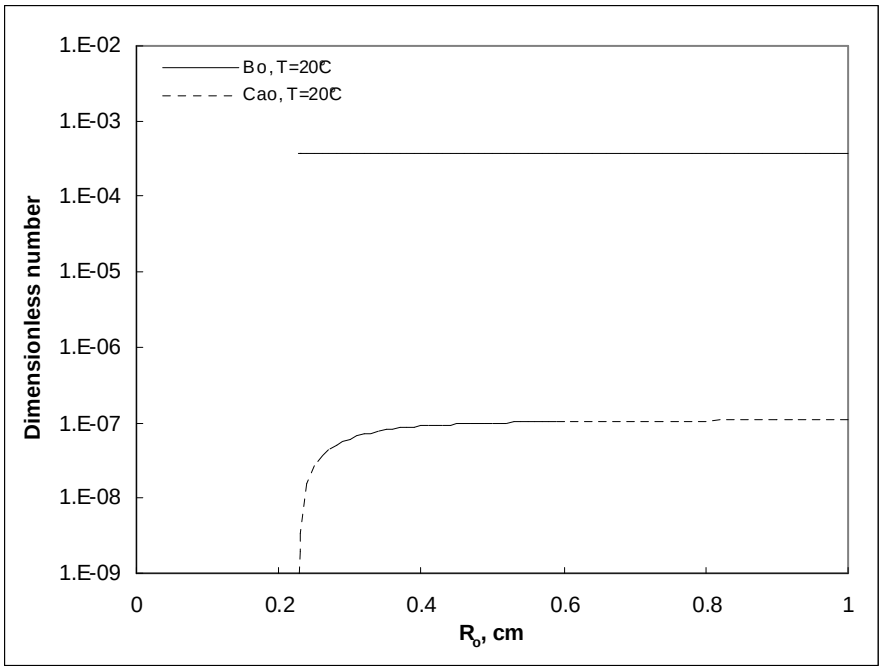

(a)

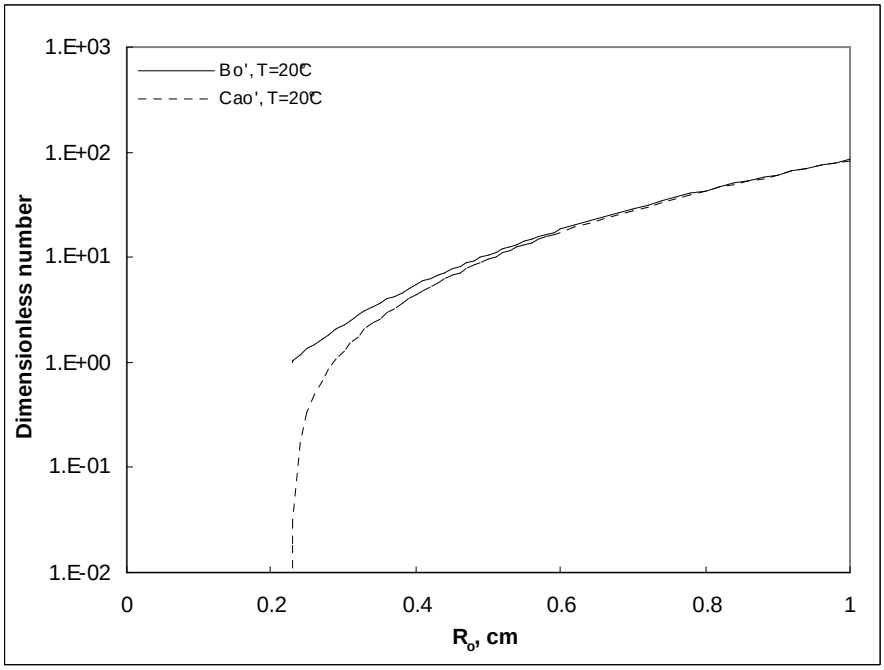

(b)

Figure 4-1 Comparison of existing and modified dimensionless numbers as a function of blob radius at T = 20 ^{o}C; (a) existing numbers Bo and Ca_o and (b) modified numbers Bo' and Ca'_o

4.2.2 Effects of Temperature

Modified dimensionless numbers are calculated with respect to the temperature (Figure 4-2; Table 4-1). To evaluate temperature changes, fixed values are given to the coefficients C_{Bo} and $C_{Ca,o}$ at fixed blob radius. The temperature-dependent changes of Bo' and Ca_o' are exactly proportional to that of Bo and Ca_o, more exactly, to the term $\frac{(\rho_w - \rho_o)}{\sigma \cos\theta}$ for Bo and $\frac{\mu_o u_o}{\sigma \cos\theta}$ for Ca_o.

As the temperature rises from 20 ^{o}C to 90 ^{o}C, the modified dimensionless number Bo' increases about 45% at any blob radius. The increase in number is due to the relatively larger decrease of the term $\sigma \cos\theta$ over the term $(\rho_w - \rho_o)$. The terms $\sigma \cos\theta$ and $(\rho_w - \rho_o)$ indicate the effects of surface tension and buoyant forces, respectively. Thus, the blob mobilization is supposed to gain its driving force from the buoyant force as temperature increases, compared to the retention force from surface tension force.

As the temperature rises from 20 ^{o}C to 90 ^{o}C, the modified dimensionless number Ca_o' increases about twice at R_o = 0.25 cm. The increase in number is due to the increase of the term $\mu_o u_o$, indicating the effects of drag force. As the blob velocity increases with the increasing temperature, the drag force increases greatly along with the decrease of surface tension force. This relationship decreases as the blob radius increases. The increase of the number Ca_o' is approximately 50% at R_o = 0.6 cm. From this observation, the surface tension force is significant at smaller blob radius over the whole temperature range and makes a greater contribution to the retention force than the drag force. At R_o = 0.25 cm, the ratio of the surface tension to the drag force is 3:1 at T = 20 ^{o}C. This ratio reduces to 1:1 at T = 90 ^{o}C and demonstrates that the surface tension force and the drag force make the same contributions to the retention force. However, at R_o = 0.6 cm, the drag force comprises most of the retention force with a ratio of the drag to the surface tension forces of 17:1 at T = 20 ^{o}C. This demonstrates that the surface tension contributes only 6% of the total retention force. This percentage goes down to 4% with a ratio of 25.5:1 at T = 90 ^{o}C.

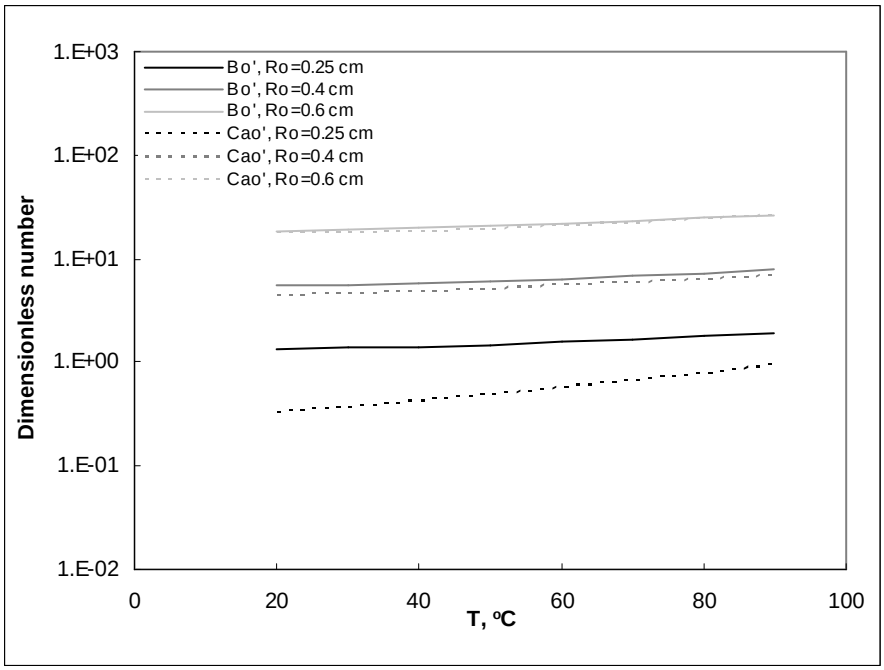

Figure 4-2 Modified dimensionless numbers Bo' and Ca_o' as a function of temperature between 20 °C and 90 °C at R_o = 0.25, 0.4 and 0.6 cm

Table 4-1 Modified dimensionless numbers Bo' and Ca_o' as a function of temperature between 20 ^oC and 90 ^oC at R_o = 0.25, 0.4 and 0.6 cm

T, ^oC	R_o = 0.25 cm		R_o = 0.4 cm		R_o = 0.6 cm	
	Bo'	Ca_o'	Bo'	Ca_o'	Bo'	Ca_o'
20	1.325	0.325	5.426	4.426	18.312	17.312
30	1.366	0.366	5.594	4.594	18.878	17.878
40	1.417	0.417	5.806	4.806	19.595	18.595
50	1.482	0.482	6.070	5.070	20.485	19.485
60	1.561	0.561	6.394	5.394	21.579	20.579
70	1.658	0.658	6.791	5.791	22.921	21.921
80	1.777	0.777	7.280	6.280	24.569	23.569
90	1.925	0.925	7.883	6.883	26.607	25.607
	45.3	184.8	45.3	55.5	45.3	47.9

Shading indicates the percentage Increase of the number over the temperature increase from 20 to 90 ^oC

4.2.3 Effects of Blob Velocity

Blob movement in porous media can be explained by a dimensionless number like Reynolds number. Reynolds number is expressed as the ratio of inertial to viscous forces, giving the information to identify the flow type between the laminar and turbulent flow ranges. Reynolds number is defined as:

$$\mathrm{Re} = \frac{2u_o R_o \rho_w}{\mu_w}. \tag{4-7}$$

where u_o and R_o are velocity and radius of blob, and ρ_w and μ_w are density and viscosity of water.

For blobs with a radius up to 1 cm and at temperatures between 20 to 90 ^{o}C, the Reynolds number indicates that the blob movement belongs in the laminar flow regime with critical values less than unity. It is already applied to the expression of drag force including the laminar flow term only in Chapter III.

As the blob radius increases, Reynolds number increases (Figure 4-3a). At smaller radius, Reynolds number is proportional to the product of the blob radius and blob velocity. As the radius gets larger, the blob velocity becomes constant and the Reynolds number is proportional to the blob radius only.

Reynolds number increases at the elevated temperature and it is proportional to the product of the water density and water viscosity (Figure 4-3b).

At the same Reynolds number, the modified dimensionless numbers Bo' and Ca_o' increase as the temperature increases (Figure 4-4). The higher dimensionless number indicates the more favorable conditions for flow running through the porous media with the decrease of surface tension force.

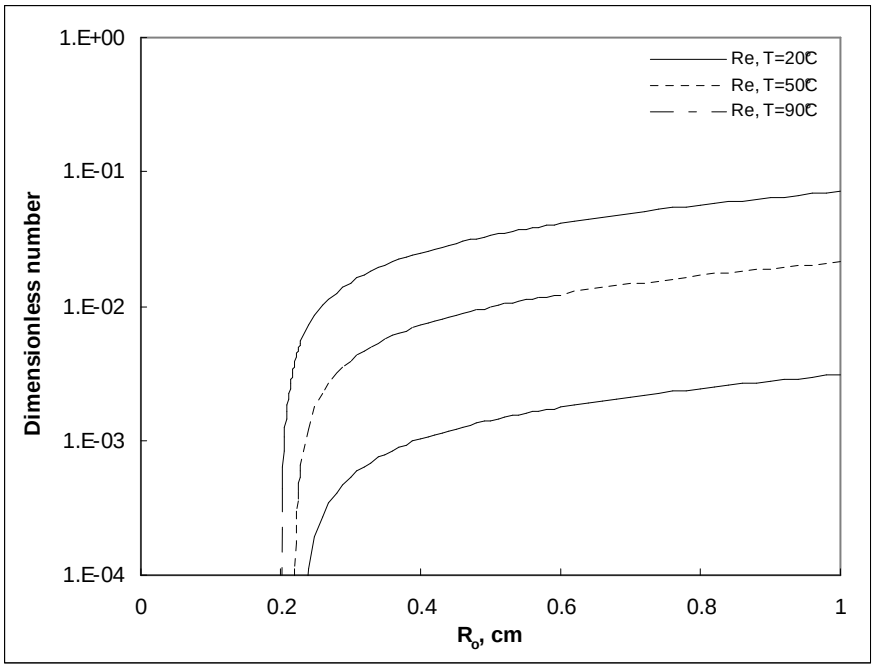

(a)

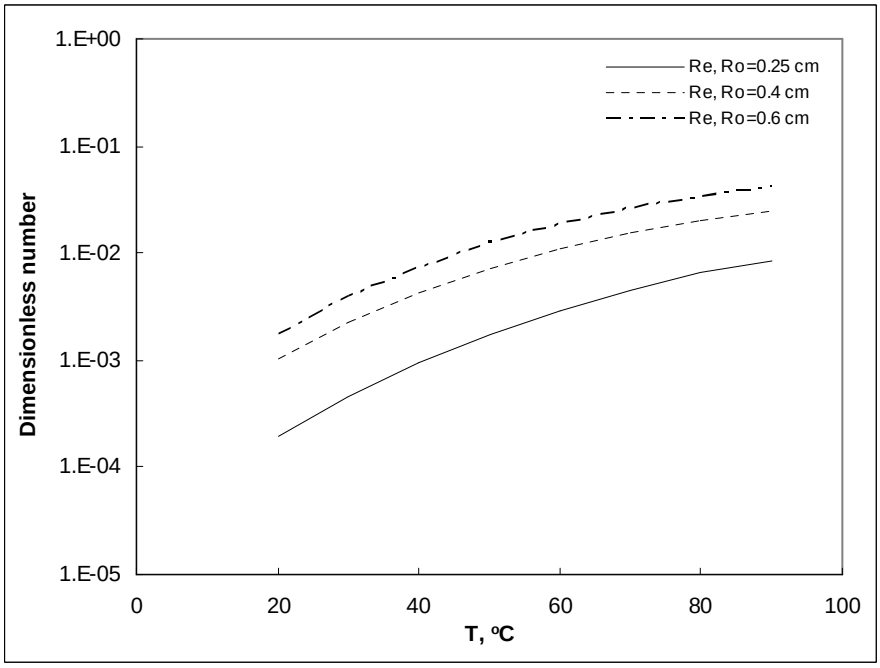

(b)

Figure 4-3 Reynolds number as a function of (a) blob radius (up to 1 cm) and (b) temperature (20 to 90 ^{o}C)

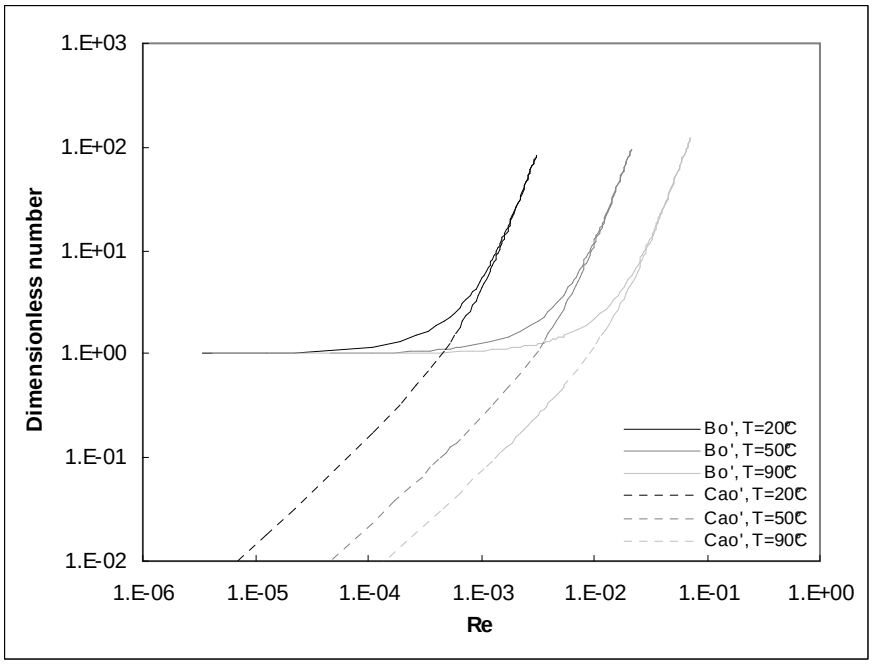

Figure 4-4 Modified dimensionless numbers Bo' and Ca_o' as a function of Reynolds number at T = 20, 50 and 90 ^{o}C

4.3 Analysis on a Trapped NAPL Blob with Water Flow

From the Pennell's definition (Equation (4-3)), the trapping number is expressed as the summation of the bond number and capillary number. When it is analyzed in conjunction with the force balance approach, it seems this trapping number is not applicable to explain the result of force balance approach. Instead, another similar expression is useful in explaining the result of force balance approach. The newly defined expression is the linear combination of the bond number and capillary number using proportionality coefficients. Proportionality coefficients are mainly comprised of blob radius and permeability. The coefficients are multiplied to the bond and capillary numbers to define their modified dimensionless numbers. The use of coefficients is necessary to integrate reality into the analysis of the pore-scale characteristics of porous media for a more understanding of fluid movement. It makes changes in some of fluid properties, like the fluid saturation and its relative permeability, quantitatively explainable from the changes in fluid size when the fluid exists only in a discrete form.

From the force balance equation, dimensionless numbers can be modified by proportionality coefficients.

$$\sum F = F_b + F_p - F_{st} - F_d = 0 \tag{4-8}$$

$$= \Delta\rho g \frac{4}{3}\pi R_o^3 + A\frac{\mu_w (u_w - u_o)}{kk_{rw}}\frac{4}{3}\pi R_o^3 - 2\pi R'\sigma\cos\theta - A\frac{\mu_o u_o}{kk_{ro}}\frac{4}{3}\pi R_o^3 = 0 \tag{4-9}$$

Dividing all other terms by the third term (expressing the surface tension force) gives,

$$Bo' = \frac{\Delta\rho g \frac{4}{3}\pi R_o^3}{2\pi R'\sigma\cos\theta} = \frac{2\Delta\rho g R_o^3}{3R'\sigma\cos\theta} = \frac{2R_o^3}{3R'kk_{rw}} Bo = C_{Bo} Bo \tag{4-10}$$

$$Ca'_{o,1} = \frac{A\frac{\mu_o u_o}{kk_{ro}}\frac{4}{3}\pi R_o^3}{2\pi R'\sigma\cos\theta} = \frac{2AR_o^3}{3R'kk_{ro}}Ca_o = C^1_{Ca,o}Ca_o \tag{4-11}$$

$$Ca'_{o,2} = \frac{A\frac{\mu_w u_o}{kk_{rw}}\frac{4}{3}\pi R_o^3}{2\pi R'\sigma\cos\theta} = \frac{2AR_o^3}{3R'kk_{rw}}\left(\frac{\mu_w}{\mu_o}\right)Ca_o = C^2_{ca,o}Ca_o \tag{4-12}$$

$$Ca'_w = \frac{A\frac{\mu_w u_w}{kk_{rw}}\frac{4}{3}\pi R_o^3}{2\pi R'\sigma\cos\theta} = \frac{2AR_o^3}{3R'kk_{rw}}Ca_w = C_{ca,w}Ca_w \tag{4-13}$$

where $Bo = \frac{(\rho_w - \rho_o)gkk_{rw}}{\sigma\cos\theta}$, $Ca_o = \frac{\mu_o u_o}{\sigma\cos\theta}$, $Ca_w = \frac{\mu_w u_w}{\sigma\cos\theta}$,

$$C_{Bo} = \frac{2R_o^3}{3R'kk_{rw}},\ C^1_{ca,o} = \frac{2AR_o^3}{3R'kk_{ro}},\ C^2_{ca,o} = \frac{2AR_o^3}{3R'kk_{rw}}\left(\frac{\mu_w}{\mu_o}\right), \text{ and } C_{ca,w} = \frac{2AR_o^3}{3R'kk_{rw}}.$$

Bo' is the modified dimensionless number corresponding to bond number (Bo) and $Ca'_{o,1}$ and $Ca'_{o,2}$ are the modified dimensionless number corresponding to capillary number for oil phase (Ca_o) and Ca'_w is the modified dimensionless number corresponding to capillary number for water phase (Ca_w). $Ca'_{o,1}$ is the dimensionless number having the same meaning and expression as Ca'_o in Section 4.2. $Ca'_{o,2}$ is the dimensionless number showing the effects of the drag force against the water flow due to the relative velocity between water and blob velocities.

4.3.1 Effects of Blob Radius

Existing and modified dimensionless numbers are calculated with respect to the blob radius (Figure 4-5). The existing dimensionless numbers Bo, $Ca_{o,1}$, $Ca_{o,2}$ and Ca_w do not provide a meaningful explanation to the role played by driving and retention forces after the blob mobilization (Figure 4-5a). Meanwhile, modified dimensionless numbers Bo', $Ca'_{o,1}$, $Ca'_{o,2}$ and Ca'_w provide some useful information for the blob mobilization (Figure 4-5b).

Bo' and $Ca'_{o,1}$ play the major role of the driving force and retention force. As the driving force, Bo' and Ca'_w are examined and Bo' is 20 times as large as Ca'_w. And, as the retention force, $Ca'_{o,1}$ and $Ca'_{o,2}$ are examined and $Ca'_{o,1}$ is larger than $Ca'_{o,2}$ by three orders of magnitude.

However, Ca'_w can contribute much more to the driving force under favorable conditions like increasing water velocity or increasing oil saturation. Ca'_w increases in direct proportion to the water velocity. For example, the above calculation is done at u_w = 1 m/d and if the water velocity goes up to 20 m/d, Ca'_w will increase 20 times.

And also, the elevated oil saturation can cause Ca'_w to increase by decreasing the water relative permeability Ca'_w. For example, the above calculation is done at S_o = 0.2 and the corresponding $k_{rw}\left(=(1-S_o)^3=(1-0.2)^3=0.512\right)$. If the oil saturation increases up to 0.5, then the corresponding k_{rw} will be $0.125\left(=(1-S_o)^3=(1-0.5)^3=0.125\right)$ and Ca'_w will increase more than 4 times.

$Ca'_{o,2}$ can also contribute much more to the retention force under favorable conditions like increasing oil saturation. From the initial oil saturation (S_o = 0.2), the corresponding relative permeabilities k_{ro} and k_{rw} are 0.008 $\left(=S_o{}^3=0.2^3=0.008\right)$ and 0.512, respectively. If the oil saturation, S_o, increases from 0.2 to 0.5, both k_{ro} and k_{rw} will be 0.125. It causes k_{ro} to increase more than 15 times and k_{rw} to decrease more than 4 times. In conclusion, $Ca'_{o,2}$ can contribute about 60 times more than ever to the total retention force.

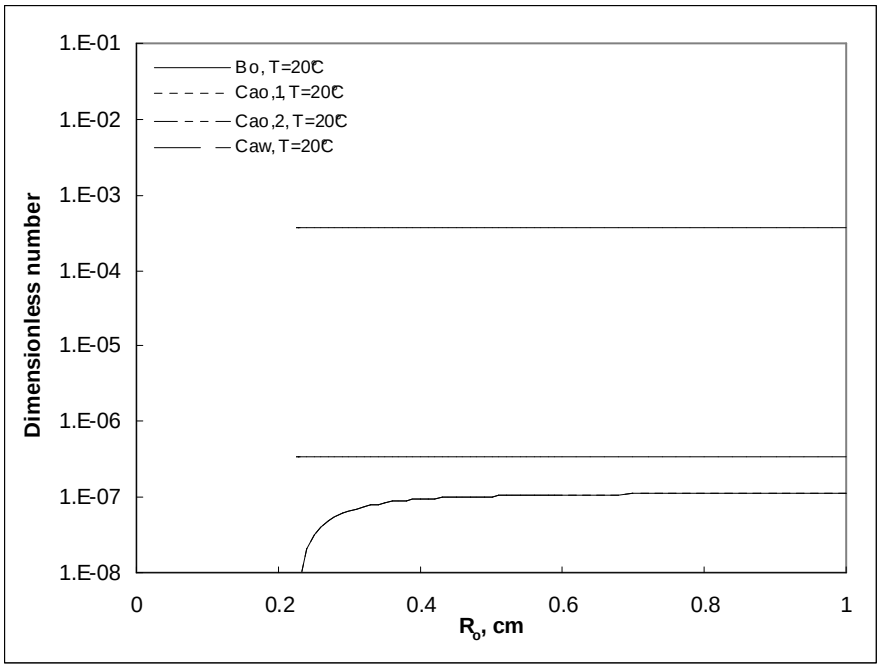

(a)

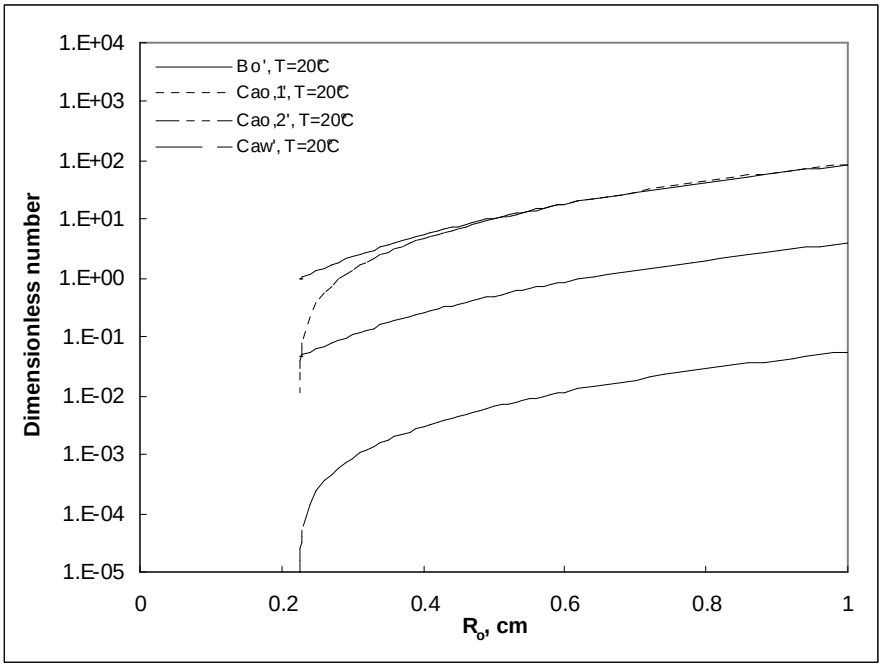

(b)

Figure 4-5 Comparison of existing and modified dimensionless numbers as a function of blob radius at T = 20 ^{o}C; (a) existing numbers Bo, $Ca_{o,1}$, $Ca_{o,2}$ and Ca_{w} and (b) modified numbers Bo', $Ca'_{o,1}$, $Ca'_{o,2}$ and Ca'_{w}

4.3.2 Effects of Temperature

As the temperature increases, the modified dimensionless numbers Bo', $Ca'_{o,1}$, and $Ca'_{o,2}$ increase, but Ca'_w decreases. The increase of Bo' is due to the relatively rapid decrease of surface tension force compared to buoyant force. The increases of $Ca'_{o,1}$ and $Ca'_{o,2}$ are due to the relatively large increase of blob velocity compared to the decrease of oil and water viscosities, respectively. That is, the increase of blob velocity causes the increasing effects of drag force from $Ca'_{o,1}$ and the increasing effects of friction force between water and oil phases from $Ca'_{o,2}$. Meanwhile, the decrease of Ca'_w is due to the decrease of push force by the decrease of water viscosity.

At the smaller blob radius (R_o = 0.25 cm), the close-to-one values of dimensionless numbers Bo' and $Ca'_{o,1}$ show that the role of surface tension force maintains at the elevated temperature even though it reduces gradually with the escalating temperature. However, at the larger blob radius (R_o = 0.6 cm), the higher values (ranging between 18 and 27) of these dimensionless numbers show that the surface tension force provide only a small contribution of a few percent to the total retention force, compared to the drag force.

The decrease of push force observed from the decrease of Ca'_w can be explained by the fact that the blob mobilization gets easier because the decrease of water viscosity at the higher temperature makes the blob slide more smoothly on the water surface being contacted by the blob.

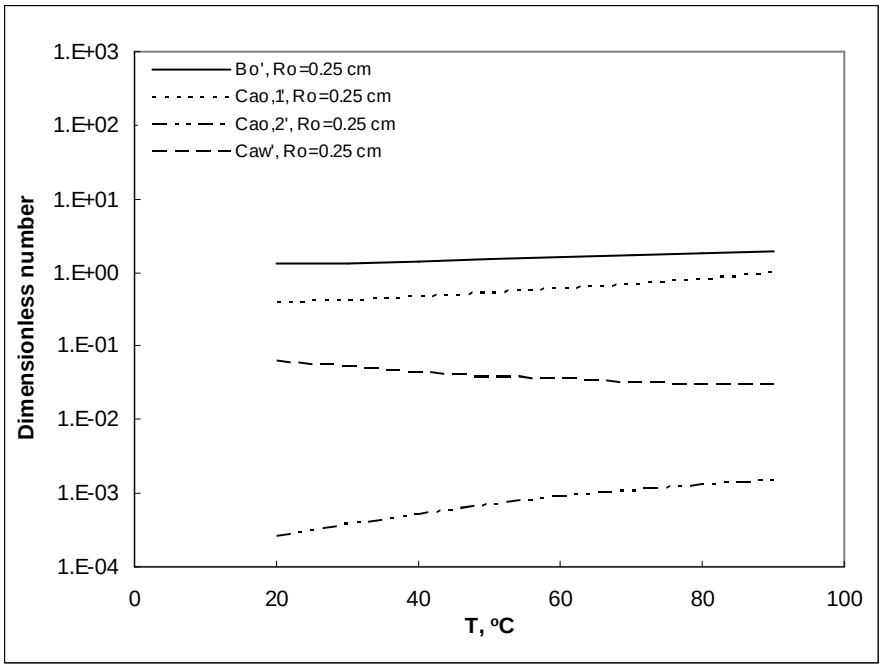

(a)

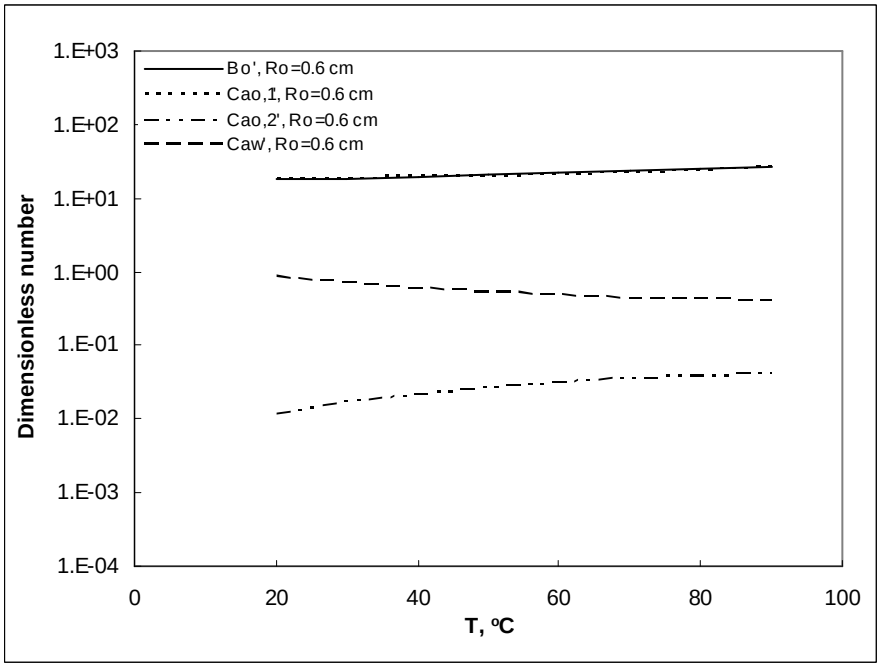

(b)

Figure 4-6 Modified dimensionless numbers Bo', $Ca'_{o,1}$, $Ca'_{o,2}$ and Ca'_{w} as a function of temperature at (a) R_o = 0.25 cm and (b) R_o = 0.6 cm

4.3.3 Effects of Blob Velocity

Under conditions without and with water flow, Reynolds number is compared to see the effects of water velocity (Figure 4-7). The existence of water flow does not give any significant change to Reynolds number. The change of number is only a few percent with respect to blob radius (Figure 4-7a). For example, the change is about 4.7 % at R_o = 1 cm and T = 20 ^{o}C. It means that the water velocity does not increase the blob velocity much. And the change is getting smaller as the temperature increases to 90 ^{o}C. The change is about 1.4 %. From these observations, it is inferred that effects of both buoyant force and temperature still play the major role on the blob mobilization, compared to the effects of water velocity. However, if the water velocity increases much higher, the effects of water velocity for the blob mobilization can be much more significant and the change of Reynolds number will be much larger.

From the comparison between modified dimensionless numbers and Reynolds number (Figure 4-8), the following observations are indicated.

First, the modified dimensionless numbers $Ca'_{o,1}$ and $Ca'_{o,2}$ are controlled by blob velocity at the lower Reynolds number while numbers Bo' and Ca'_w are not. The Reynolds number increases abruptly at the lower blob radius in proportion to the blob velocity. Meanwhile, the numbers Bo' and Ca'_w also increase as the Reynolds number does, but the increase in these numbers is being masked by the rapid increase in the Reynolds number at the lower blob radius.

Second, all of the modified dimensionless numbers are controlled by blob radius at the higher Reynolds number. After the blob velocity reaches steady state (that is, after the blob velocity becomes constant), the Reynolds number and other dimensionless numbers change in proportion to the blob volume, that is, the cube of blob radius. From Figure 4-8, the slope shows the relationship between those parameters and dimensionless numbers, including Reynolds number.

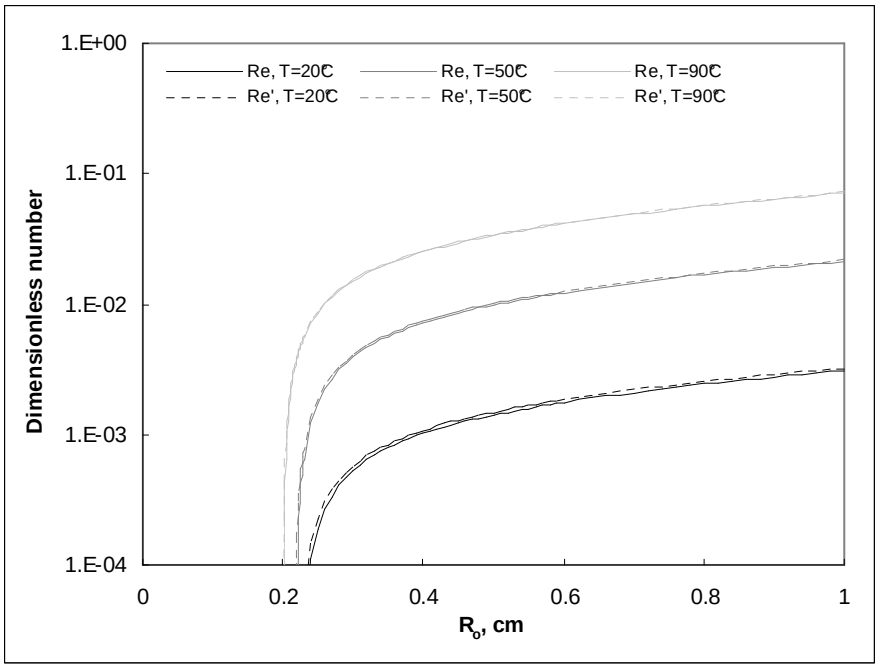

(a)

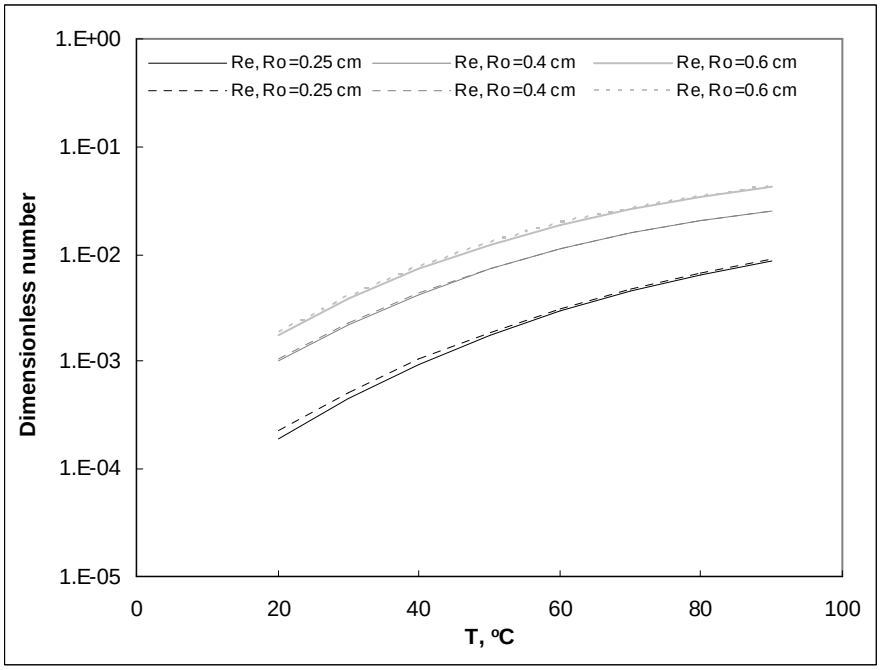

(b)

Figure 4-7 Reynolds number under condition without and with water flow as a function of (a) blob radius (up to 1 cm) and (b) temperature (20 to 90 ^{o}C)

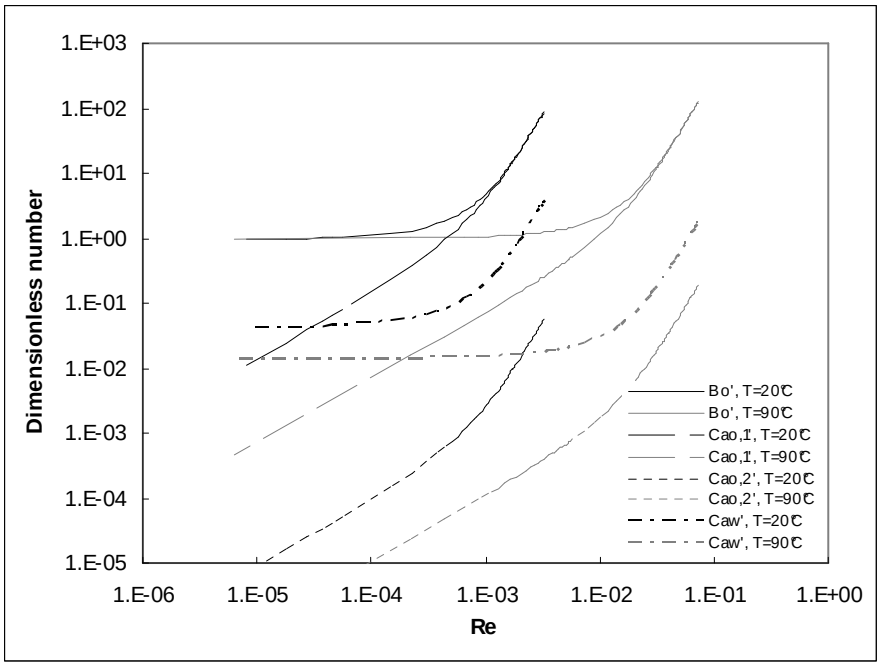

Figure 4-8 Comparison of modified dimensionless numbers Bo', $Ca'_{o,1}$, $Ca'_{o,2}$ and Ca'_{w} and Reynolds number at T = 20 and 90 ^{o}C

CHAPTER V

CRITICAL CONDITIONS ON THE ENHANCEMENT OF NAPL BLOB MOBILIZATION

5.1 Effects of Water Velocity on NAPL Blob Mobilization

5.1.1 Critical Water Velocity

In Chapter III, critical conditions of NAPL blob mobilization in porous media were investigated with respect to blob radius and temperature. In addition to these factors, the water velocity also can influence the blob mobilization. In this chapter, the effects of water velocity for the initiation of blob mobilization are observed in combination with factors mentioned above.

With the existence of water flow, one-phase (water) flow is considered for the examination and Equations (3-9a) and (3-9b) can be used to observe critical conditions of water velocity for the initiation of blob mobilization. According to equations, the push force increases as the water velocity increases while buoyant and surface tension forces do not change. Thus, the driving force increases along with the increase of water velocity and overcomes the retention force initiate the blob mobilization at certain water velocity (Figures 5-1). From the Equation (3-9b) and the assumption mentioned above, the critical water velocity can be calculated as

$$u_{w,crit} \geq \frac{kk_{rw}}{A\mu_w}\left(\frac{3R'\sigma\cos\theta}{2R_o^3} - \Delta\rho g\right) \qquad (5\text{-}1)$$

and it is 26.5 m/d. For the sand or gravel aquifer, the typical groundwater velocity has a range of 5 – 50 ft/d (1.5 – 15 m/d).

And, as the water velocity increases, the critical blob radius for blob mobilization decreases. Considered the increase of water velocity, the mobilization of a blob is possible at the smaller radius from Equation (3-9c) because the increasing push force along with the increasing water velocity makes the driving force larger (Figures 5-2 and 5-3). For example, the critical blob radius is 0.224 cm at u_w = 1 m/d. Meanwhile, at u_w = 26.5 m/d, the critical blob radius is 0.174 cm. And, at the water velocity higher than 26.5 m/d, the critical blob radius becomes smaller. This blob radius (R_o = 0.174 cm) represents the same volume of blob as that of a single pore. Thus, this water velocity (u_w = 26.5 m/d) provides the critical condition for the initiation of blob mobilization to distinguish singlet and doublet in the blob size. From the calculation, the critical blob radius becomes as small as 0.152 cm at u_w = 50 m/d and the corresponding oil saturation is 0.67, meaning the blob volume is 67 % of the unit pore volume.

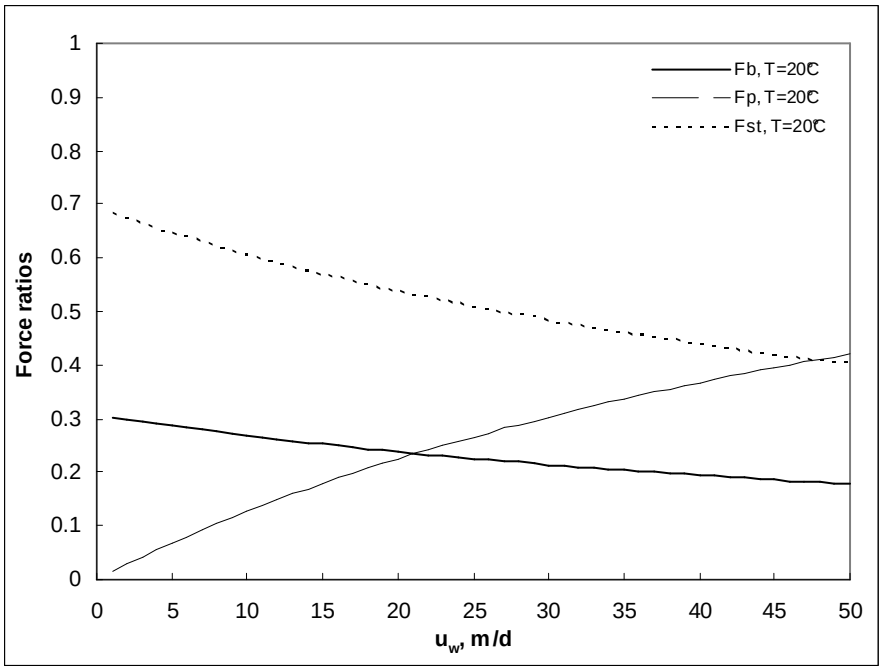

(a)

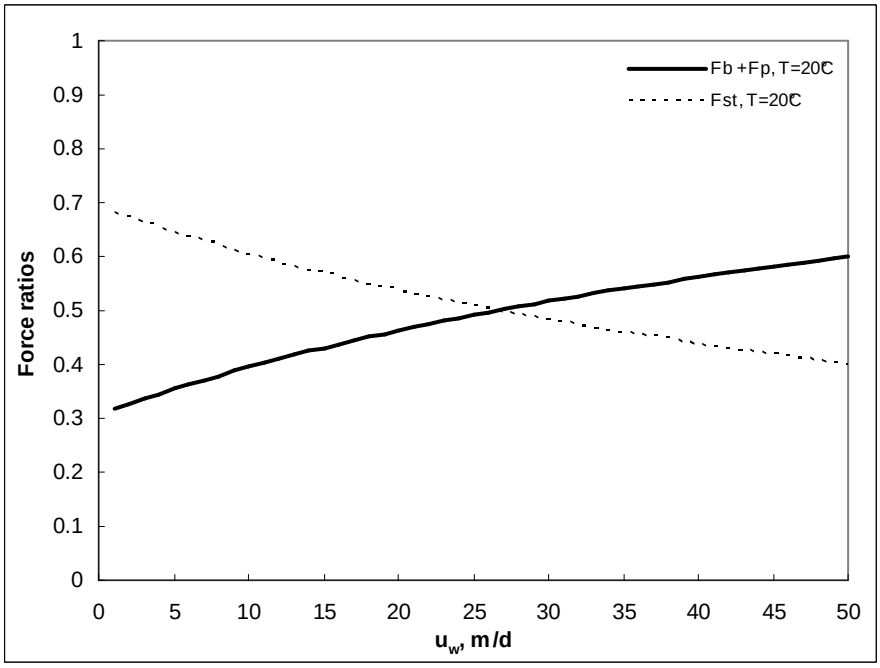

(b)

Figure 5-1 Force ratios versus water velocity for the blob mobilization.
(a) Ratios between F_b, F_p, and F_{st}; (b) ratios between $F_b + F_p$ and F_{st}

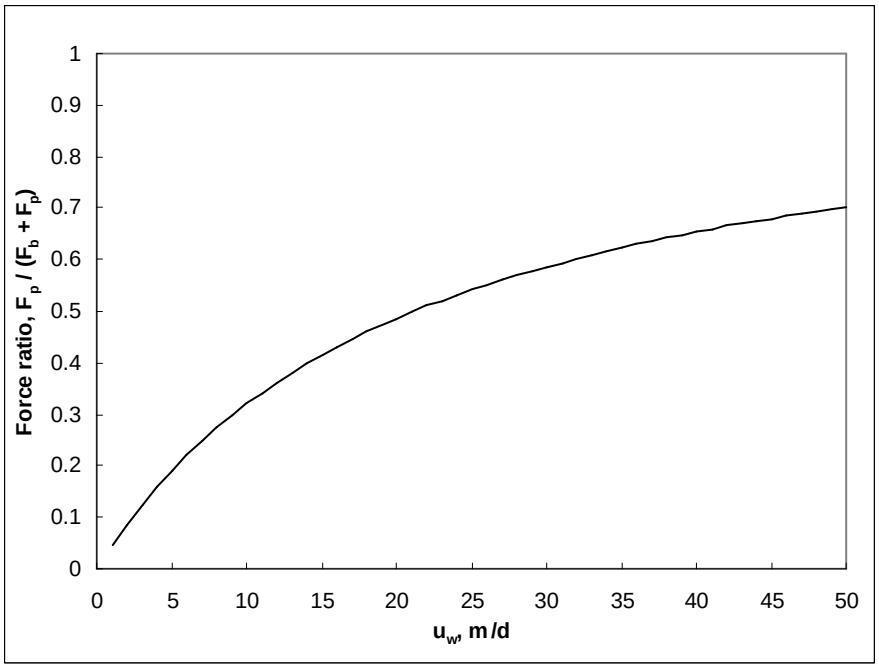

Figure 5-2 Increasing contribution of push force to the driving force at increasing water velocity

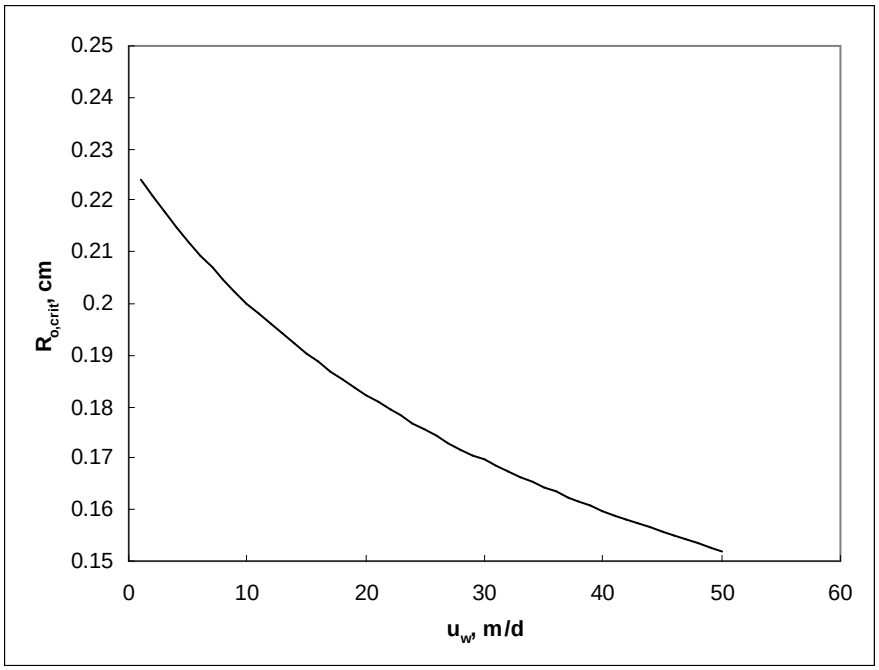

(a)

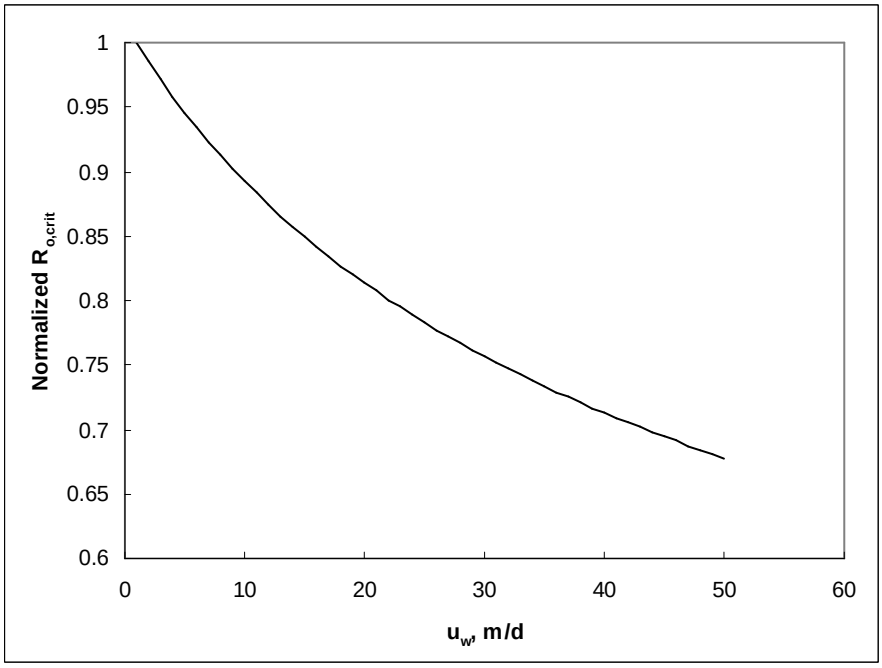

(b)

Figure 5-3 (a) Critical blob radius for the mobilization as a function of water velocity and (b) ratio of critical blob radius at reference water velocity (u_w = 1 m/d) to that at interest water velocity

5.1.2 Combined Effects of Water Velocity and Temperature

When two factors of water velocity and temperature are simultaneously considered to determine the critical condition of blob mobilization, it does not show a linear trend. When the effects of temperature are observed at the fixed water velocity, the critical blob radius for the mobilization is calculated from Equations (3-9a) through (3-9c). From Equation (3-9c), the calculated critical blob radius is defined as

$$R_{o,crit} = \left(\frac{3R'\sigma \cos\theta}{2\left(\Delta\rho g + A\frac{\mu_w u_w}{k k_{rw}} \right)} \right)^{1/3} . \qquad (5\text{-}2)$$

The critical blob radius for the mobilization decreases at the low water velocity as the temperature increases (Figure 5-4). Meanwhile, the critical blob radius increases at the high water velocity over the increasing temperature.

For example, the critical blob radius decreases from 0.224 cm to 0.202 cm at u_w = 1 m/d and increases from 0.152 cm to 0.168 cm at u_w = 50 m/d (Table 5-1). This is due to the different contribution of push force to the driving force for the blob mobilization at low and high water velocities, respectively.

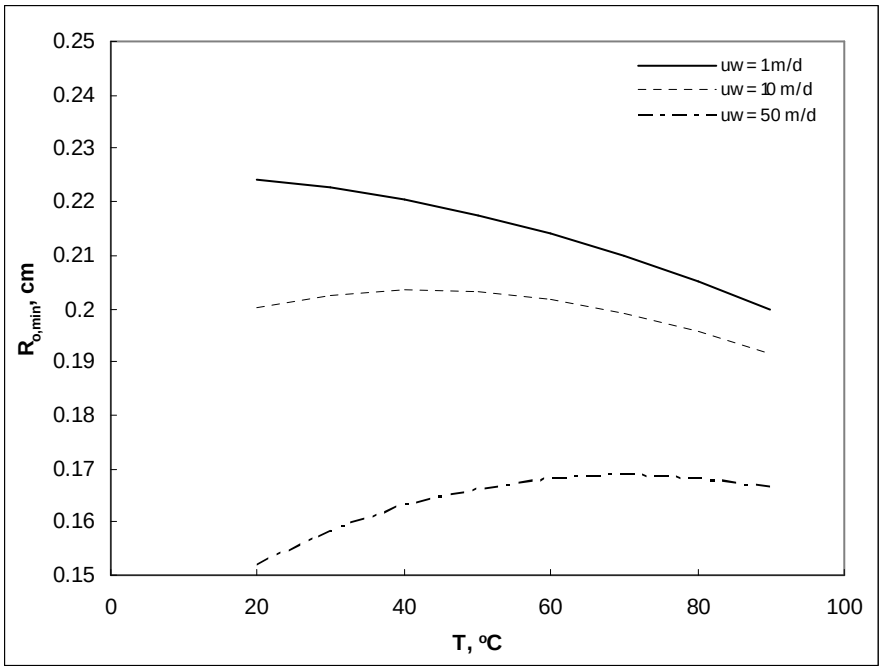

(a)

Figure 5-4 Critical blob radius for the mobilization as a function of temperature at interest water velocity

Table 5-1 Critical values of blob radius for the mobilization as a function of water flow velocity and temperature

T, ^{o}C	$R_{o,crit}$, cm		
	u_w = 1 m/d	u_w = 10 m/d	u_w = 50 m/d
20	0.224	0.200	0.152
30	0.223	0.203	0.158
40	0.220	0.203	0.163
50	0.217	0.203	0.166
60	0.214	0.202	0.168
70	0.210	0.199	0.169
80	0.205	0.196	0.168
90	0.200	0.192	0.166

Buoyant force and surface tension force are independent to the water velocity, but push force is dependent. So, the magnitude of push force changes according to the water velocity. At u_w = 1 m/d, the push force is about 20 times smaller than the buoyant force in magnitude (Figure 5-5a). However, the push force is about twice larger than the buoyant force at u_w = 50 m/d (Figure 5-5b). It says that the contribution of push force to the driving force, expressed as the summation of buoyant force and push force in magnitude, is insignificantly small at u_w = 1 m/d, but it becomes significantly large at u_w = 50 m/d (Table 5-2). Thus, the change of driving force in magnitude is much different at low and high water velocities, respectively.

When the temperature increases from 20 ^{o}C to 90 ^{o}C, force magnitudes change as the temperature changes, that is, buoyant force increases, and push and surface tension forces decrease as the temperature increases. And, the change of force magnitude for buoyant, push and surface tension forces is about 3, 69 and 30%, respectively. Along with these changes, the driving force decreases about 2.1 and 47.1% at u_w = 1 and 50 m/d, respectively. It explains the reason why the critical blob radius decreases at u_w = 1 m/d and it increases at u_w = 50 m/d. At u_w = 1 m/d, the decreases of surface tension force is larger than that of driving force.

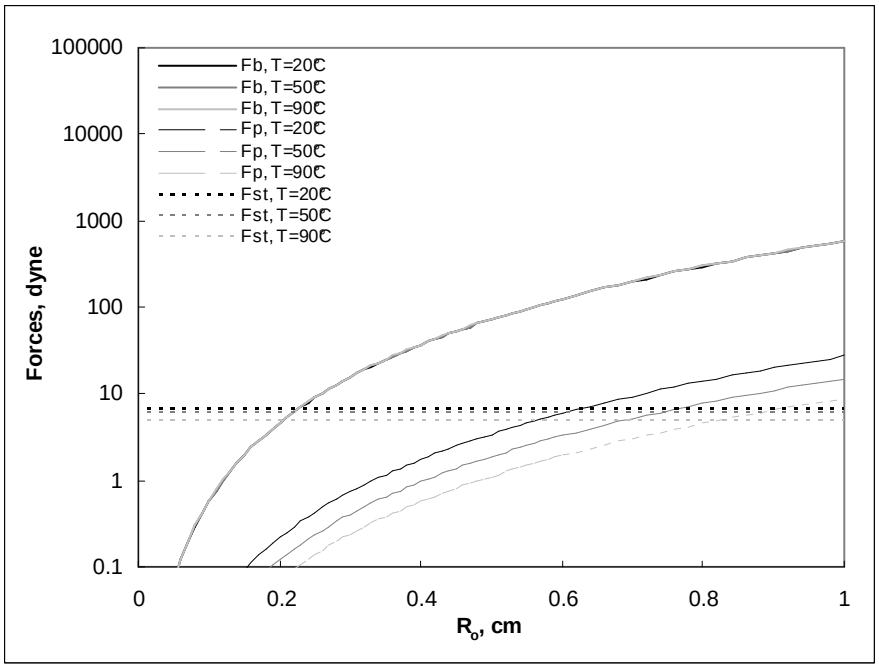

(a)

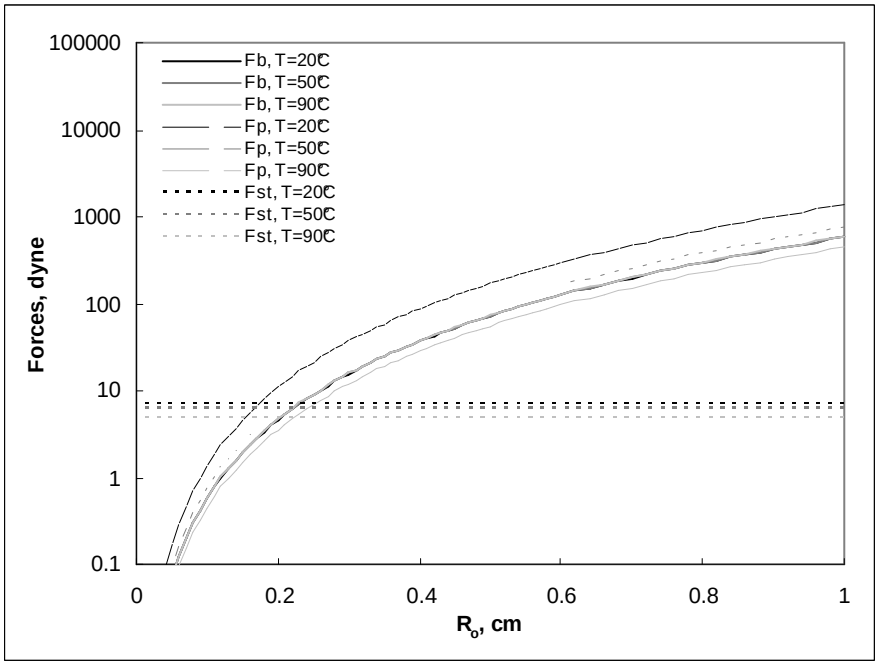

(b)

Figure 5-5 Magnitudes of buoyant, push and surface tension forces as a function of blob radius (a) at u_w = 1 m/d and (b) at u_w = 50 m/d

Table 5-2 Percentage contribution of push force to the driving force as a function of water velocity

T, °C	$F_p/(F_b+F_p)$, %		
	u_w = 1 m/d	u_w = 10 m/d	u_w = 50 m/d
20	4.5	32.1	70.3
30	3.6	27.4	65.3
40	3.0	23.6	60.7
50	2.5	20.6	56.5
60	2.2	18.2	52.7
70	1.9	16.2	49.2
80	1.7	14.6	46.0
90	1.5	13.2	43.2

Thus, the critical condition of blob mobilization becomes more favorable. Meanwhile, at u_w = 50 m/d, the decreases of driving force is larger than that of surface force. Thus, the critical condition of blob mobilization becomes less favorable.

The critical blob radius for the mobilization reduces at a certain temperature as the water velocity increases (Figure 5-6). However, the reducing rate of blob radius varies according to the temperature. When the water velocity changes from 1 m/d to 50 m/d, the calculated rates from the semi-log plot is 0.00761, 0.00538 and 0.00371 d/m at u_w = 1, 10 and 50 m/d, respectively. The decreases of critical blob radius at the escalated temperature indicate the increases of contribution of push force to the driving force because its increases are proportional to the water velocity. However, at the increasing temperature, the initial contribution of push force to the driving force is smaller because the corresponding water viscosity is lower. The smaller the initial push force, the smaller the increasing contribution of push force to the driving force with the increasing temperature.

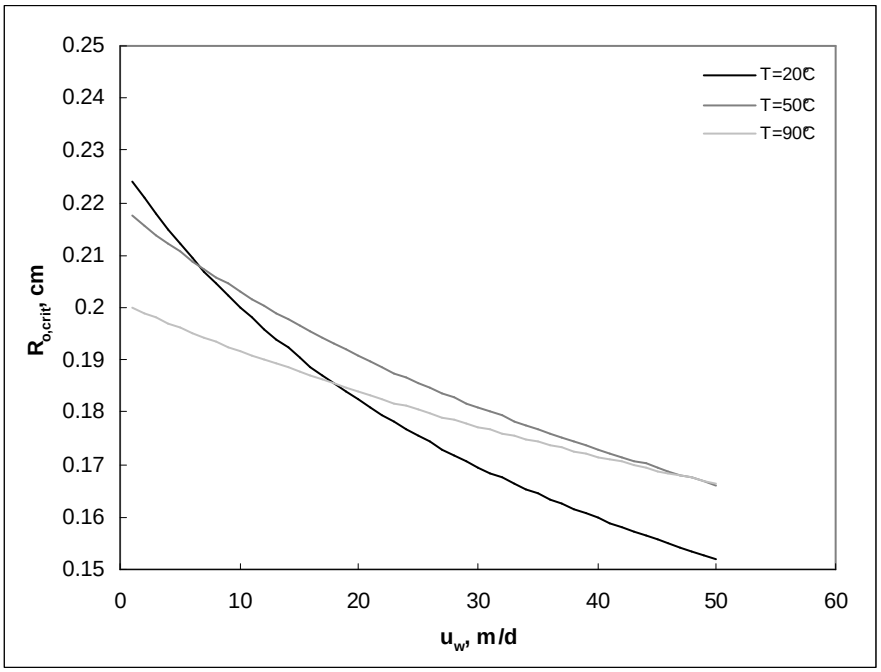

(a)

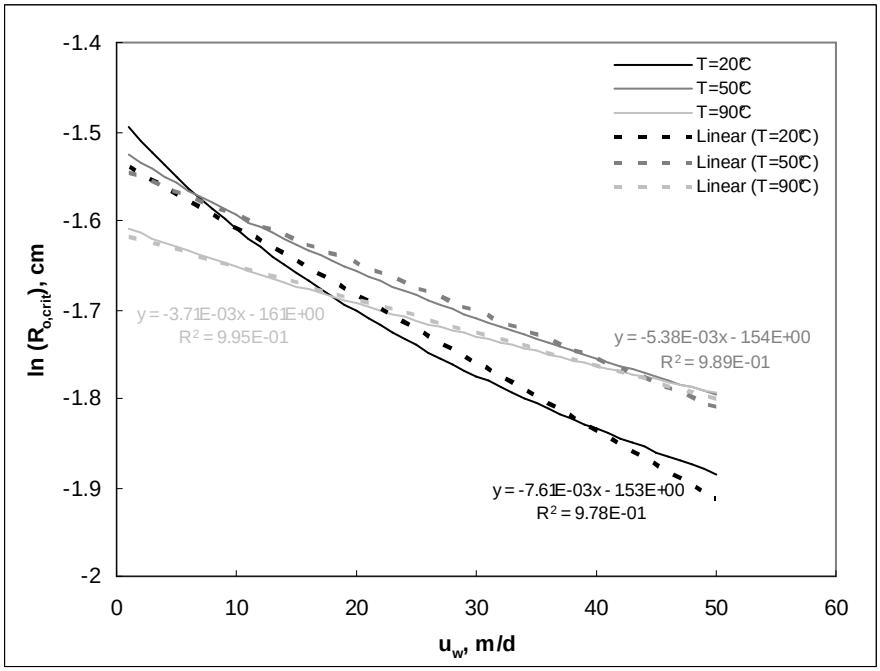

(b)

Figure 5-6 (a) Critical blob radius for the mobilization and (b) its reducing rate as a function of water velocity at interest temperature

5.1.3 Terminal Blob Velocity

The terminal blob velocity after the blob mobilization increases as the temperature increases (Figure 5-7a). However, the rate of blob velocity increases with the increasing water velocity: this is, the increasing rate of terminal blob velocity is 1.59×10^{-6}, 1.79×10^{-6} and 2.66×10^{-6} cm/s·°C at u_w = 1, 10 and 50 m/d, respectively (Table 5-3). This happens because the magnitude of push force is increasing in proportion of water velocity and thus its contribution to the driving force is accordingly increasing.

Meanwhile, the terminal blob velocity after the blob mobilization increases as the water velocity increases, too (Figure 5-7b). And, the change rate of blob velocity increases with the increasing temperature. Using the Equation (3-10d), the change rate of blob velocity with the variable of water velocity can be expressed as

$$u_o = a' \times u_w + b' \tag{5-3}$$

$$a' = \frac{kk_{ro}}{A\mu_o\left(1+\frac{k_{ro}}{k_{rw}}\frac{\mu_w}{\mu_o}\right)}\left(\frac{A\mu_w}{kk_{rw}}\right) = \frac{1}{\frac{k_{rw}}{k_{ro}}\frac{\mu_o}{\mu_w}\left(1+\frac{k_{ro}}{k_{rw}}\frac{\mu_w}{\mu_o}\right)} = \frac{1}{\frac{k_{rw}}{k_{ro}}\frac{\mu_o}{\mu_w}+1} = \frac{k_{ro}\mu_w}{k_{rw}\mu_o + k_{ro}\mu_w} \tag{5-4}$$

$$b' = \frac{kk_{ro}}{A\mu_o\left(1+\frac{k_{ro}}{k_{rw}}\frac{\mu_w}{\mu_o}\right)}\left(\Delta\rho g - \frac{3R'\sigma\cos\theta}{2R_o^3}\right). \quad (5\text{-}5)$$

The coefficient, a´ represents the ratio of change of blob velocity to that of water velocity, indicating the influence of water velocity to the blob velocity. This proportionality coefficient is the function of relative permeabilities and viscosities of oil and water phases, i.e., $a' = f(k_{rw}, k_{ro}, \mu_w, \mu_o)$. This coefficient has the constant value at the interest temperature. However, the value is varying as the temperature changes because the viscosities are changing. So, the coefficient is the function of temperature because the viscosities are the function of temperature, i.e., $a' = f(k_{rw}, k_{ro}, \mu_w(T), \mu_o(T)) = f(T)$. Under the given condition, the dimensionless coefficient changes from 6.39×10^{-4} to 1.52×10^{-3} when the temperature changes from 20 ^{o}C to 90 ^{o}C (Table 5-4; Figure 5-8). That is, the blob velocity changes more rapidly at the elevated temperature.

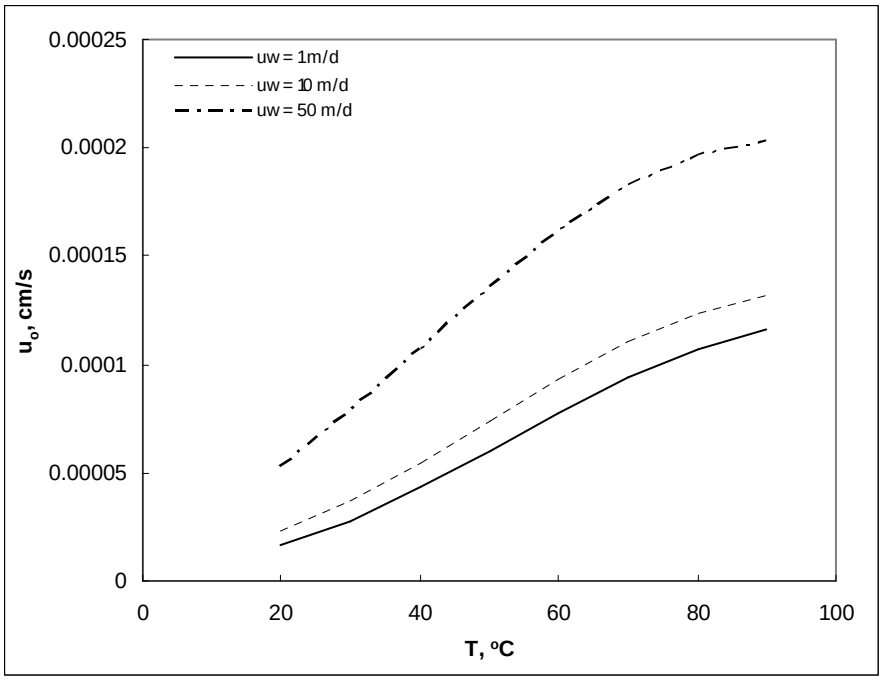

(a)

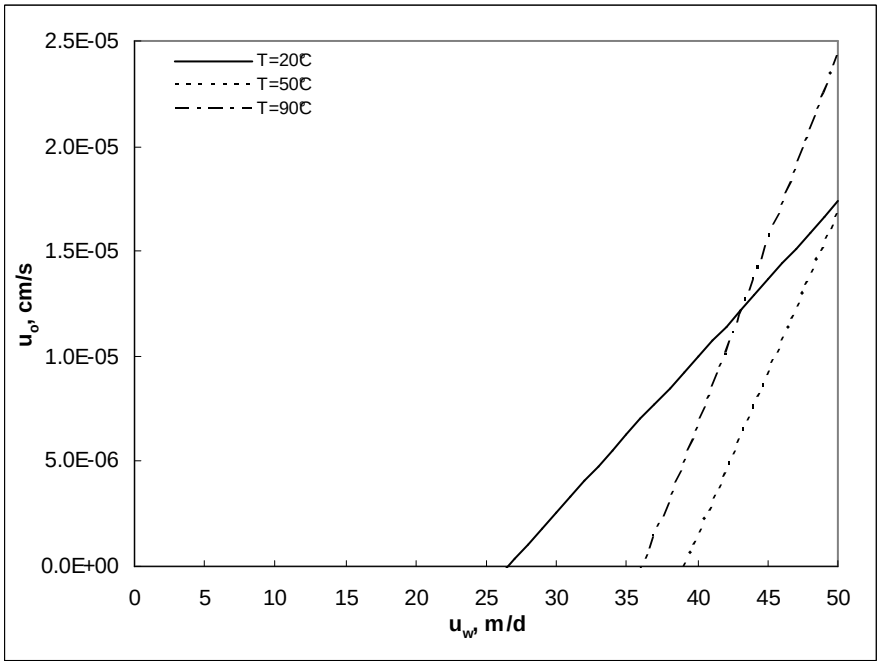

(b)

Figure 5-7 Terminal blob velocity as a function of (a) temperature and (b) water velocity

Table 5-3 Terminal blob velocity for NAPL blob mobilization as a function of water flow velocity and temperature

T, °C	u_o, cm/s		
	u_w = 1 m/d	u_w = 10 m/d	u_w = 50 m/d
20	1.620E-05	2.286E-05	5.245E-05
30	2.787E-05	3.708E-05	7.801E-05
40	4.291E-05	5.463E-05	1.067E-04
50	6.016E-05	7.401E-05	1.356E-04
60	7.785E-05	9.325E-05	1.617E-04
70	9.409E-05	1.103E-04	1.825E-04
80	1.073E-04	1.236E-04	1.963E-04
90	1.164E-04	1.322E-04	2.026E-04
From the linear fitting line, u_o (cm/s) = $a \times T$ (°C) + b,			
a, cm/s·°C	1.59×10^{-6}	1.79×10^{-6}	2.66×10^{-6}

Table 5-4 Proportionality coefficient a' from Equation (5-3) as a function of temperature

T, °C	a' from Equation (5-3)	
	(cm/s)/(m/d)	dimensionless
20	7.397E-07	6.391E-04
30	1.023E-06	8.842E-04
40	1.301E-06	1.124E-03
50	1.539E-06	1.330E-03
60	1.711E-06	1.478E-03
70	1.803E-06	1.558E-03
80	1.816E-06	1.569E-03
90	1.760E-06	1.521E-03

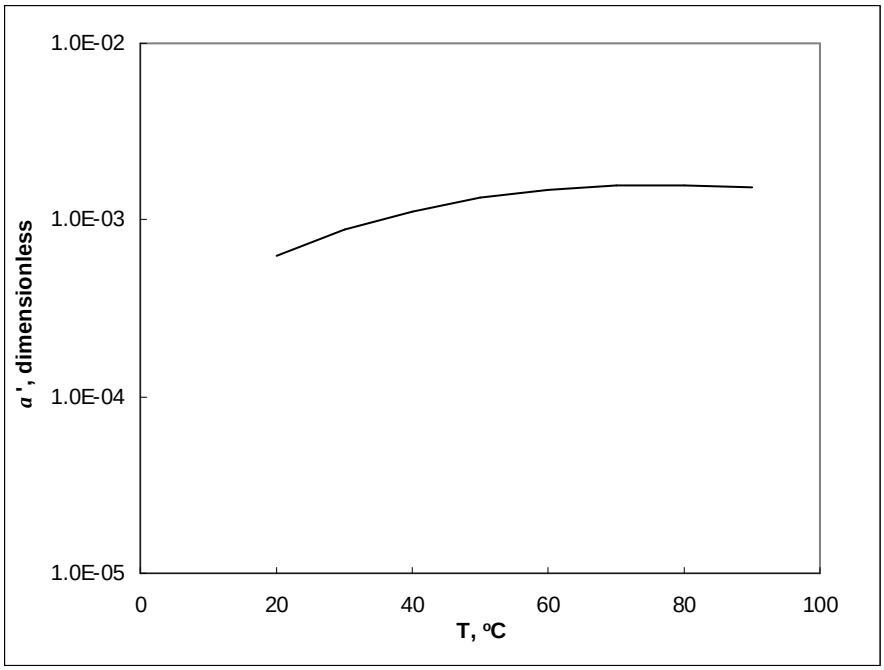

Figure 5-8 Proportionality coefficient *a*' from Equation (5-3) as a function of temperature

5.2 Effects of Varying Relative Permeability on the Blob Mobilization

At the macro scale of soil system, saturation and permeability of oil phase are considered constant. Meanwhile, as the soil system scales down to the micro scale (pore scale), the saturation of oil phase is considered varying according to the blob size. Thus, the relative permeability of oil phase has varying value along with the varying saturation.

Based on the definition of soil geometry at Chapter II, Figure 5-9 illustrates the relationship between saturation and relative permeability of oil phase. At a certain blob size, oil saturation increases when the point of observation moves gradually from the macro scale of representative elemental volume (REV) to the micro scale of single pore. For example, the oil saturation increases from 0.2 to 0.94 at R_o = 0.17 cm. Then, the change of oil saturation is followed by the change of relative permeability of oil phase from 0.008 to 0.831 with the corresponding change of oil saturation.

With this change, the magnitude of push force changes accordingly while buoyant and surface tension forces does not (Figure 5-10a). Along with the constant water flow velocity (u_w = 1 m/d), the push force increases as the oil saturation increases and the corresponding relative permeability of water phase decreases. The increase of push force is clearly seen with the calculated force ratio (Figure 5-10b). The ratio shows the significant increase of push force and decrease of other forces at oil saturation larger than 0.5. And finally, this increase provides the positive contribution to the driving force and as the oil saturation increases and go beyond 0.7, the contribution of push force to the driving force exceeds that of buoyant force (Figure 5-11a). This also provides the more favorable condition for the blob mobilization at the higher oil saturation (Figure 5-11b).

At the higher temperature, forces shows the same trend with the change of force magnitude; the push force increases and other forces does not change with respect to oil saturation. However, magnitudes of forces change with respect to temperature. When the temperature changes from 20 °C to 90 °C, all of forces decrease and the extent of decreases is 2.5, 67.5 and 30.5 % for buoyant, push and surface tension force, respectively (Figure 5-10a). From the force ratios between forces, the ratio of buoyant force rises and the ratios of push and surface tension forces lower (Figure 5-10b). It can be known that the change is possible because the extent of decreases of buoyant force is relatively smaller than those of other forces. And because of this fact, the contribution of push force to the driving force decreases as the temperature increases (Figure 5-11a). And also, the point which the driving force exceeds the retention force appears at the higher oil saturation than that at T = 20 °C because the relatively huge decrease of push force causes the total driving force to lower, compared to the retention force (Figure 5-11b).

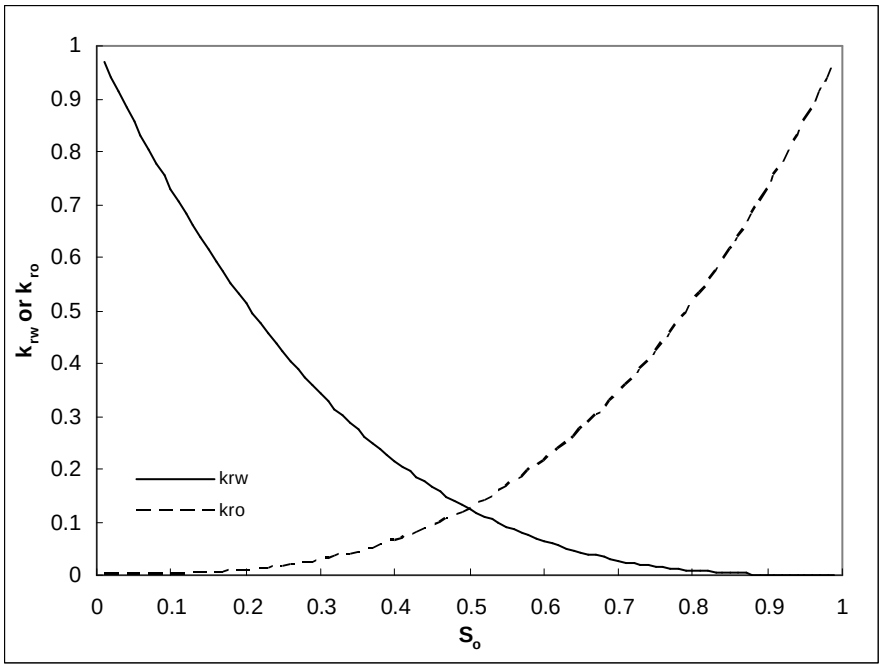

(a)

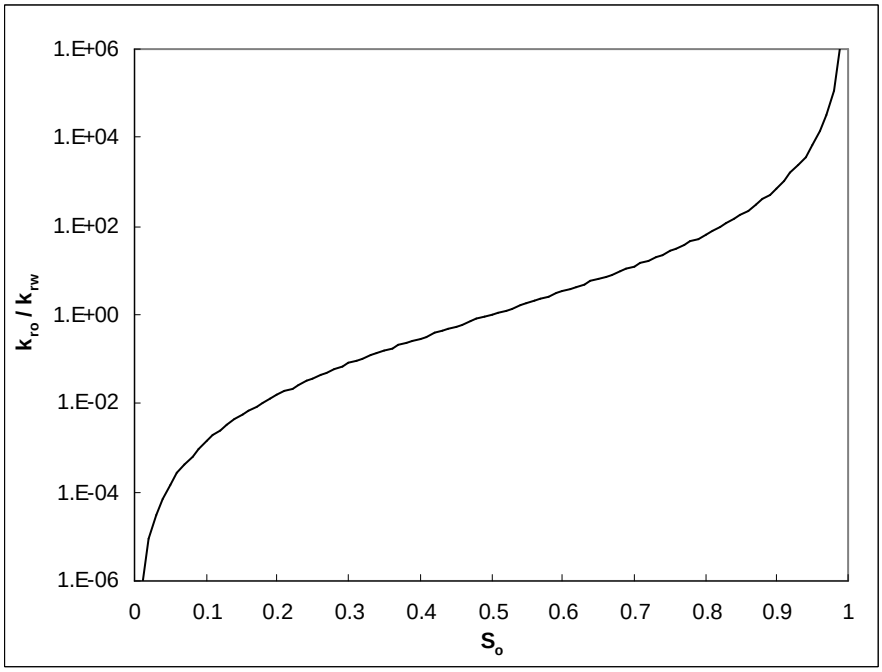

(b)

Figure 5-9 (a) Relative permeabilities of oil and water phases and (b) ratio of relative permeabilities as a function of oil saturation

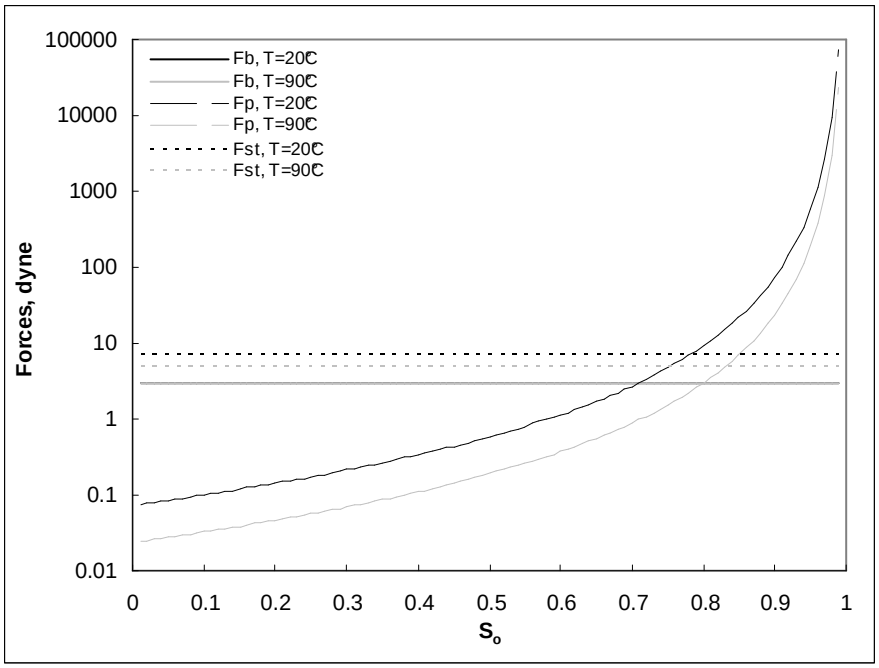

(a)

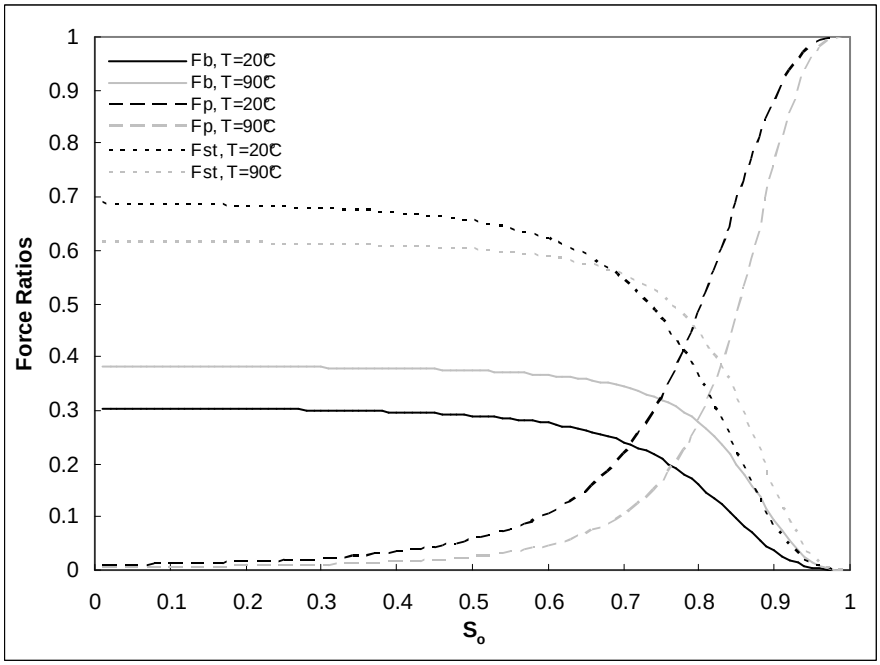

(b)

Figure 5-10 (a) Magnitudes of buoyant, push and surface tension forces and (b) force ratios between forces as a function of oil saturation

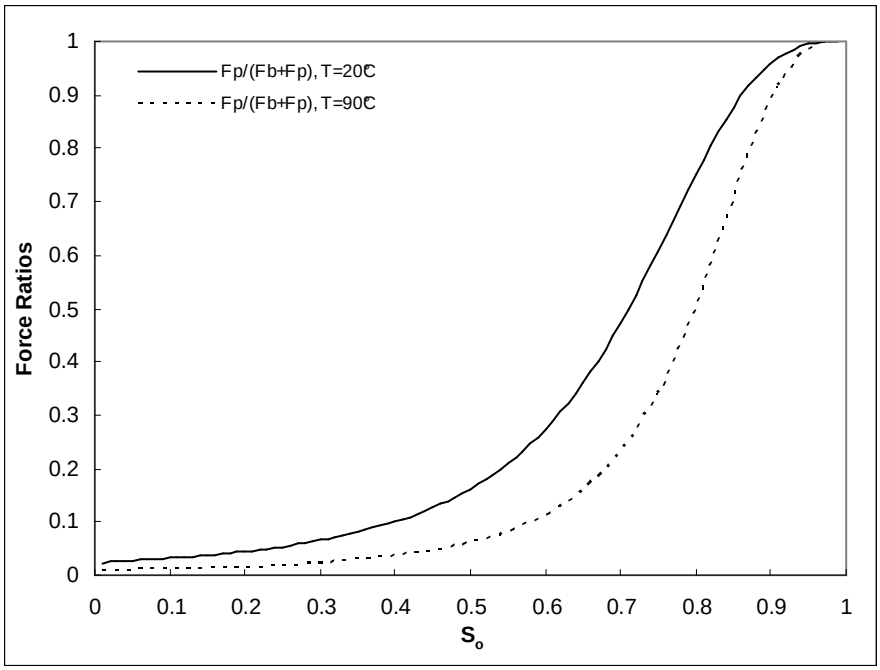

(a)

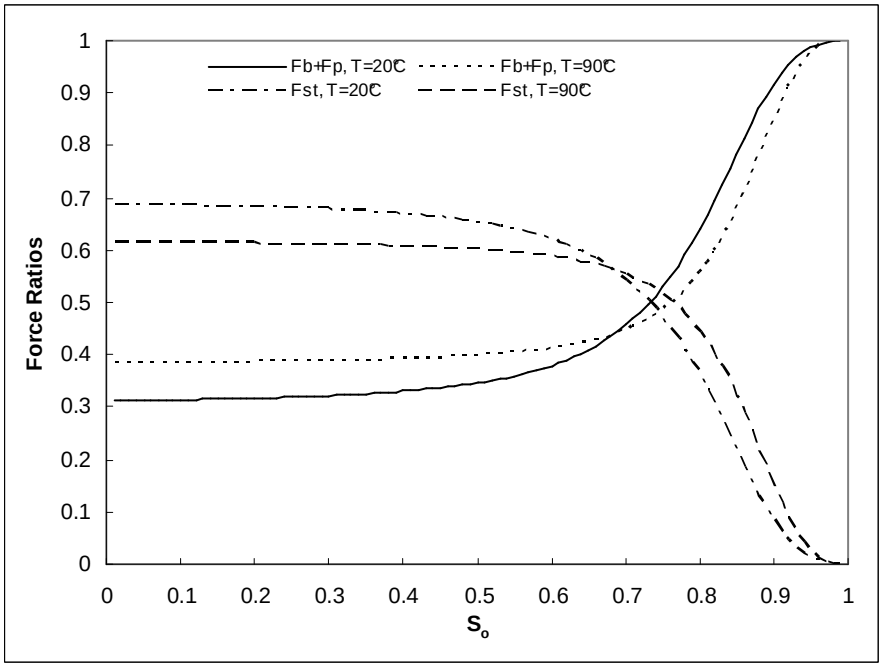

(b)

Figure 5-11 (a) Force ratio of push force to the driving force, showing the extent of contribution of push force to the driving force and (b) force ratios of the driving force ($F_b + F_p$) and the retention force (F_{st}) as a function of oil saturation

5.3 Terminal Blob Velocity with Varying Relative Permeability

The blob velocity is calculated once again from force balance equations. Equations (3-10a) through (3-10d) set up for the mobilization of a trapped NAPL blob in a pore with the water flow are used for this calculation. All the conditions are same except for the relative permeability: the relative permeability is variable according to the blob radius and the corresponding oil saturation (Figure 5-9). As the oil saturation changes, the water saturation also changes. But, this change is limited by the fact that the summation of both of saturations goes to unity.

5.3.1 Consideration of Blob Radius

The calculation of blob velocity with varying permeability is compared to that with constant permeability, shown at Section 3.3.3. At first, the terminal blob velocity at the varying permeability scenario reaches to water velocity applied to the system (u_w = 1 m/d = 1.157×10^{-3} cm/s) at certain blob radius, meanwhile the blob velocity does not reach to the water velocity at the constant permeability scenario. That is, the blob velocity at the varying permeability scenario is 1.157×10^{-3} cm/s and the velocity at the constant permeability scenario is 1.620×10^{-5} cm/s (Figure 5-12). The difference between two velocities is as large as two orders. Also, the pattern of increase of blob velocity is different.

With the constant permeability scenario, the blob starts to move at the blob radius of 0.225 cm and its velocity reaches to 99% of the terminal velocity (nearing the steady-state velocity) at the blob radius of 0.81 cm. Meanwhile, with the varying permeability scenario, the blob starts to move at the blob radius of 0.159 cm and its velocity reaches to 99% of the terminal velocity at the blob radius of 0.171 cm. This fact says that the increase of the blob velocity happened dramatically fast with the varying permeability scenario. It can be explained by the increase of oil permeability and the resultant decrease of water permeability. The increase of oil permeability plays the role of reducing the drag force and the decrease of water permeability plays the role of increasing the push force. And when the magnitude of relative permeability is looked over under the above condition, the change of magnitude in push force is much more significant than that in drag force because the change of water relative permeability is more sensitive to the change of blob radius than that of oil relative permeability.

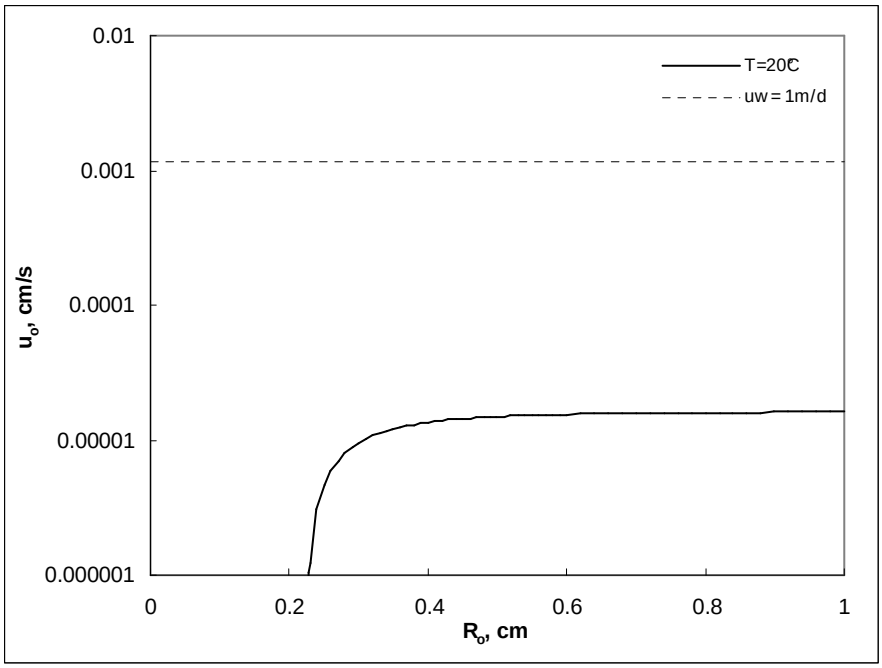

(a)

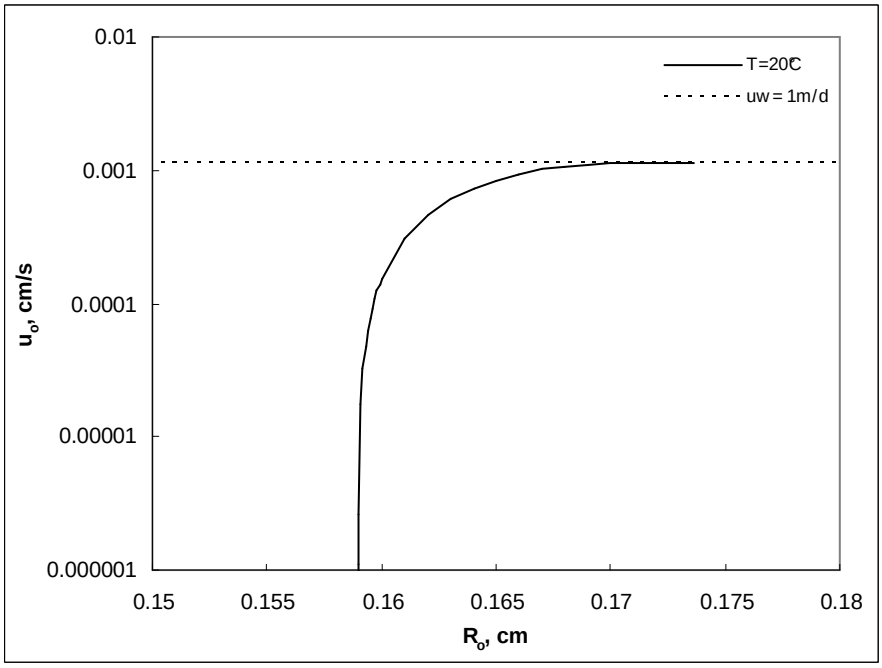

(b)

Figure 5-12 Blob velocity as a function of blob radius under (a) the constant permeability condition and (b) the varying permeability condition

5.3.2 Consideration of Temperature

As the temperature increases, the difference between blob velocities of two scenarios from varying and constant permeability is getting smaller (Figure 5-13). However, the difference is still significant. At T = 90 ^{o}C, the blob velocity with constant permeability scenario is 1.164 $\times$ 10^{-4} cm/s, meanwhile the blob velocity with varying permeability reaches to the water velocity (u_w = 1 m/d = 1.157 $\times$ 10^{-3} cm/s). Thus, the difference between those two velocities is by an order.

Considered the temperature range of 20 to 90 ^{o}C, the blob velocity at the varying permeability scenario reaches to the water velocity, meanwhile the velocity still does not reach to the water velocity at any temperature.

5.3.3 Consideration of Water Velocity

The terminal blob velocities of two scenarios with different types of permeability are clearly different. The increase of terminal blob velocity with respect to water velocity is shown with both constant and varying permeability scenario (Figure 5-14; Table 5-5). But, the blob velocity with constant permeability scenario is much lower than the water velocity (Figure 5-14a), meanwhile the blob velocity with varying permeability scenario reaches to the water velocity regardless of the magnitude of water velocity (Figure 5-14b).

From both of scenarios, the critical blob radius for the blob mobilization decreases as the water velocity increases. That is, the smaller blob can start up at the higher water velocity. And, the blob velocity reaches to the steady state at the smaller blob radius as the water velocity increases. This phenomena is clearly seen at the constant permeability scenario, meanwhile it is not at the varying permeability scenario.

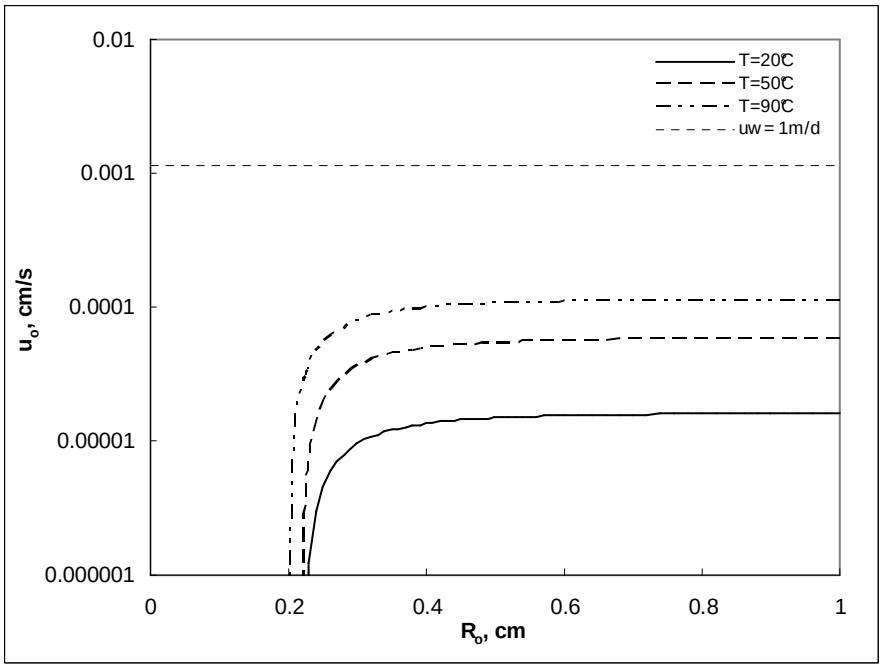

(a)

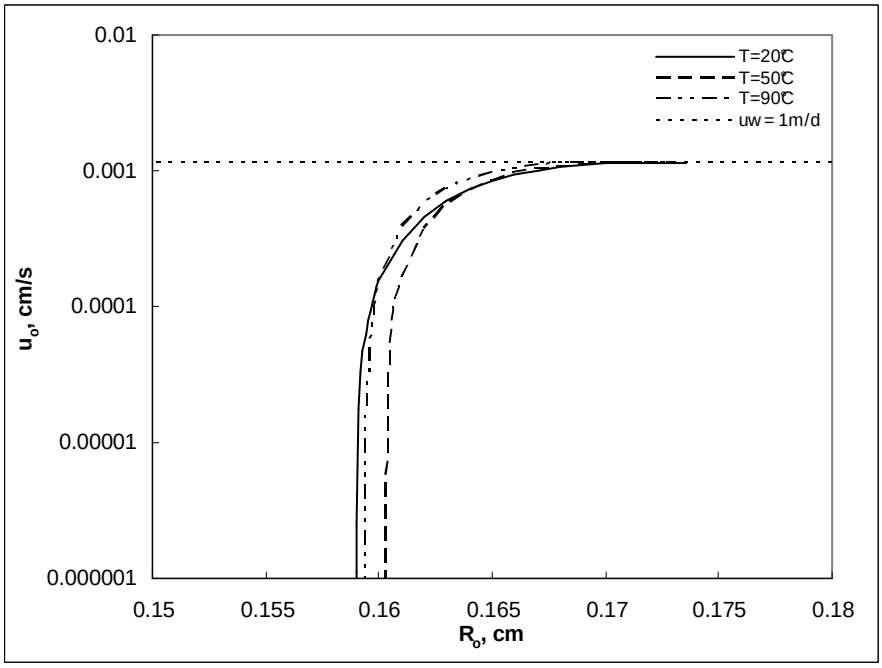

(b)

Figure 5-13 Blob velocity as a function of blob radius at different temperatures under (a) the constant permeability condition and (b) the varying permeability condition

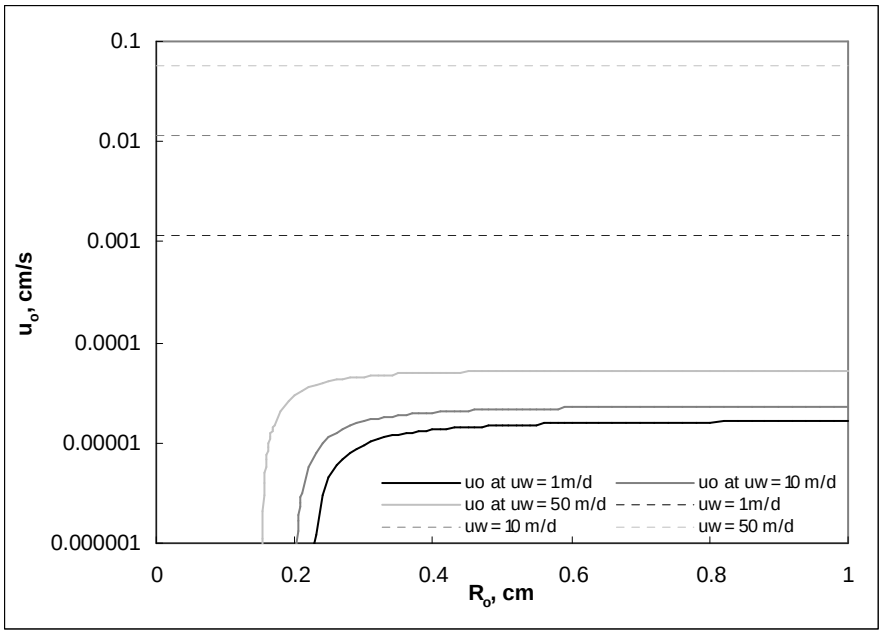

(a)

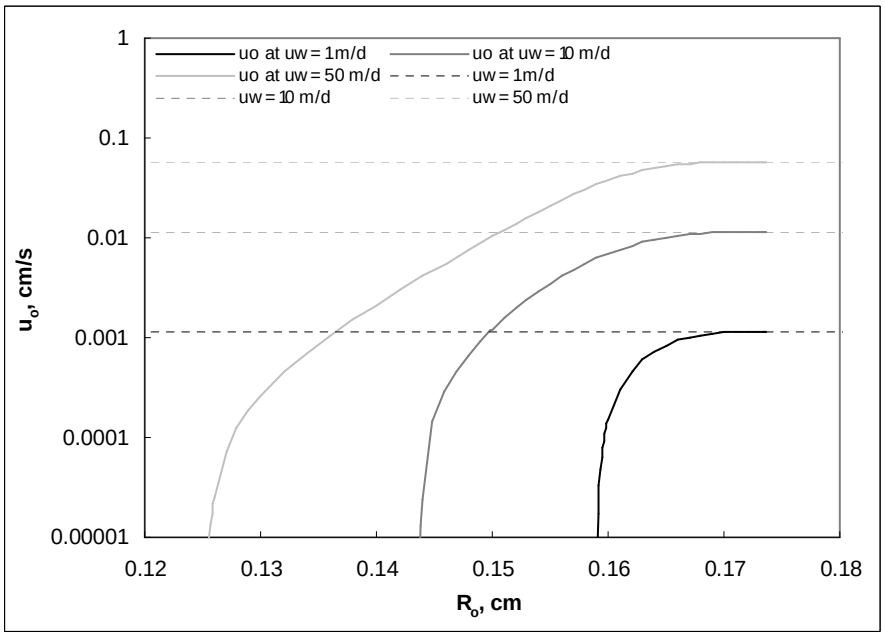

(b)

Figure 5-14 Velocity of blob mobilization as a function of blob radius at different water velocities under (a) the constant permeability condition and (b) the varying permeability condition

Table 5-5 Terminal blob velocity with constant and varying permeability scenarios over water velocity

u_w		u_o, cm/s	
m/d	cm/s	constant permeability scenario	varying permeability scenario
1	1.157E-03	1.620E-05	1.157E-03
10	1.157E-02	2.286E-05	1.157E-02
50	5.787E-02	5.245E-05	5.787E-02

5.4 Dimensionless Numbers with Varying Relative Permeability

5.4.1 Effects of Blob Radius

As the blob radius increases, all of modified dimensionless numbers Bo', $Ca'_{o,1}$, $Ca'_{o,2}$ and Ca'_{w} increases under the varying permeability scenario, too (Figure 5-15). But, the increasing trend is somewhat different from that of constant permeability scenario. Under the constant permeability environment, all the numbers are influenced by the blob radius (Figure 5-15a), meanwhile those numbers are influenced by oil (or water) relative permeability under the varying permeability environment (Figure 5-15b). Especially, Bo' and Ca'_{w} show the significant difference between those two environments. Under the environment of constant permeability and normal groundwater velocity, Bo' from the buoyant force plays a major role of the driving force. However, under the environment of varying permeability, Ca'_{w} from the push force does the role of the driving force. It can be thought that the increase of oil saturation along with the increasing blob radius causes the NAPL (or water) phase more (or less) permeable (i.e., movable) in a pore. $Ca'_{o,1}$ and $Ca'_{o,2}$ also shows the same change of playing role for the retention force. Under the environment of constant permeability and normal groundwater velocity, $Ca'_{o,1}$ from the drag force plays a major role of the retention force. However, under the environment of varying permeability, $Ca'_{o,2}$ from the drag force between fluid phases does the role of the retention force.

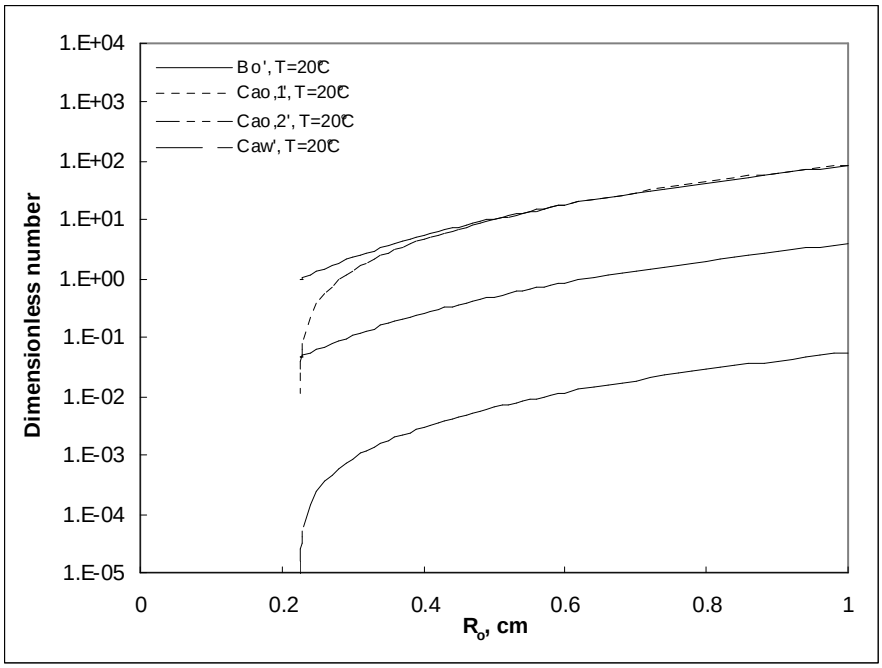

(a)

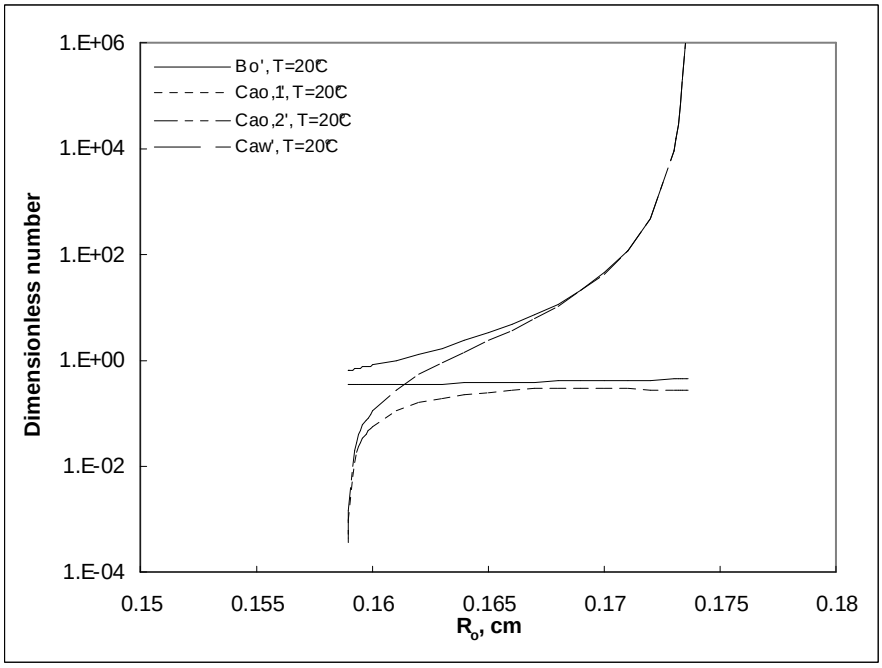

(b)

Figure 5-15 Modified dimensionless numbers as a function of blob radius at T = 20 ^{o}C; (a) with constant permeability and (b) with varying permeability

5.4.2 Effects of Temperature

The increase of temperature does not change the trend of change of dimensionless numbers, compared to that at reference temperature (i.e. room temperature, T = 20 ^{o}C). However, the temperature-dependent change of values of dimensionless numbers is observed. $Ca'_{o,1}$, $Ca'_{o,2}$ and Ca'_{w} decrease as the temperature increases, meanwhile Bo' increases (Figure 5-16). Decreases of first three numbers are influenced by the big drop-down of water (or NAPL) viscosity, but Bo' is not influenced by the decrease of viscosity. Instead, the significant decrease of the combined term of interfacial tension and contact angle gives Bo' the relatively increasing number over the temperature.

5.4.3 Effects of Water Velocity

All of modified dimensionless numbers shows the same trend of change with respect to the blob radius at the higher water velocity (u_w = 10 m/d), compared to that at reference water velocity (u_w = 1 m/d) (Figure 5-17). But, some different phenomena are observed. First, as mentioned in the previous chapter, the smaller critical blob radius for the blob mobilization is observed at the higher water velocity.

Second, at the smaller blob radius, $Ca'_{o,2}$ is larger than $Ca'_{o,1}$, and then this phenomena is overturned after some point of blob radius (Figure 5-17a).

This is different from that at u_w = 1 m/d, i.e. $Ca'_{o,1}$ is always larger than $Ca'_{o,2}$ over the range of blob radius considered. From Equations (4-11) and (4-12), the ratio of numbers between $Ca'_{o,1}$ and $Ca'_{o,2}$ can be expressed as $\left(\frac{k_{rw}}{k_{ro}}\right)\left(\frac{\mu_o}{\mu_w}\right)$ and if this ratio is larger than unity, $Ca'_{o,1}$ is larger than $Ca'_{o,2}$. So, the critical blob radius for this ratio is 0.157 cm. That is, at the smaller blob radius than 0.157 cm, $Ca'_{o,1}$ is larger than $Ca'_{o,2}$ and after this radius, $Ca'_{o,2}$ becomes larger than $Ca'_{o,1}$. This critical blob radius is much smaller (0.151 cm) at the elevated temperature (T = 90 ^{o}C) and this is because the ratio of $\left(k_{rw}/k_{ro}\right)$ becomes lower at elevated temperature due to the effects of thermal expansion of NAPL blob. Nevertheless, $Ca'_{o,1}$ and $Ca'_{o,2}$ shows numbers of much smaller than unity, that is, over this range of blob radius, the surface tension force plays a major role of the retention force.

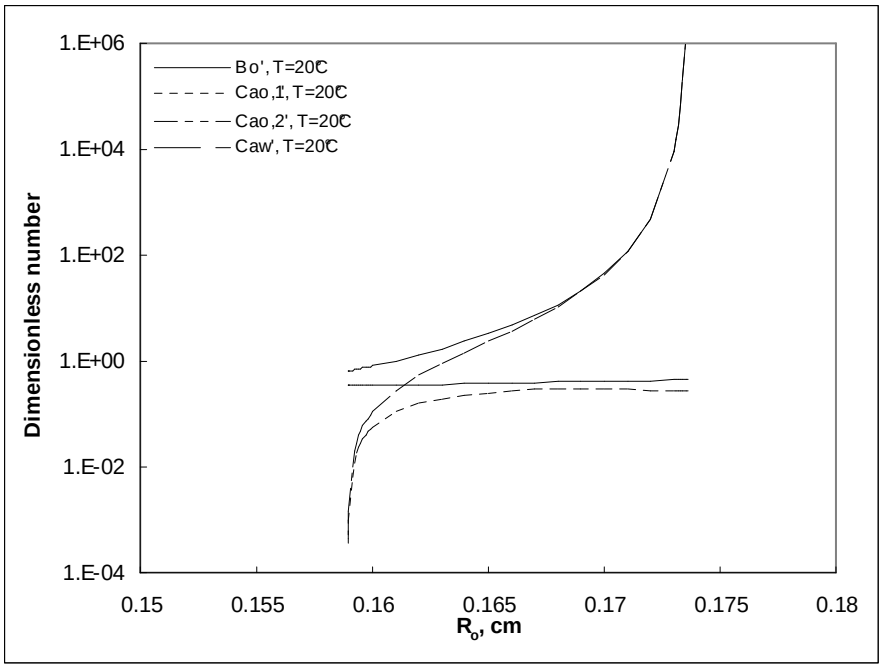

(a)

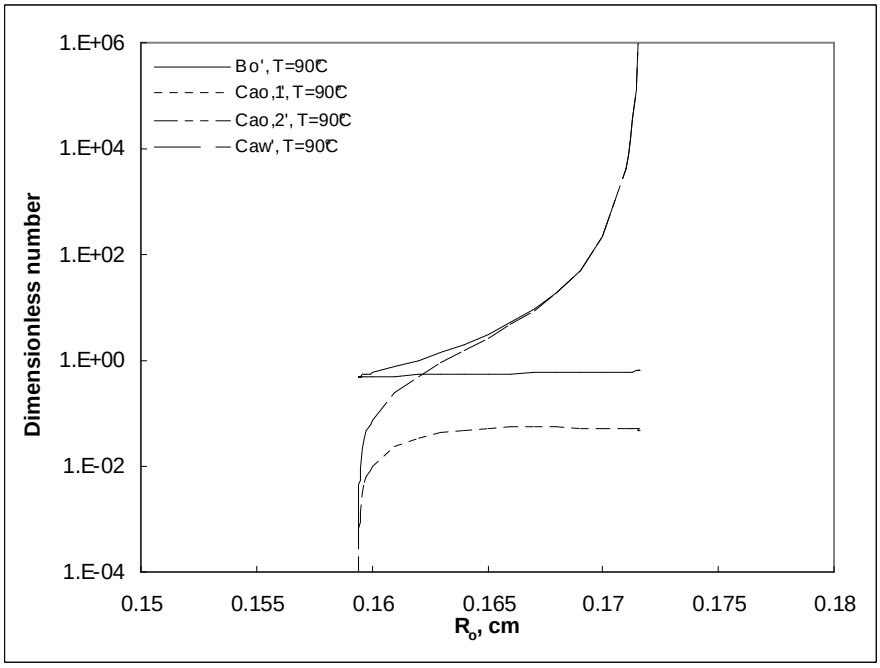

(b)

Figure 5-16 Modified dimensionless numbers as a function of blob radius under the condition of varying permeability and constant water velocity (u_w = 1 m/d); (a) at T = 20 ^{o}C and (b) T = 90 ^{o}C

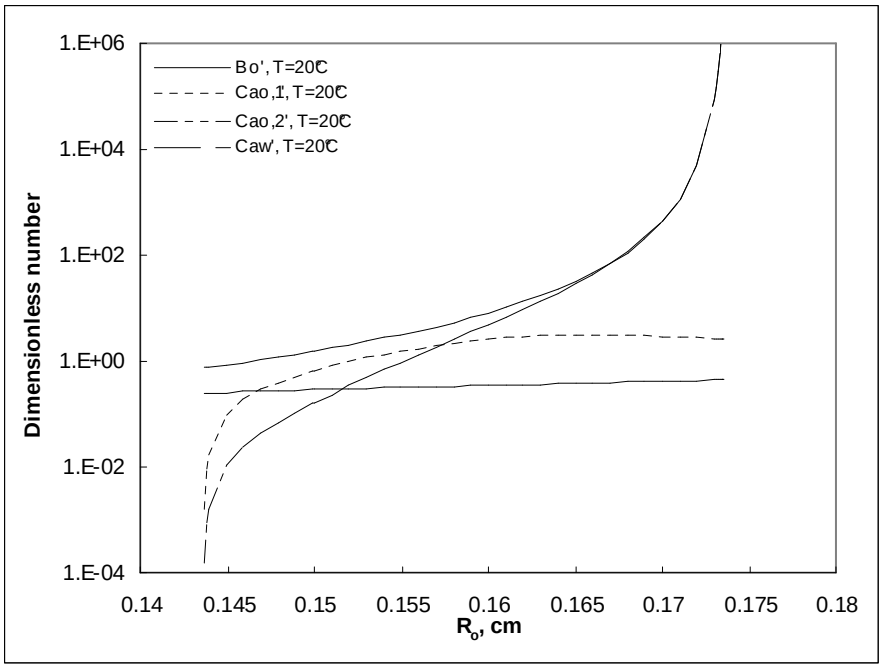

(a)

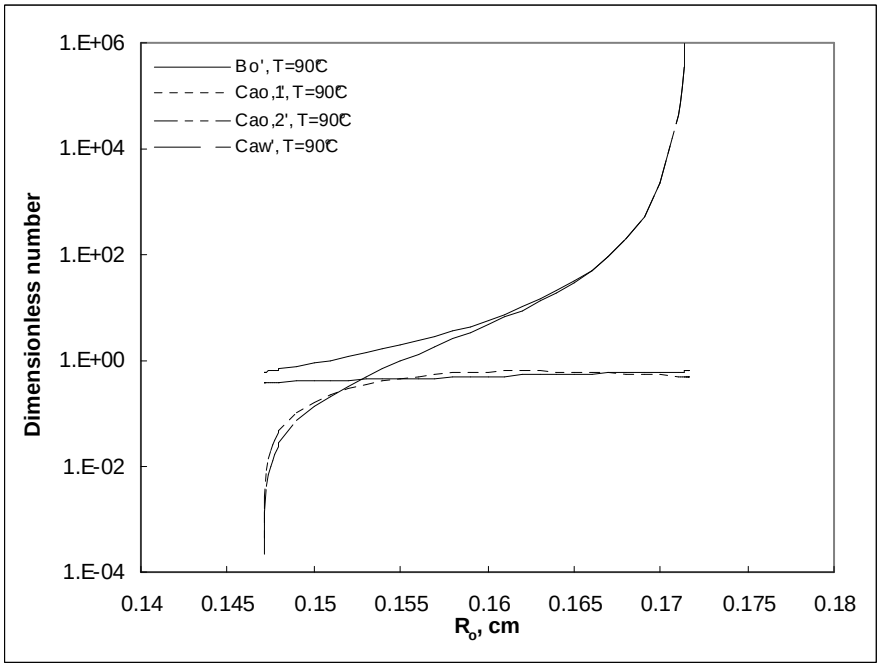

(b)

Figure 5-17 Modified dimensionless numbers as a function of blob radius under the condition of varying permeability and constant water velocity (u_w = 10 m/d); (a) at T = 20 ^{o}C and (b) T = 90 ^{o}C

CHAPTER VI

SUMMARY AND CONCLUSION

The objectives of this research are to analyze the possible benefits of remediating the NAPL-contaminated subsurface by thermal techniques (for this study, hot water flooding). Specifically, this research focuses on how the temperature influences the mobilization of the immobile NAPL blob (specifically Voltesso 35, a viscous LNAPL) in porous media.

Force balance analysis shows the critical conditions for the initiation of blob mobilization in porous media in terms of blob radius, temperature and the water flow. First, the critical blob radius of stagnant blob in the pores for the initiation of blob mobilization is 0.228 cm (blob volume as 2.3 times of unit pore volume). At the elevated temperature (T = 90 ^{o}C), the critical blob radius decreases up to 0.203 cm (blob volume as 1.6 times of unit pore volume). The number of unit pore volume, equivalent to the blob volume, also decreases from 2.3 to 1.6 units.

When the water flow exists in porous media, the water flow lowers the critical blob radius under the same environment and condition. With the natural velocity of water flow (u_w = 1 m/d), the critical blob radius for the blob mobilization is 0.224 cm at T = 20 °C. And at the elevated temperature (T = 90 ^{o}C), the critical blob radius is 0.202 cm. The number of unit pore volume, equivalent to the blob volume, also decreases from 2.1 to 1.6 units. Under the range of naturally existing velocity, the water flow does not contribute much to the blob mobilization, compared to the effects of temperature from the decrease of interfacial tension.

However, at the elevating water velocity, the contribution of water flow to the blob mobilization increases significantly. With the high water flow (u_w = 26.5 m/d), the critical blob radius for the blob mobilization is 0.174 cm at T = 20 °C. This blob radius represents the same volume of blob as that of a single pore. Thus, this water velocity provides the critical condition for the initiation of blob mobilization to distinguish singlet and doublet in the blob size.

In the meantime, this critical water velocity increases as the temperature increases. At T = 90 °C, the critical water velocity is 43.6 m/d. It indicates that when the water velocity is considered as a factor to affect the mobilization of such a small blob as singlet, it requires the highly increasing velocity.

Terminal (or steady-state) blob velocity at the steady-state blob motion is another characteristic of blob mobilization observed by force balance analysis. Terminal blob velocity in the pores without the water flow is 1.55×10^{-5} cm/s at T = 20 ^{o}C. At the elevated temperature (T = 90 ^{o}C), terminal blob velocity increases up to 1.15×10^{-4} cm/s.

When the water flow exists in porous media, the water flow raises terminal blob velocity under the same environment and condition. With the natural velocity of water flow (u_w = 1 m/d), terminal blob velocity is 1.62×10^{-5} cm/s at T = 20 ^{o}C. And at the elevated temperature (T = 90 ^{o}C), terminal blob velocity is 1.16×10^{-4} cm/s. Under the range of naturally existing velocity, the water flow contributes little to enhance the blob mobilization, compared to the effects of temperature. When terminal blob velocity is compared to water velocity (u_w = 1 m/d = 1.16×10^{-3} cm/s), it is lower by two order at T = 20 ^{o}C and by one order at T = 90 ^{o}C.

Terminal blob velocity increases in linear proportion to the water velocity. The proportionality coefficient is a function of viscosities and relative permeabilities of water and oil phases, i.e., $a' = f(k_{rw}, k_{ro}, \mu_w, \mu_o)$. And, two viscosities are a function of temperature, so the proportionality coefficient is a function of temperature [$a' = f(k_{rw}, k_{ro}, \mu_w(T), \mu_o(T)) = f(T)$]. This dimensionless proportionality coefficient changes from 6.39×10^{-4} to 1.52×10^{-3} when the temperature changes from 20 ^{o}C to 90 ^{o}C. That is, terminal blob velocity changes more rapidly at the elevated temperature.

When the observation of blob mobilization moves from REV scale (macro-scale) to pore-scale with respect to the point of view, terminal blob velocity shows the different phenomena according to the change of oil saturation. Oil saturation which is defined as constant at macro-scale varies according to the change of blob volume. Accordingly, varying oil saturation provides changing relative permeability of oil phase. Thus, oil permeability also changes and it becomes a factor to affect the blob mobilization at pore-scale. Unlike the terminal blob velocity at macro-scale with constant oil permeability lowered by one or two order than water velocity, the terminal blob velocity at pore-scale with varying oil permeability reaches to the water velocity when a singlet-type blob is observed in a pore. This is explained by the fact that the increase of oil permeability and the corresponding decrease of water permeability cause the drag force to decrease and the push force to increase, respectively. It means, for the blob mobilization, the decrease of total retention force by decreasing drag force and the increase of total driving force by increasing push force.

Dimensional analysis using dimensionless numbers shows the evaluation of the effects of forces exerted on a NAPL blob trapped in the pores to delineate the blob

mobilization in porous media. For the analysis, the modified forms of existing dimensionless numbers are introduced. Unlike existing dimensionless numbers, modified dimensionless numbers are expressed as a function of blob radius to show the effects of blob volume from buoyant and drag forces.

First, without the water flow, modified dimensionless numbers Bo' and Ca'_o, corresponding to existing dimensionless numbers Bo and Ca_o, show that the buoyant force is balanced by the surface tension force at very small blob radius (R_o = 0.25 cm). And at R_o > 0.25 cm, the combined drag and surface tension forces balance the buoyant force and the drag force only balances the buoyant force at R_o > 0.6 cm. This phenomenon happens at the smaller blob radius as the temperature increases. It is due to the relative increases of buoyant and drag forces by the decrease of interfacial tension and the increase of blob velocity.

With the existence of water flow, dimensionless numbers show the same trend with respect to the blob radius and temperature. Dimensionless numbers Bo' and $Ca'_{o,1}$ do a major role of blob mobilization, compared to $Ca'_{o,2}$ and Ca'_w. However, at pore-scale with varying oil permeability, dimensionless numbers $Ca'_{o,2}$ and Ca'_w become a major role of blob mobilization due to the increase of oil permeability and the corresponding decrease of water permeability. Meanwhile, Ca'_w increases in proportion to water velocity and provides more contribution to the total driving force at the elevated water velocity.

REFERENCES

Anton, L., Hilfer, R., 1999. Trapping and mobilization of residual fluid during capillary desaturation in porous media. Physical Review E 59(6), 6819–6823.

Bear, J.A., 1972. Dynamics of Fluids in Porous Media, American Elsevier Publishing Company, New York.

Bruell, C.J., Ryan, D.K., Duggan, J.W., Crawford, S.C., Barker, C.C., 1997. Effects of pore size on the mobilization of petroleum hydrocarbons by surfactant enhanced soil flushing, Technical completion report. Water Resources Research Center, University of Massachusetts at Amherst, Publication No. 172.

Corapcioglu, M.Y., Cihan, A., Drazenovic, M., 2004. Rise velocity of an air bubble in porous media: theoretical studies. Water Resources Research 40, 1-9.

Corey, A.T., 1954. The interrelation between gas and oil relative permeability abilities. Producer's Monthly 19, 32-41.

Corey, A.T., 1994. Mechanics of Immiscible Fluids in Porous Media, 3rd Ed. Water Resources Publications, Highlands Ranch, CO.

Davis, B.M., Istok, J.D., Semprini, L., 2002. Push-pull partitioning tracer tests using radon-222 to quantify non-aqueous phase liquid contamination. Journal of Contaminant Hydrology 58, 129–146.

Davis, E.L., 1997. How Heat Can Enhance In-situ Soil and Aquifer Remediation: Important Chemical Properties and Guidance on Choosing the Appropriate Technique. EPA/540/S-97/502. United States Environmental Protection Agency, Washington, DC.

Davis, E.L., 1998. Steam Injection for Soil and Aquifer Remediation. EPA/540/S-97/505. United States Environmental Protection Agency, Washington, DC.

Dullien, F.A.L., 1979. Porous Media: Fluid Transport and Structure, Academic Press, New York.

Dury, O., Fischer, U., Schulin, R., 1999. A comparison of relative nonwetting-phase permeability models. Water Resources Research 35, 1481–1493.

Fu, X., Imhoff, P.T., 2002. Mobilization of small DNAPL pools formed by capillary entrapment. Journal of Contaminant Hydrology 56, 137–158.

Gioia, F., Urciuolo, M., 2006. Combined effect of bond and capillary numbers on hydrocarbon mobility in water saturated porous media. Journal of Hazardous Materials 133, 218–225.

Graton, L.C., Fraser, H.J., 1935. Systematic packing of spheres with particular relation to porosity and permeability. Journal of Gology 43(8), 785–909.

Han, J.S., 2007. The Role of Colloidal Particles on the Migration of Air Bubbles in Porous Media. Ph.D. dissertation, Texas A&M University.

Jayaram, S., 1993. Effects of thermal and viscous drag forces on AC breakdown characteristics of transformer oil". Conference Record of IEEE - CEIDP Annual Meeting, Pocono Manor, PA, 396–401.

Keller, A.A., Chen, M., 2003. Effect of spreading coefficient on three-phase relative permeability of nonaqueous phase liquids. Water Resources Research 39 (10), 1288.

Li, Y.S., Abriola, L.M., Phelan, T.J., Ramsburg, C.A., Pennell, K.D., 2007. Experimental and numerical validation of the total trapping number for prediction of DNAPL mobilization. Environmental Science and Technology 41, 8135−8141.

Mercer, J.W., Cohen, R.M., 1990. A review of immiscible fluids in the subsurface: properties, models, characterization and remediation. Journal of Contaminant Hydrology 6, 107–163.

Morrow, N.R., Chatzis, I., Taber, J.J., 1988. Entrapment and mobilization of residual oil in bead packs. SPE Reservoir Engineering 3, 927–934

Munson, B.R., Young, D.F., Okiishi, T.H., 1998. Fundamentals of Fluid Mechanics, 3rd Ed. John Wiley & Sons, New York.

Niven, R.K., 2002. Physical insight into the Ergun and Wen & Yu equations for fluid flow in packed and fluidised beds. Chemical Engineering Science 57, 527–534.

O'Carroll, D.M., Sleep, B.E., 2007. Hot water flushing for immiscible displacement of a viscous NAPL. Journal of Contaminant Hydrology 91(1), 247–266.

Pennell, K.D., Pope, G.A., Abriola, L.M., 1996. Influence of viscous and buoyancy forces on the mobilization of residual tetrachloroethylene during during surfactant flushing. Environmental Science & Technology 30(4), 1328−1335.

Pirson, S.J., 1958. Oil Reservoir Engineering. McGraw Hill, New York.

Poston, S.W., Ysrael, S., Hossain, A.K.M.S., Montgomery, E.F., Ramey, H.J., Jr., 1970. The effect of temperature on irreducible water saturation and relative permeability of unconsolidated sands. SPE Journal 10(2), 171−180.

Powers, S.E., Abriola, L.M., Weber, W.J., Jr., 1994. An experimental investigation of nonaqueous phase dissolution in saturated subsurface systems: transient mass transfer rates. Water Resources Research 30(2), 321−332.

Powers, S.E., Loureiro, C.O., Abriola, L.M., Weber, W.J., Jr., 1991. Theoretical study of the significance of nonequilibrium dissolution of nonaqueous phase liquids in subsurface systems. Water Resources Research 27(4), 463−477.

Roosevelt, S.E., Corapcioglu, M.Y., 1998. Air bubble migration in a granular porous medium: experimental studies. Water Resources Research 34(5), 1131−1142.

Rubin, H., Yaniv, S., Spiller, M., Köngeter, J., 2008. Parameters that control the cleanup of fractured permeable aquifers. Journal of Contaminant Hydrology 96, 128−149.

She, H.Y., Sleep, B.E., 1998. The effect of temperature on capillary pressure-saturation relationships for air-water and perchloroethylene-water systems. Water Resources Research 34(10), 2587–2597.

Sleep, B.E., Ma, Y.F., 1997. Thermal variation of organic fluid properties and impact on thermal remediation feasibility. Journal of Soil Contamination 6(3), 281–306.

Wyllie, M.R.J., 1962. Relative permeability, in Petroleum Production Handbook, vol. 2, Reservoir Engineering. SPE, Richardson, TX, pp. 25.1-25.14.

Wilson, J.L., Conrad, S.H., Mason, W.R., Peplinski, W., Hagan, E., 1990. Laboratory investigations of residual liquid organics from spills, leaks, and disposal of hazardous wastes in groundwater. EPA/600/6-90/004. United States Environmental Protection Agency, Washington, DC.

Yoon, S.H., 2007. Pore-scale Analysis of Solubilization and Mobilization of Trapped NAPL Blobs in Porous Media. Ph.D. dissertation, Texas A&M University.

VITA

Name: MIN AHN

Address: Department of Civil Engineering, Texas A&M University,
3136 TAMU, College Station, TX 77843-3136

Email Address: ahnmin@hotmail.com

Education: B.A., Geology, Seoul National University, 1992
M.S., Geology, Seoul National University, 1996
M.S., Civil Engineering, Texas A&M University, 2003
Ph.D., Civil Engineering, Texas A&M University, 2008